Shape Memory Polymers Produced via Additive Manufacturing

by

Trenton M. Cersoli

Submitted in Partial Fulfillment of the Requirements

for the Degree of

Master of Science in Engineering

in the

Chemical Engineering

Program

YOUNGSTOWN STATE UNIVERSITY

May 2021

Shape Memory Polymers Produced via Additive Manufacturing

Trenton Cersoli

I hereby release this **thesis** to the public. I understand that **thesis** will be made available from the OhioLINK ETD Center and the Maag Library Circulation Desk for public access. I also authorize the University or other individuals to make copies of this thesis as needed for scholarly research.

Signature:

Trenton M. Cersoli, Student Date

Approvals:

Dr. Pedro Cortes, Thesis Advisor Date

Dr. Eric MacDonald, Committee Member Date

Dr. Frank Li, Committee Member Date

Dr. Salvatore A. Sanders, Dean of Graduate Studies Date

Acknowledgments

With thanks and love to my family. Additional thanks to my parents for their support and sacrifices to allow me to pursue my interests. My success is always ours.

A special thank you to Dr. Pedro Cortes for his support and guidance throughout my time at YSU. Thank you for entertaining all of our crazy ideas.

There are too many others to thank in this short space. To all my friends, colleagues and more, I valued every memory we shared at Youngstown State University.

Thanks to the Air Force funding that allowed this and many other works to be investigated. The present work has been funded by the Secure Engineering for Trusted Systems project through the US Air Force. Grant FA8650-14-D-1724/004.

ABSTRACT

Smart materials provide a useful route for the fabrication of self-sensing actuators and deployable structures. In areas such as the aerospace industry, where weight and space savings are of the highest importance, shape memory polymers (SMPs) can be advantageous in creating these smart structures. Additive manufacturing offers additional benefits to fabricate polymers in more geometrically complex configurations than obtainable with traditional manufacturing techniques. If additive manufacturing and shape memory polymers can successfully be combined, the fabrication of smart, geometrically complex structures will be attainable. This work aims to fabricate shape memory polymers using two techniques of additive manufacturing: material extrusion and stereolithography (SLA). The use of commercially available shape memory polymer pellets is explored as a feedstock for material extrusion. Additionally, a commercially available photopolymer for SLA printers has been reformulated to improve its mechanical performance to act as a thermal shape memory polymer. With the ability to prepare SMPs via additive manufacturing, functional actuators and antennas were fabricated, to explore the potential applications of these materials.

Table of Contents

Figures

1 Introduction

1.1 Background

Developments in both manufacturing techniques and materials over the last two decades has expanded the horizon on feasibility and imagination in design. As manufacturing of many materials has progressed from traditional techniques (injection molding, film casting, subtractive machining), the original constraints for fabricating a part have been erased. Now, with advanced manufacturing techniques, designing parts for their application, instead of within the bounds of a manufacturing technique is possible. With the widespread use of additive manufacturing, more complex and organic structures are now accessible to a variety of industries. Industry sectors including biomedical, aerospace, and maritime are some of the largest contributors to both improve manufacturing techniques, and improved materials to fully utilize the potential of additive manufacturing. Advanced manufacturing builds on innovation in manufacturing techniques to explore new production of parts and materials.

With a growing library of materials and manufacturing methods, more applications for such techniques are discovered each year. An industrial focus on lightweight, and space saving structures has drawn significant attention to the fabrication of so called “smart” materials. In the aerospace sector, a focus on lightweight, strong, and morphing parts is of interest [1]. In situations where space, and weight is of the utmost importance, the creation of deployable and self-assembling structures can be utilized to

occupy less space, while maintaining functionality of a part [2]. While the incorporation of smart materials has been examined for this purpose, the full potential of smart materials can be maximized by combining them with other advanced manufacturing techniques.

1.2 Additive Manufacturing

Additive manufacturing techniques allow for more freedom of design, and the fabrication of complex geometries, not possible with conventional techniques (such as injection molding). Overcoming some limitations of additive manufacturing, new materials are being developed and investigated to produce high performance, composite, and / or multifunctional materials. In the past couple decades, small scale additive manufacturing has seen a shift from rapid prototyping to end-use polymer parts offering complex geometries [3], customizable fabrication [4], and creating composite parts for added strength [5].

Figure 1.1 Consumer Goods Produced via Additive Manufacturing. (a) Adidas Shoes, showing complex geometry [3], and (b) 3D printed dentures, showing unique customization [4].

1.3 Market Growth of Additive Manufacturing

Since its conception in 1984, and first 3D printing venture in 1986 (3D Systems Santa Clarita, CA) additive manufacturing has seen significant growth in market impact and expanded technologies. Most notably, the open source Rep-Rap project (2005) has allowed for open source development of Fused Filament Fabrication machines upon the patent expiration fused deposition modeling machines [6]. The overall market growth of 3D printing is projected to reach $53 billion (USD) by 2029, from its recorded value around 9 billion in 2018 [7]. Total additive manufacturing growth, projected to 2029 (Figure 1.2) also shows significant growth in hardware for additive manufacturing, and an even larger growth in the materials available for these techniques [7]. Academic research continues to grow since the conception of additive manufacturing, with the number of publications in this field increasing from hundreds to thousands of new publications a year [8].

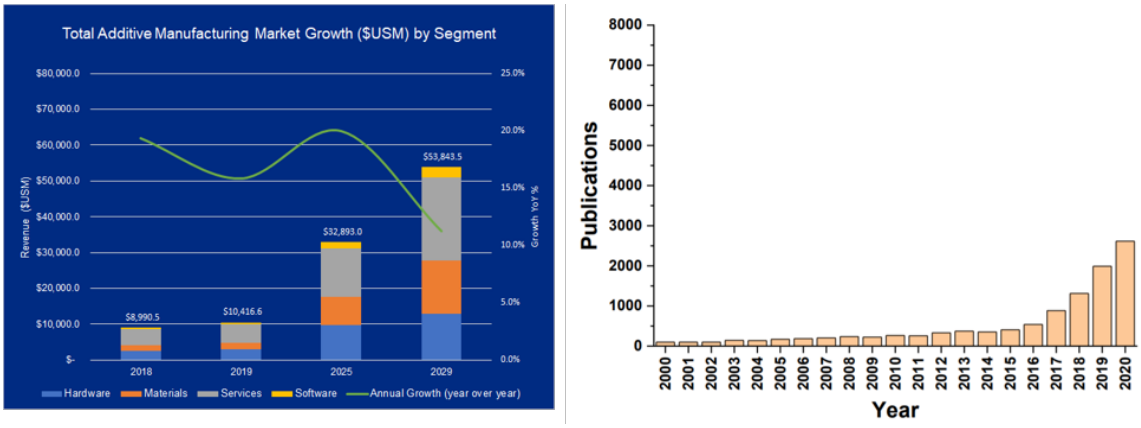

Figure 1.2 Market Growth of Additive Manufacturing. (left) Total market growth up to 2029 [7], and (right) publications in "additive manufacturing" from 2000 to 2020 [8].

1.4 Shape Memory Polymers

As the additive manufacturing market continues to grow, applications of new technologies and new materials continue to rise. Smart materials are of particular interest, in that, they unlock even more possibilities to be imagined. Shape memory polymers and shape memory alloys are the most prominent form of shape changing smart materials, that are often responsive to temperature. These materials allow for changes in geometry of a part based on a thermal input.

Unlike conventional polymer materials, parts fabricated with shape memory polymers can orient themselves from a temporary to a fixed geometry. As temperature of the polymer is increased, SMP's transition from a glassy to rubbery phase. In the rubbery state, SMP's can be easily deformed, and cooling allows for the storage of a temporary shape. Once returned above the transition temperature of the material, the part becomes rubbery once again and can return to its "permanent" shape. The shape recovery process of a deployable hinge is shown below (Figure 1.3), showcasing how the permanent shape of the SMP is recovered with the addition of heat into the system.

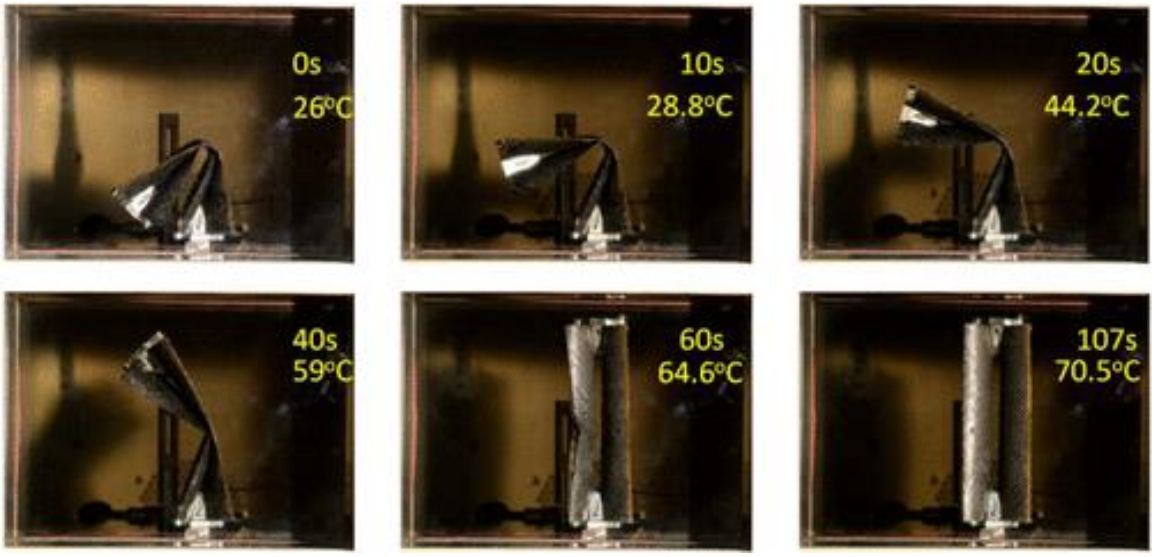

Figure 1.3 The shape recovery of a deployable shape memory polymer composite hinge [9]. As temperature increases, the shape memory part returns to its original shape, from the temporary folded shape of the deployable structure.

The applicability of shape memory polymers has been explored in many different industries including: biomedical [10,11], electronic actuators, aerospace, and authentication devices [12]. Specifically, the usability of shape memory polymers as actuators and deployable structures is explored in this work. Because shape memory polymers offer shape changing functionality with several advantages: low-cost, low-density, and high degrees of elastic deformation in the rubbery phase, they are of specific interest of shape memory polymers for aerospace applications [13]. Indeed, shape memory polymers are being explored as deployable trusses for antennas and solar arrays [14]. A deployable truss utilizing shape memory polymer as the recovery phase is shown below () [14].

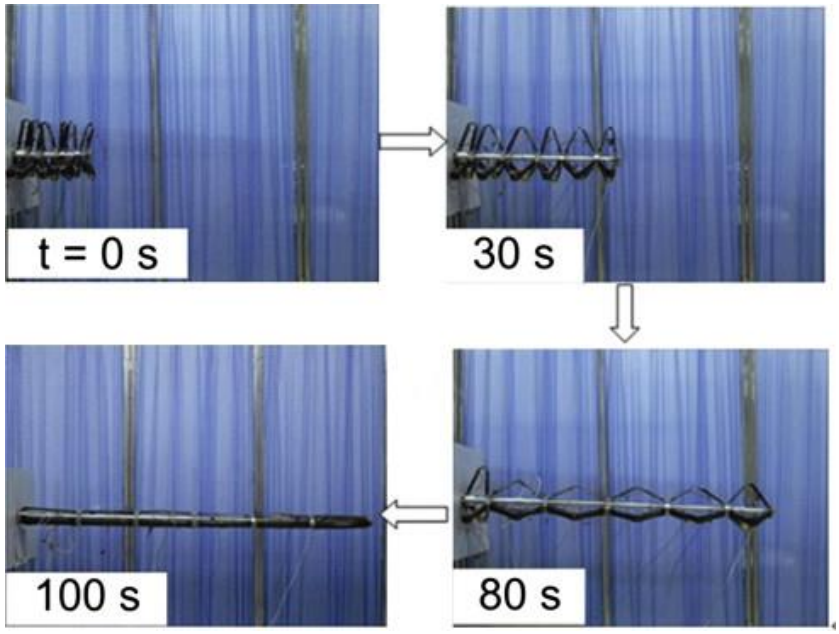

Figure 1.4 Deployable truss structure for aerospace applications. An epoxy based SMP is reinforced with carbon fibers (black), and the final shape is recovered in 100 seconds at elevated temperature.

1.5 Motivation for the thesis

While recent work aims to fabricate shape memory polymers via additive manufacturing, fabrication techniques and applications are few. Additive manufacturing allows for complex structures to be manufactured, and shape memory polymers may be used to create functional hybrid systems. Of specific interest, is the creating of deployable and reconfigurable functional antennas, as well as temperature sensitive actuators both produced via additive manufacturing. This research is focused on filling the gap between additive manufacturing and shape memory polymers, with an aim to fabricate smart functional electronics.

1.6 Objectives of this Research

The purpose of this research project is to produce smart materials with additive manufacturing techniques. Specifically, this work examines shape memory polymers prepared with two techniques of additive manufacturing: vat polymerization and material extrusion. Validating the functionality of smart materials is conducted, and functional applications are explored for these SMP systems.

Four minor objectives are identified in this work to accomplish the overall goal:

- Test the ability of a commercially available shape memory polymer to be used on an open-source desktop 3D Printer.
- Formulate a shape memory polymer to be used on a Desktop SLA machine.
- Validate and investigate the shape memory properties of the formulated material.
- Demonstrate the fabrication of electronic actuators or deployable structures produced via additive manufacturing.

1.7 Structure of this Thesis

This thesis is composed of five Chapters, organized in the following manner:

- Chapter one outlining the problem and structure of this work.
- Chapter two consists of a literature review or relevant research in 3D printing of shape memory polymers, polymer formulation, and application use cases.

- Chapter three describes the research methodology and materials used in this work.
- Chapter four shows the results and discussions for shape memory polymers produced via two techniques of additive manufacturing.
- Finally, chapter five summarizes the entirety of the work on the 3D printing of shape memory polymers.

2 Literature Review

2.1 Additive Manufacturing

While additive manufacturing, commonly known as 3D printing, encompasses a wide range of materials and technologies, the review of this section will be focused on the additive manufacturing of polymer materials. The fabrication of polymer parts can be further divided into the fabrication of thermoplastic and thermosetting materials. Namely, this review will briefly cover preparations of photosensitive resins via stereolithography and digital light projection, as well as preparation of thermoplastic via material extrusion techniques. While the method of polymer deposition or curing may differ between these two distinctions, the fundamental fabrication of parts via additive manufacturing is similar across all technologies. Here, a 3D computer aided design (CAD) model is converted into slices, or layers, and fabricated in a layer-by-layer fasion (Figure 2.1) [15]. After the object has been built, it can proceed through traditional post-processing steps (machining, sanding, polishing, and grinding).

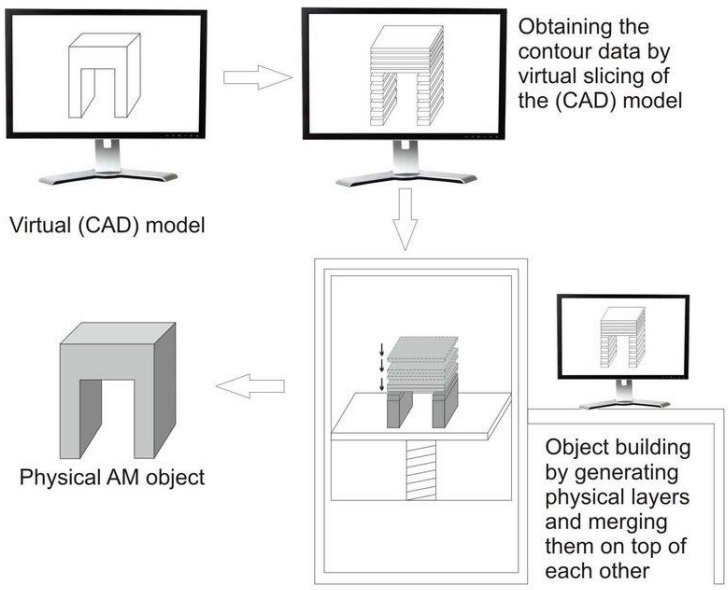

Figure 2.1 Overview of additive manufacturing process. A computer aided design (CAD) is used to draw a three-dimensional object. The object is then placed in a slicing software, and movement commands (.gcode) for the 3D printer were generated [15].

2.1.1 Material Extrusion

Arguably the most popular 3D printing technique for hobbyists and professionals is that of fused filament fabrication (FFF). According to a 2020 report on trends in additive manufacturing (Makerbot, LLC) FFF 3D printing accounts for 77% of 3D printing technologies currently used by professionals. In this process, polymer pellets are first extruded into a circular cross section filament. Then, the filament is fed into a 3D printer and remelted to be deposited in a layer-by-layer manufacturing process (Figure 2.2). This technology is not only widely available, but inexpensive and now showcases a wide range of materials including Nylon, Polycarbonate, Polystyrene, PEEK, and more [16,17].

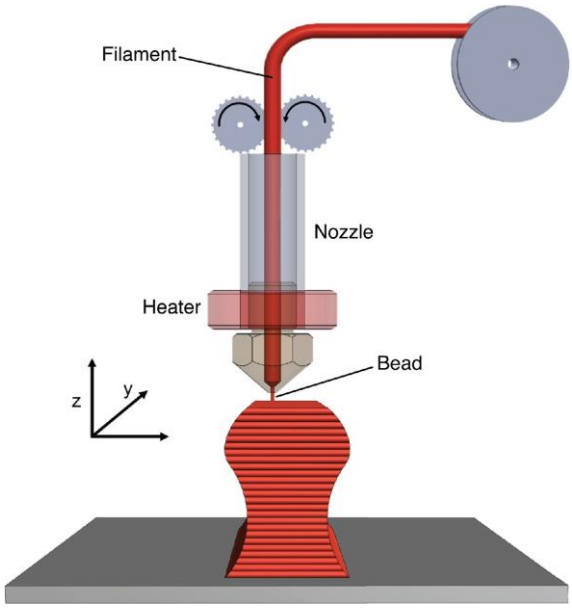

Figure 2.2 Model of the fused filament fabrication 3D printing process [18] A thermoplastic filament is driven through a hot-end to extrude the molten polymer filament.

A recent extension of material extrusion and fused filament fabrication printing is direct pellet extrusion technology. Unlike filament fabrication, where polymer pellets are extruded into a filament prior to being utilized in the printer; in pellet extrusion, polymer pellets or granules are used as feedstock directly for the printer, and the printer is equipped with a small extruder for direct pellet extrusion printing [19–22]. While still able to reach the resolution of FFF 3D printers (down to 0.1mm) [23], this approach of thermoplastic printing has several benefits over conventional FFF printing. Namely, direct pellet extrusion allows for: higher volumetric flow rate of extruded material, the ability to fabricate large (on the scale of meters) parts using a single printer [24], and less thermal processing of materials [20,25].

Parts fabricated using material extrusion techniques mentioned above exhibit several unique characteristics. Since a polymer bead is deposited in a layer by layer

approach, the resolution of the manufactured parts is highly dependent on the layer height of these objects. Figure 2.3 shows a sample cross section of a printed square profile produced through material extrusion. In this process, the polymer bead is cooled (via a fan) upon deposition, since the previous layer must provide support for the subsequent layers on top of it, a molten polymer bead is adhered to the semi-cooled previous layer. As a result, parts fabricated with material extrusion are anisotropic, exhibiting a lower mechanical strength in the z direction [26,27].

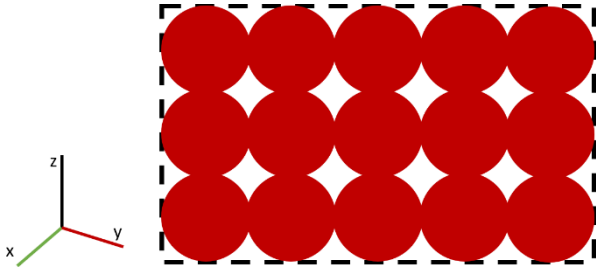

Figure 2.3 Cross-section of a square composed of extruded beads of filament. Extruded beads of filament (red) exhibit gaps between extrusions contributing to the anisotropy in extruded parts.

2.1.2 Vat Polymerization Techniques for Additive Manufacturing

Unlike the material extrusion techniques described above, both stereolithography and digital light projection utilize photosensitive polymers to cure a printed object (see Figure 2.4). In fact, the first patented technology of 3D printing was in the form of stereolithography by Charles Hull in 1984 [28]. Today, stereolithography printing accounts for 27% of the use cases for professionals working with additive manufacturing [29]. Vat polymerization encompasses both stereolithography and digital light projection, and many similarities are shared between these two approaches to manufacture 3D objects.

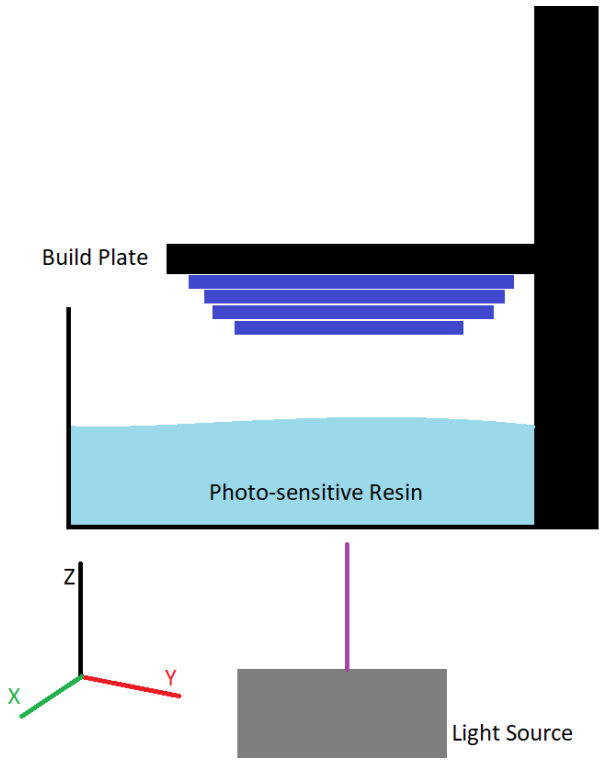

Figure 2.4 Graphical representation of vat-polymerization technique. Here, an inverted build platform moves into the vat of photo-sensitive resin to expose each layer to the light source.

2.1.2.1 Stereolithography (SLA) 3D Printing

Stereolithography (SLA) 3D printing provides the ability to produce a range of photopolymerizable materials, high resolution models, in a variety of price ranges to the consumer. SLA machines can range in both price in size from free standing professional machines costing upwards of $250,000 [30], to desktop SLA printers under $5,000 [31]. With new machines available for purchase each year, the materials library of SLA printers, much like materials extrusion, is constantly evolving. Unlike the limitations of thermoplastics for material extrusion printers, SLA printers have materials ranging from: rigid/glassy, elastomers, high-temperature materials, ceramics, and hydrogels [32].

Stereolithography printers, like most additive manufacturing techniques, build up slices of an object in a layer-by-layer fashion. SLA printers are available in both inverted, where the build platform is suspended above the liquid polymer, or normal configuration, where the build platform moves downward from the resin vat. SLA 3D printers offer a higher resolution than FFF 3D printers, where the x-y resolution is determined by the spot size of the laser used. SLA printers can offer an x-y resolution of 150 microns, and z-axis resolution as low as 25 microns [33].

2.1.2.2 Digital Light Projection (DLP) 3D Printing

Digital light projection, or DLP, is a 3D printing process that works in many ways similar to SLA, but often at a lower price. DLP printers utilize a digital LCD screen to cure the resin in the printer, instead of costly laser and galvanometer components used in SLA 3D printers. Often, the tradeoff for this is a smaller build volume, as the entire x-y build area is dictated by the size of the digital display. Desktop DLP printers range in build volumes from 100 x 60 mm to 190 x 120mm [34], but can be found for as low as $200 [35]. While having a smaller x-y build area, the resolution of DLP printers can be as low as 50um, with the x-y resolution controlled by the pixel resolution of the digital display, versus the laser spot size controlling the x-y resolution of SLA printers [34]. While not used explicitly in this work, DLP printers cannot be ignored when examining 3D printing of smart materials.

2.1.2.3 Photopolymerizable Resins for SLA and DLP Printing

Not only do DLP and SLA 3D printers possess similar hardware configurations; but also, the materials used for both SLA and DLP 3D share many similarities in the formulation. As the specific curing energy for both SLA and DLP printing is often

405nm light, the polymerization mechanism proceeds in the same manner [36–38]. In fact, commercially available photo-sensitive resins are sold for use in both DLP and SLA printers [39]. The basic formulation for these photosensitive polymers consists of oligomers, crosslinkers, and photoinitiators [40,41]. Here, the oligomer and monomer units can be mono, di, tri, or multifunctional, and vary in both chain length and composition.

As might be expected, each commercial SLA printer manufacturer often produces proprietary resins for use in the machines they produce and sell. However, the functional reaction groups of these resins share several similarities; specifically, the use of acrylate functional groups is prevalent across many SLA and DLP resins [38,40–42]. Acrylate functional groups offer fast reactivity with free radicals and can range in properties to create different end-use functionality. Likewise, a photoinitiator can be selected based on the desired wavelength of light, or stability, but most vat-polymerization techniques utilize a photoinitiator to generate free radicals and lead the reaction of free radical polymerization. The basic process for free radical polymerization is shown in Figure 2.5 [43], where free radicals provide initiation, and the polymer is formed through propagation of monomers and oligomers, and termination is achieved through multiple avenues. The use of photoinitiators allows for the rapid generation of radicals under 405nm light, to create solid layers of the object rather quickly (< 2 seconds).

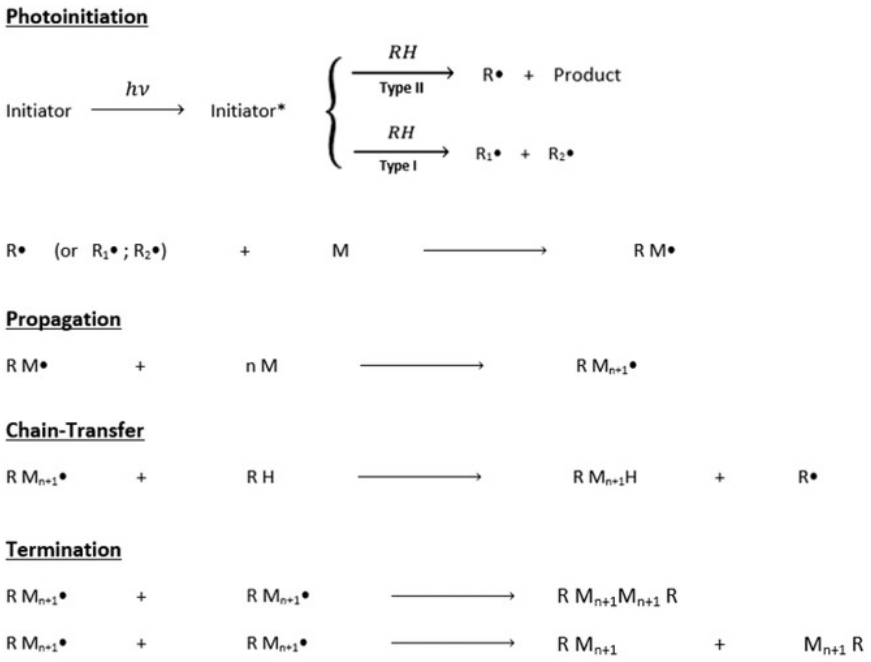

Figure 2.5 Free radical polymerization process. Photoinitiation for vat polymerization occurs with a UV laser. Propagation, chain transfer, and termination take place before the next layer is manufactured.

As the manufacturing process is often focused on having a low cure-time for each layer, parts produced via SLA/DLP printers utilize a post-processing and post-cure step. Parts directly removed from the printer exhibit uncured resin on the surface, which can affect surface finish and accuracy. Often, the 'green' parts are subjected to a solvent wash to remove excess material, followed by a final flood cure under UV-lights to react the residual crosslinkers and photoinitiators in the manufactured part. It has been shown, by Aznart et al, that post-curing UV exposure has an effect on the resulting modulus and final mechanical properties more than any other processing parameter in preparing SLA 3D printed parts [44]. Parts fabricated in a green state allow for the rapid production of layers, and the final post-cure gives the part its final strength.

While photopolymerizable resins allow for the production of thermoset materials, another advantage is the production of parts exhibiting near-isotropic properties. It has been shown that parts produced via SLA and DLP exhibit mechanical properties with little dependence on part orientation during fabrication [37,44–46]. In contrast to the anisotropic limitation of parts fabricated with material extrusion techniques, vat polymerized parts exhibit similar strength in each direction of the printing. Semi-isotropic properties are a useful advantage that vat polymerization techniques possess over material extrusion.

2.1.3 Additive Manufacturing Techniques

The above-described techniques for additive manufacturing (material extrusion, and vat polymerization) are only a selection of the available techniques used in research and industry. However, these techniques are among the most accessible and popular techniques for the preparation of polymer materials, apart from selective laser sintering and Multi-jet fusion techniques. Table 1 summarizes the advantages and disadvantages of the most relevant 3D printing techniques to this work.

Table 2-1. Comparison of Common Polymer 3D Printing Techniques

3D Printing Technique	Materials	Resolution	Polymer Solidification	Advantages	Disadvantages
Fused Filament Fabrication (FFF)	Thermoplastics (Nylon, PLA, ABS, PET-G, Peek, etc..)	Down to 0.1 mm	Polymer melt (solidified with active cooling)	Widely available, wide material library, low cost	Anisotropic material properties, limited to thermoplastic materials
Pellet Extrusion	Same as FFF	Same as FFF	Same as FFF	Large-scale additive manufacturing possible	Same as FFF
Stereolithography (SLA)	Thermosets, Flexible, ridged, ceramic, etc)	140um (x-y) 25um in z	Free-radical polymerization, post-curing in UV chamber	High resolution, formulation of many materials and fillers	More expensive, materials require post-curing
Digital Light Processing (DLP)	Same as SLA	Down to 50um	Same as SLA	Low-cost options, very high resolution	Lower build area

2.2 Shape Memory Polymers

The previous section has examined several techniques of additive manufacturing. In addition, several materials have been enumerated that can be produced via these techniques. Thermoplastic, thermosetting polymers, and other materials can all be produced in an additive fashion. Shape memory polymers may provide a useful method of fabricating smart, deployable, space-savings, or functional actuators. To capitalize on the complex geometries obtainable via additive manufacturing, if shape memory polymers can be 3D printed, geometrically complex and smart parts can be fabricated. As

new materials for 3D printing continue to be developed, the manufacturing of smart materials is undeniably of interest.

2.2.1 Overview of Shape Memory Polymers

2.2.1.1 Characteristics of Shape Memory polymers

Shape memory polymers (SMPs) are a common type of smart material able to memorize a permanent shape, while being reconfigurable into multiple temporary shapes (see Figure 2.6). While traditional materials exhibit static properties, smart materials often exhibit a useful change in properties due to some external stimulus (magnetic fields, temperature changes, changes in current, or pH). Shape memory polymers are a type of smart materials that can undergo large deflections due to an increase in temperature. This allows for a specific geometry to be manufactured (molded, cast, or 3D printed) out of shape memory polymer material, and then later be deformed into a separate geometry. A simple example of this is fabricating a flat bar of shape memory polymer and heating the bar and bending it around a rod. Shape memory polymers can lock in this temporary shape once the polymer network has cooled. The part will stay in this secondary geometry until a new thermal stimulus is applied.

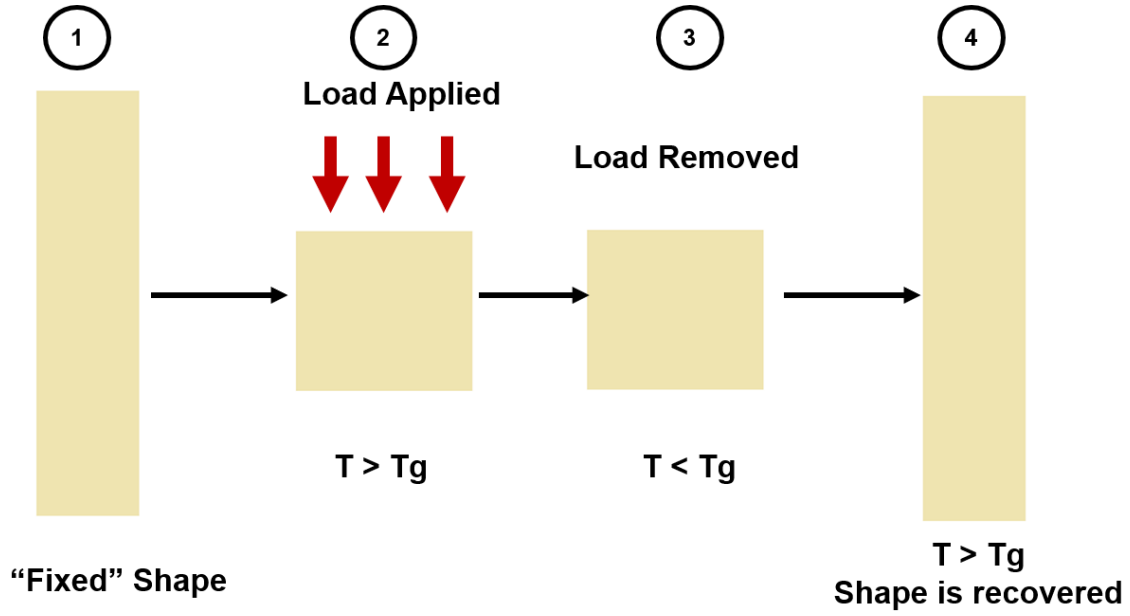

Figure 2.6 Graphical representation of the thermal shape memory effect of SMP's. Step 1, showcases the permanent shape that is manufactured. After heating, a load is applied in step 2, and the part is cooled below Tg. After the load is removed (step 3), the part is fixed in the temporary shape. A final heating above Tg allows the part to recover to its permanent shape (step 4).

Numerous stimuli can be utilized to recover the permanent shape and set the temporary deformation of a shape memory material. Research has focused on photo-responsive shape memory polymers, utilizing a reversible crosslinking reaction initiated with ultraviolet light [47]. Another approach involved creating switching points based on reversible bonds, such as: hydrogen bonding, ionic bonds, and reversible covalent bonds [48].Further still, are shape memory polymers that are responsive to electromagnetic radiation. Often electromagnetic-responsive shape memory polymers are composites fabricated with nano or micro particles (conductive fillers, metal powders, or carbon nano materials) and are actuated by external magnetic fields, or joule heating [48].

Shape memory polymers have several defining characteristics that separate them from other polymeric materials. One of the most defining characteristics is the modulus

change of the material across different temperatures. A typical storage modulus vs. temperature curve, obtained by dynamic mechanical analysis, displays a significant drop in the modulus as the temperature of the shape memory polymer is increased (see Figure 2.7) [49]. This change in modulus of the material can be two to three orders of magnitude lower at elevated temperatures [49–51]. A drastic change in modulus allows for the material two have two distinct phases: rubbery and glassy. The dramatic distinction of the rubbery and glassy phase allows for high deformations to a part at higher temperatures to be "locked" after cooling to the glassy phase. In essence, the glassy state of the polymer holds the permanent shape, and temporary deformations in the rubbery phase are set at elevated temperatures, free-constrained recovery of the part to the rubbery phase allows for the permanent shape to be returned.

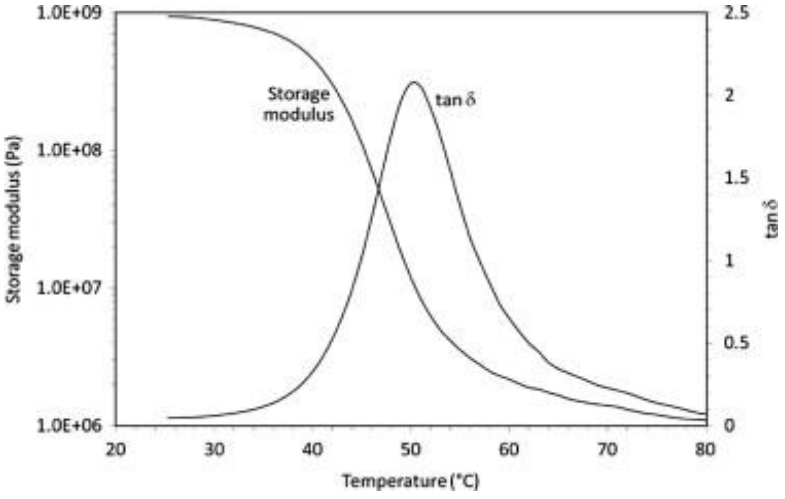

Figure 2.7 Sample DMA curve of a shape memory polymer. As temperature increases, the storage modulus of the SMP drops over 2 orders of magnitude.

2.2.1.2 Shape recovery

Given that shape memory polymers exhibit different geometries in response to a thermal stimulus, one of the most unique characteristics of SMP's is the relationship between temperature, stress, and strain of a given sample. Thermomechanical analysis of shape memory polymers is often used to characterize the recovery of a sample to its permanent shape. It has been shown (see section 2.2.1.1) that the free recovery of shape memory polymers is achieved when the part is in the "rubbery" state. The stress-strain of a sample can be evaluated under a temperature change to illustrate its ability to recover a permanent shape (see Figure 2.8) [52].

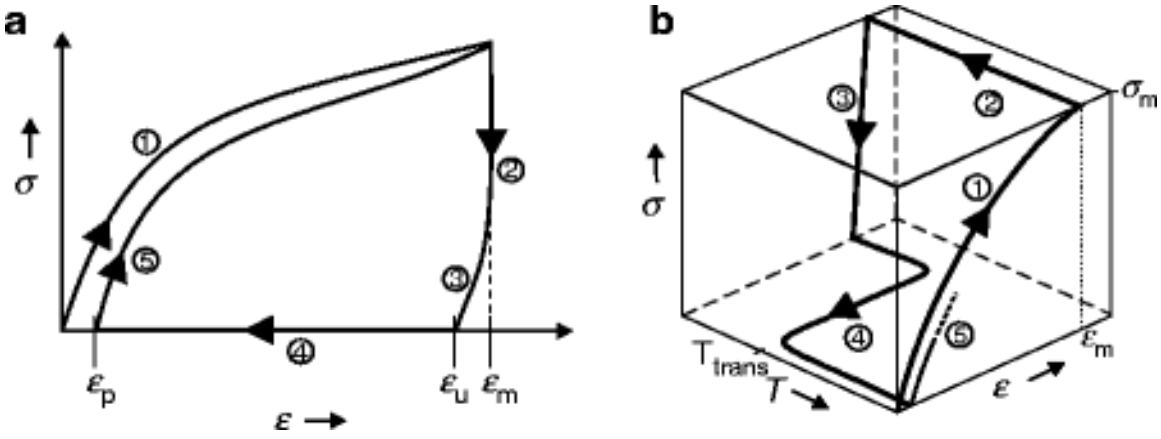

Figure 2.8 Schematic of a thermomechanical cycle on a shape memory polymer sample. (a) Strain-controlled recovery of SMP under different steps (1, 2, 3, 4). (b) T vs. stress vs strain for a SMP sample, undergoing a shape programming and recovery. In both images, step 1 corresponds to stretching at T > Tg, 2 cooling under load, 3 unloading at T < Tg, 4 heating T > Tg with no external load, and 5 the start of the second cycle (repeat of step 1).

2.2.2 Switching mechanisms of shape memory polymers

The recovery of the permanent shape of SMPs is dictated through several unique mechanisms that hold the part in a state of hysteresis. Netpoint connections within the polymer network allow for recovery of the permanent shape. SMP's can be formulated in both thermosetting and thermoplastic polyurethanes, and can have switching domains based both on chemical bonds, or physical connections [53]. This results in six different categories (see . Table 2-2) of netpoint types based on glass transition temperature, or melting temperature, and further divided by chemical crosslinks, and hard domains [52].

Table 2-2. Netpoint categories responsible for shape recovery in different shape memory polymers [52]**.**

		Reversible netpoints determining temporary shape	
		Switching domain associated to T_g	Switching domain associated to T_m
Netpoints determining permanent shape	Chemical crosslinks	**Cat. A-I:** Chemically crosslinked amorphous polymer networks **Examples:** a) Copolyesterurethane networks [8] b) Crosslinked Polystyrene [11] c) Poly[(*L*-lactide)-*ran*-glycolide] dimethaycrylates based networks [13]	**Cat. A-II:** Chemically crosslinked semi-crystalline polymer networks **Examples:** a) Networks from poly(ε-caprolactone) dimethacrylate and n-butyl acrylate [9] or cyclohexyl methacrylate [10] b) Crosslinked Poly(cyclooctene) [12] c) Poly[(ε-caprolactone)-*graft*-poly (ethylene glycol)] networks [10]
	Hard domain associated to T_m	**Cat. B-I:** Thermoplastics with crystalline hard and amorphous switching domains **Examples:** a) Copolyesterurethanes [14] b) Poly(norbornyl-*co*-POSS) [17]	**Cat. B-II:** Thermoplastics with crystalline hard and switching domains **Examples**: a) Polyetherurethanes [15, 16] b) Polyesterurethanes [18, 19] c) Poly(ethylene oxide-*block*-ethylene terephthalate) [20]
	Hard domain associated to T_g	**Cat. C-I:** Thermoplastics with amorphous hard and switching domains **Examples:** Polyetherurethanes from methylene bis(p-cyclohexyl isocyanate), 1,4-butanediol, and poly(tetramethylene glycol) [21]	**Cat. C-II:** Thermoplastics with amorphous hard and crystalline switching domains **Examples:** Block copolymers from styrene and butadiene [22, 23]

Several approaches exist to create these netpoints within a polymer to elicit the shape memory effect, two of which will be explored in more detail. Firstly, shape memory polymers having a network stability based on crystallizable netpoints (cat b-II, table 1) such as polyurethane based shape memory polymers, exhibiting a distinct crystallization temperature. Secondly, shape memory polymers are later examined in this work exhibiting the shape memory effect based on the glass transition temperature. Lacking a distinct crystallization point, these thermosetting shape memory polymers are chemically crosslinked amorphous networks (see Cat A-1, . Table 2-2). In this case, a switchable netpoint is achieved through crosslinking of polymer chains in the network. In essence, different morphologies within a polymer matrix aid in establishing a temperature memory effect.

2.2.3 Synthesis of Shape Memory Polymers

Given that there are multiple netpoint configurations (chemical crosslinks, physical connections, and physical entanglement), several strategies exist to formulate and modify polymers to exhibit the shape memory effect. Formulation techniques for thermal shape memory polymers can be summarized by two techniques: “crosslinking of linear or branched polymers, and (co)polymerization/poly(co)condensation of one or several (co)monomers” that allow for the preparation of a polymer network able to undergo shape deformation and recovery [54]. Through the process of co-polymerization, polymer networks of co-continuous polymer phases can be generated including: co-polymers, semi-interpenetrating networks, and interpenetrating polymer networks (IPNs) (seeFigure 2.9).

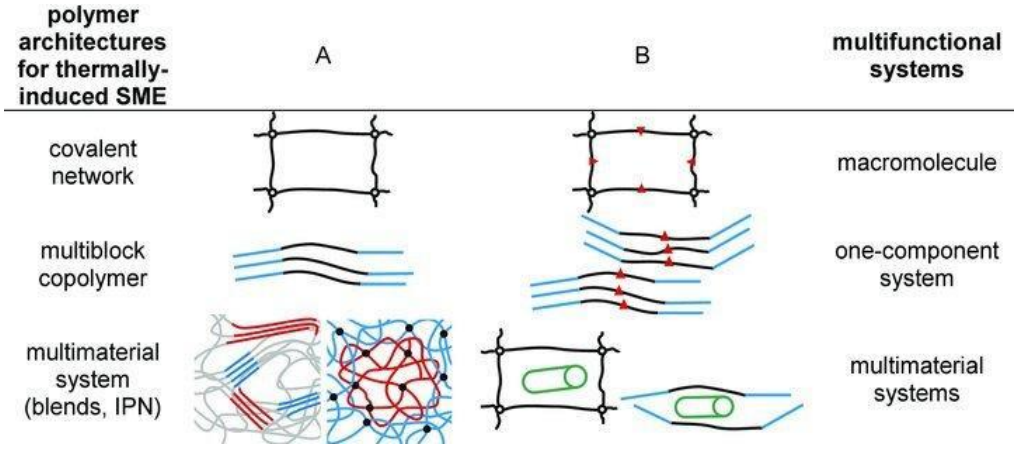

Figure 2.9 Graphic representation of polymer networks prepared with co-polymerization, and co-continuous polymerization [54]**.** For thermally induced shape memory polymers, multimaterial polymer blends can co-polymerize (as shown by polymer A (red) and polymer b (blue) to form a shape memory network.

The synthesis of shape memory polymers via copolymer phases is often used to elicit the shape memory effect and modify properties of the rigid and glassy state. Focusing on the prepolymers used to establish a hard and soft domain in the polymer network, where the hard domain aids in the netpoints used to set the permanent, and temporary shape, and soft domains allowing for deformations and the presence of the rubbery phase. Polymer chain length has a large effect on the entanglement and viscoelastic response of the polymer matrix. Ferrero et al (2016) examined molecular weight (polymer chain length) effect on the extension of the rubbery phase of the polymer network in poly(rac-d,l)lactides [55]. Through examining this, they found that modifying the chain length of starting materials successfully allowed for a decrease in the modulus of the rubbery phase, finding a change in the ratio of glassy to rubbery modulus of 655-1545 [55]. Certainly, the improvement of phases in a shape memory polymer is dependent on its starting materials, and network formation.

2.2.3.1 Fused Filament Fabrication of Shape Memory Polymer

Recent work has shown the applicability of extruding thermoplastic shape memory polymers on commercial FFF machines. Most commonly, work in fused filament fabrication focuses on modifying currently available materials [56,57], and utilizing commercially available shape memory polymers [58–60]. Both techniques utilize the shape memory polymers into a polymer extruder to develop a circular cross-sectional filament to be printed with a common FFF 3D printer. As such, these shape memory polymers must be thermoplastic in nature, often utilizing the crystallization temperature as the switching point in the polymer network.

Multiple approaches of fabricating thermoplastic-based shape memory polymers have been investigated. Yang et al (2016) fabricated 3D printed shape memory polymers by extruding a commercially available Diaplex MM-4520 SMP, into a filament and printed samples on a commercially available FFF 3D printer (MakerBot, LLC) [61]. Yang et al studied process parameters on the effect of the overall quality of SMP parts fabricated through this technique (surface roughness, mechanical properties, and dimensional accuracy). Yang et al was able to prepare SMP parts via FFF printing, and showcased this by fabricating a gripping arm actuated by a thermal stimulus [61]. Similarly, other work has showcased the use of similar polymer pellets extruded into a filament for 3D printing [60]. Overall, this approach benefits from combining two existing technologies: pelletized shape memory polymers, and widely available FFF 3D printers. This technique is accessible, but parts fabricated with this technique are subject to the same constraints and limitations of FFF 3D printing and are limited by the characteristics of the starting material.

2.2.3.2 Vat polymerization techniques for Shape Memory Polymers

Conversely, the approach of preparing shape memory polymers for use in vat polymerization techniques is more open-ended, offering more combinations of starting materials to be used to achieve the same goal. Indeed work has been done incorporating common monomers such as polycaprolactone [62], epoxy-acrylate polymers [63], epoxidized soybean oil [64], and others to achieve shape memory polymers for preparation via vat polymerization.

Research work on vat polymerization for SMP's includes modifying the formulation to allow for unique transformation temperatures. For example, Yu et al (2015) explored the fabrication of "sequential shape changing components" by tailoring the monomer to crosslinker ratio to elicit different transformation temperatures [65]. This technique showcases that the formulation of the resin allows for a different response to be displayed from the samples, a useful technique in designing materials for a specific end use case. Choong et al (2017) successfully 3D printed copolymer networks of tert-butyl acrylate and diethylene glycol diacrylate with glass transition temperatures ranging from 53 to 74 °C [66].

Furthermore, the shape memory effect has been realized in commercially available resins for SLA 3D printing. Most notably, Inverardi et al (2020) discovered the presence of the thermal shape memory effect in the commercially available "Clear Resin" (Formlabs, Somerville, MA)[67]. This effect has been attributed to the large glass transition of the material, and further confirmed by dynamic mechanical analysis exhibiting a distinct rubbery plateau [67]. Inverardi et al utilized the broad glass transition temperature to deform a part fabricated at two transformation temperatures, 40 °C, and

100 °C. This allows for the sequential folding to be achieved from a single material, fabricating a "latching" mechanism by programming one step of deformation at 100 °C, and a secondary deformation at 40 °C [67]. Upon recovery in hot water (60 °C) the first deformation is recovered, and after a longer time at 60 °C, the final permanent shape is recovered (see Figure 2.10).

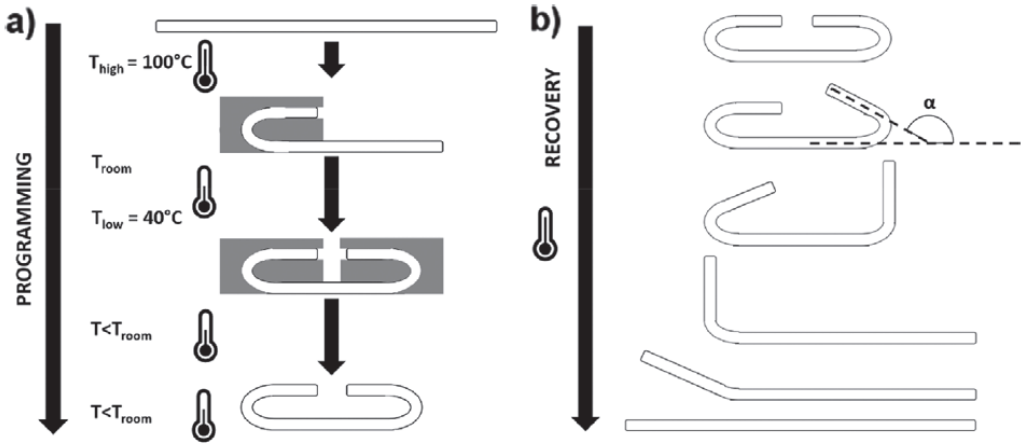

Figure 2.10 The design of a multi-shape memory part via broad glass transition temperatures. The programming of the part (a) is performed at two temperatures, while recovery (b) is performed at one temperature, allowing for a shape recovery of sequential deformations.

2.2.4 Mechanical Performance of Shape Memory Polymers produced via Additive Manufacturing

While it is possible to 3D print shape memory polymers via both material extrusion and SLA techniques, the properties of these SMP's vary widely. As previously mentioned, in addition to the basic mechanical performance (tensile strength, flexural strength) the most important mechanical properties of shape memory polymers are the

change in elastic modulus with respect to temperature, the shape fixity ratio, and shape recovery percentage. The previously stated limitations of each additive manufacturing technique may contribute to anisotropic distribution of these properties.

The properties of additively manufactured shape memory polymers have been characterized by several researchers in this field. Villacres et al (2018) and Yang et al (2016) both utilized commercially available SMP pellets and reported mechanical properties similar to that of the manufacturer's data. Here, the ultimate tensile strength MPa varied from 22 – 60 MPa for the same commercially available shape memory polymer pellets (see Table 2-3). As previously stated, vat polymerization techniques for shape memory polymers can vary greatly based on the monomers and crosslinkers used. As such, the mechanical properties of these systems can also vary, but a summarization of some of the current research work on characterizing these systems is outlined in Table 2-3.

Table 2-3 Mechanical Properties of Shape Memory Polymers produced via Additive Manufacturing:

Research	Additive Manufacturing Technique	Material Used	Ultimate Tensile Strength (MPa)	Glassy Region Elastic Modulus	Rubbery Region Elastic Modulus	Shape Recovery
Villacres et al (2018) [69]	FFF	MM4520 (SMP Technologies)	35 – 60	1.4 – 2 GPa	n/a	n/a
Yang et al (2016) [69]	FFF	MM4520 Pellets (SMP Technologies)	22 – 25	n/a	n/a	n/a
Q Ge et al (2013) [70]	Photo-polymerization	*Stratasys* ink (glassy and elastomer)	n/a	1-6 MPa	1-1.5 MPa	n/a
Choong et al (2017) [71]	Vat Polymerization	tert-butyl acrylate and diethylene glycol diacrylate	20.2	230 MPa	1.66 MPa	97-99 %
Zarek et al (2016) [70]	SLA	Poly-caprolactone	n/a	150-225 MPa	1-4 MPa	>93 %
Shan et al (2020) [71]	Digital Light Projection	Epoxy acrylate, isobornyl acrylate	25 - 65 MPa	26.4 MPa	n/a	97.8 %
Inverardi et al (2019) [67]	SLA	*Formlabs* Clear Resin	25-30 MPa	4-5 GPa	18.3 MPa	98 - 99 %

2.3 Applications of Additive Manufacturing and Shape Memory Materials

2.3.1 Shape Memory Polymer Actuators

Shape memory polymers have been prepared for a variety of applications using additive manufacturing. Of interest to this work, is 3D printed shape memory polymers as thermal actuators, to be used in a sensing application or in the development of flexible electronics. For instance, Zarek et al (2016) developed an electronic circuit consisting of: shape memory polymer, silver ink conductive traces, a power supply and LED (see Figure 2.11) [71].

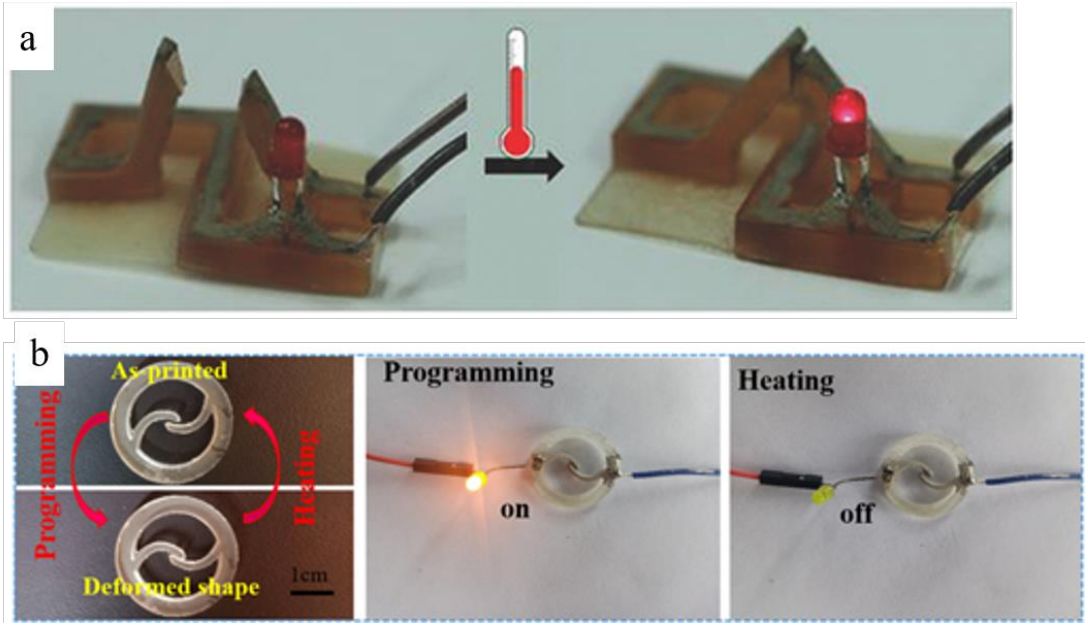

Figure 2.11 Electronic actuators fabricated with 3D Printed shape memory polymers (a) [72] **and (b)** [72]**.** (a) showing a one-way thermal switch, after shape recovery, conductive traces allow the flow of current. (b) Another shape recovering switch, after heating the shape recovers to the "off" position.

This approach showcased a circuit that illuminates an LED once the temperature reaches the transition temperature of the material. A similar system, developed by Shan et al

(2020) utilized epoxy acrylate, and isobornyl acrylate in formulating a tunable shape memory polymer [72]. Shan et al also fabricated a SMP structure that is combined with conductive traces to show the actuation of a circuit when the permanent shape is recovered (Figure 2.11).

2.3.2 Smart Antennas and Additive Manufacturing

One of the major studied uses of shape memory polymers is the fabrication of deployable structures, to minimize weight, and space; while possessing the ability for a structure to reach its final, deployed structure without the use of motors, springs, or outside actuation. In this thesis, the fabrication of a deployable antenna is examined utilizing 3D printed shape memory polymers, and relevant background information on the fabrication of antennas via additive manufacturing is needed. Additionally, relevant research regarding the use of shape memory polymers as deployable antenna materials is also important to this goal. Ultimately, research in this thesis attempts to utilize additive manufacturing of antennas and shape memory polymers to make a unique shape memory polymer, functional antenna.

The fabrication of antennas based on shape memory materials has also been examined, but research in this area is still lacking key discoveries. For example, Yongsan An et al (2018) studied the deployment of a shape memory polymer in a circular disk (see Figure 2.12), to evaluate its applicability as an antenna [73]. While not a functional antenna, Yongsan An et al highlighted the importance of deployable shape memory material antennas, even using 1-dimensional mold-cured samples of a SMP epoxy [74]. Additionally, shape memory polymer composite systems have also been studied as prototypes for deployable masts in antenna applications. However, this still consisted of a

prototype, and lacked functionality as an antenna or sensing device. It is clear there is still much research to be done to fabricate functional antennas with shape memory polymers.

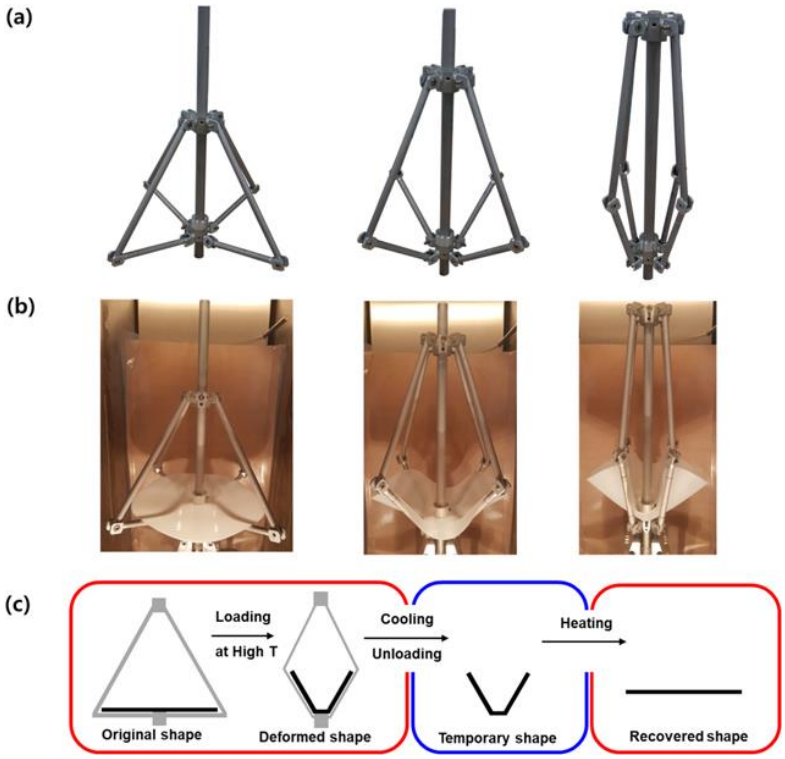

Figure 2.12 A shape memory polymer disk to showcase the geometric design of a deployable antenna. (a) the folding device utilized to set the temporary shape. (b) The shape memory polymer disc (white) being set into a temporary shape, and (c) an illustration of the shape memory cycle for the described disc [73].

One major obstacle in creating functional antennas from polymeric materials is their lack of electrical conductivity. As such, the polymer needs to be modified to improve conductivity. For instance, it can be fabricated with conductive traces or metal tape to act as a hybrid material or be coated in metal ions to provide a conductive surface on the material. Jape et al (2020) explored several of these techniques, metallizing the surface of a 3D printed antenna with copper tape, and fabricating an antenna with shape memory polymer hinges (see Figure 2.13). However, the shape memory polymer hinges

were molded, and assembled into a folding reflector antenna [75–77]. Shemelya et al, took a different approach to fabricate a spiral antenna via fused filament fabrication 3D printing. Here, the group embedded copper wire, and copper mesh into the molten plastic, using the 3D printed part to support the desired frequency of the fabricated antenna [78]. As other research has shown, incorporating metal parts onto a polymer substrate creates a hybrid antenna, with useful functionality provided by the conductive components.

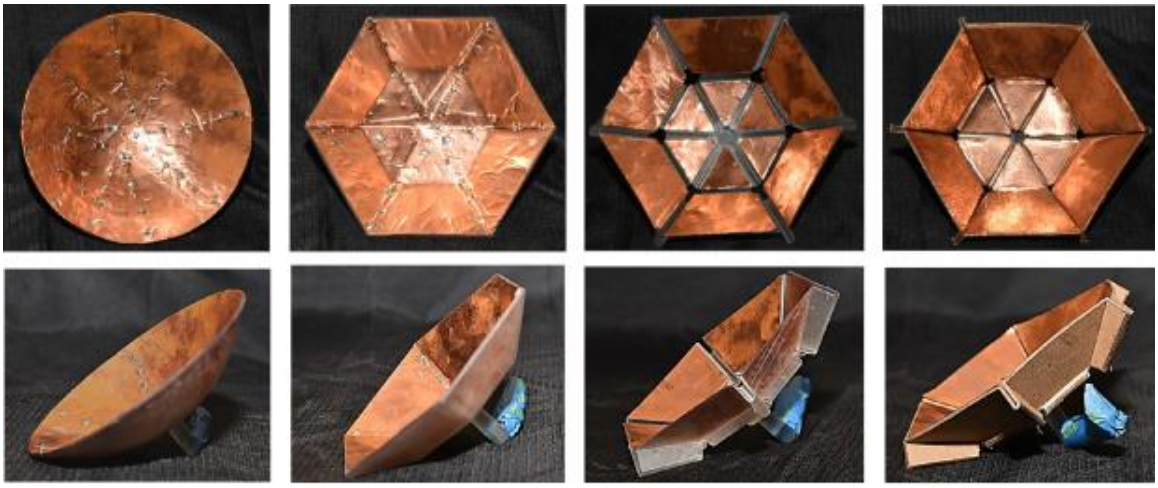

(a) Smooth parabolic reflector (3D printed). (b) Faceted parabolic reflector (3D printed). (c) Origami CAD model (3D printed). (d) AORA prototype (formed via SMP actuation).

Figure 2.13 The metallized surfaces of various 3D printed antennas fabricated by [79]**.** The smooth parabolic reflector (a) was 3D printed using a SLA technique and metalized with copper foil. (d) Consists of flat paperboard connected by shape memory polymer hinges and metallized with copper foil.

Beyond the use of copper tape to the surface of 3D printed part, liquid metals have been explored as a method to create functional electronics. With high-resolution 3D printing, such as that available by stereolithography (25 - 50μm), microfluidic channels can be printed in the polymer material and later filled with liquid metal to act as conductive channels (see Figure 2.14). A common non-toxic liquid metal used for this

purpose are alloys of indium, gallium, and tin [78]. Bharambe et al studied the performance of a dipole antenna with a reconfigurable monopole length based on pumping liquid metal through a microfluidic channel, manufactured via SLA [78]. Additionally, Zhou et al (2020) explore multiple microfluidic channels to elicit different behaviors that could be selected by pumping and removing liquid metal from the selected microfluidic channels [79]. In this case, the liquid metal could be reconfigured into five unique states all sharing a common ground plane (Figure 2.12Figure 2.14 b).

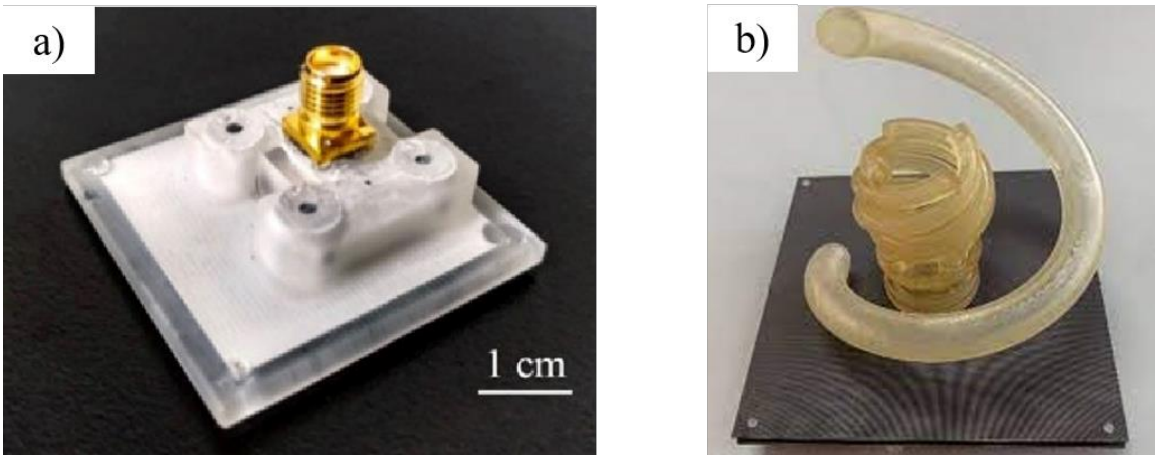

Figure 2.14 Liquid metal antennas fabricated by additive manufacturing of microfluidic channels. (a) A liquid metal microstrip patch array antenna printed on using material jetting [80]. (b) Multiple microfluidic channels attached to the same ground plane printed using SLA [79].

3 Materials and Methods

The following chapter will outline the research methodology and materials used in this work. An overview of the materials and hardware used to prepare samples via additive manufacturing is presented. Additionally, the methods and apparatuses used in examining samples in this work are described. A brief background accompanies each testing technique to justify its relevance to this research program.

3.1 Additive Manufacturing

3.1.1 Material Extrusion

The first technique utilized in this research to prepare 3D printed shape memory polymers was direct pellet extrusion. To achieve this, an open-source Makerbot M2, (Beachwood, OH, USA) FFF 3D printer was modified to utilize an open-source universal pellet extruder created by Mahor XYZ [81] (see Figure 3.1). The pellet extruder replaced the stock extruder on the Makerbot, and the stepper motor for the extrusion system. The stepper motor controlled the rotation of the extrusion screw, and polymer pellets could be used as the feedstock for the printer. The extrusion screw moved solid polymer pellets into the hot end to be melted and extruded through the cylindrical nozzle (1.5 mm). The motion control of the printer (in x, y and z) was used to deposit the extruded polymer bead into a single layer of the manufactured object.

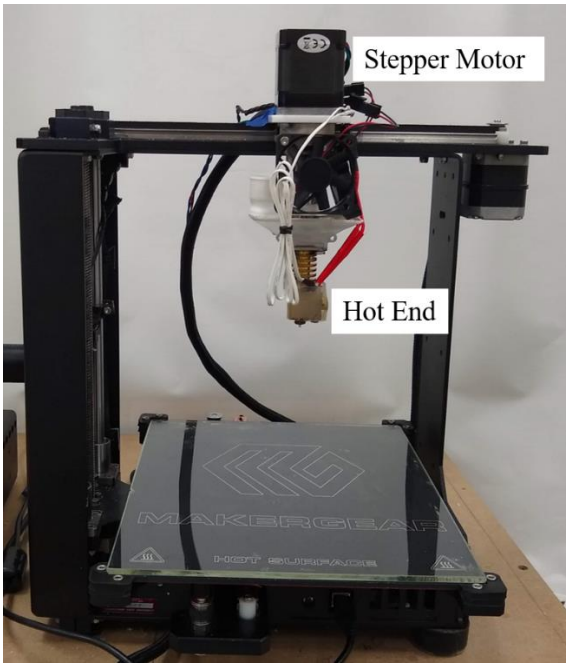

Figure 3.1 Pellet Extruder on the Makerbot M2 3D printer. The extruder stepper motor has been replaced with a new motor oriented in the vertical orientation to assist with the extrusion of polymer pellets.

The modified printer allowed for commercially available shape memory polymer pellets to be 3D printed. The polyurethane-based shape memory polymer Diaplex (MM 9020) from SMP Technologies (Tokyo, Japan) was used here. The selected polymer pellets had a recommended extrusion temperature of 190- 210 °C [82], therefore, the hot end of the printer's extruder was set slightly higher at 225 °C to extrude the pellets at a consistent rate. The bed of the printer was set to 80°C to promote adhesion of the polymer melt to the glass build platform. A printing speed of 5 mm/s was achieved in manufacturing the samples, at a layer height of 0.9 mm [83].

3.1.2 Stereolithography

3.1.2.1 Shape Memory Polymer Development

The development of a shape memory polymer for SLA 3D printing required the use of a liquid resin photopolymer. In fact, the shape memory effect was first observed in a commercially available resin, Clear v4, produced by Formlabs (Sommerville, MA, USA). Indeed, this property was confirmed by Inverardi et al (2019), however, while the shape memory effect was present, the brittle nature of Clear v4 was undesirable, and the shape memory was mostly achieved in compression [67]. To overcome this limitation, and to allow for both tensile and compressive deformations, the brittleness of the Clear v4 resin had to be mitigated. In this work, the brittleness of Clear v4 was diminished by the process of copolymerization with a highly elastic (100-200% elongation) material. Formlabs Elastic 50A, a commercially available photopolymer suitable for SLA printing was selected as the high elongation material. In essence, a 'rubber-toughened' material was created that utilized the netpoints present in the Clear v4 material, and the elasticity of Formlabs Elastic 50A to create a shape memory polymer blend for stereolithography printing.

While both resins (Clear v4 and Elastic 50A) consisted of proprietary components, rudimentary formulation information was provided in the materials safety data sheet (SDS). The contents of both Elastic 50A and Clear V4 resin are quite similar, each consisting of a blend of methacrylated oligomers, acrylated monomers, and photoinitiators. Moreover, it was made clear that the oligomer in Clear V4 was urethane dimethacyrlate, compared to the isobornyl acrylate found in Elastic 50A [86]. While proprietary aspects of the acrylated monomers and photoinitators remain undisclosed,

both resins are formulated to be printed on a Form 2 SLA printer (Formlabs, Sommerville, MA, USA) and therefore could be mixed and investigated. A summary of mechanical properties for these materials as are displayed in Table 3-1.

Table 3-1: Mechanical Properties of the Photopolymer Resins Used in This Work

Formlabs Resin	***Ultimate Tensile Strength (MPa)***	***Tensile Modulus (MPa)***	***Elongation at Break***
Clear V4	53.05	2435	3.10%
Elastic 50A	1.70	4.53	54%

Five resin mixtures were investigated, with the fraction of Elastic 50A resin increasing from 0% to 40% (by mass) in each batch. All five batches were mixed first with a stand mixer for 10 minutes, followed by sonication for 60 minutes at 40 °C (see Table 3-2). The mixed resins appeared stable and showed no visible signs of separation after a year of storage at room temperature. Following mixing, resin mixtures were printed using a Formlabs Form 2 SLA 3D printer, operated in open mode, at a layer height of 100 um. The Form 2 SLA printer initiates polymerization using a 250mW , 405nm laser, with a spot size of 140 microns [87]. After the printing, the parts were washed in an isopropyl alcohol bath for 10 minutes and dried in ambient air. To ensure complete curing of the printed parts, they were post-cured in an ultraviolet chamber (Formlabs, Inc) for 20 minutes at 60 °C.

Table 3-2. SMP Blends of Clear and Elastic Resin Examined in this Work

Batch Name	*Clear V4 (mass %)*	*Elastic 50A (mass %)*
0E100C	100%	0%
10E90C	90%	10%
20E80C	80%	20%
30E70C	70%	30%
40E60C	60%	40%

3.2 Mechanical and Rheological Characterization

The following techniques were used to ascertain the physical properties of shape memory polymers prepared via material extrusion and stereolithography. While the manufacturing of samples was different, the techniques for determination of tensile and flexural properties were identical for all samples. However, additional analysis was performed on the samples prepared via stereolithography.

3.2.1 Uniaxial Tensile

The uniaxial tensile test was based on the American Society for Testing and Materials (ASTM) standard D638, and determined properties such as the ultimate tensile strength, elongation at break, and tensile modulus. Here, dog bone shaped specimens (ASTM type IV, and type V) were placed in a universal testing device (Instron, 5967) equipped with a load cell (± 10 kN) and a motorized crosshead (see Figure 3.2). As the cross head elongated the samples in the z direction, stress and displacement data were collected. For this work, samples were tested at an extension rate of 2 mm/min, and strain

data was calculated by the crosshead displacement. In this work, a minimum of four samples were tested for each polymer blend.

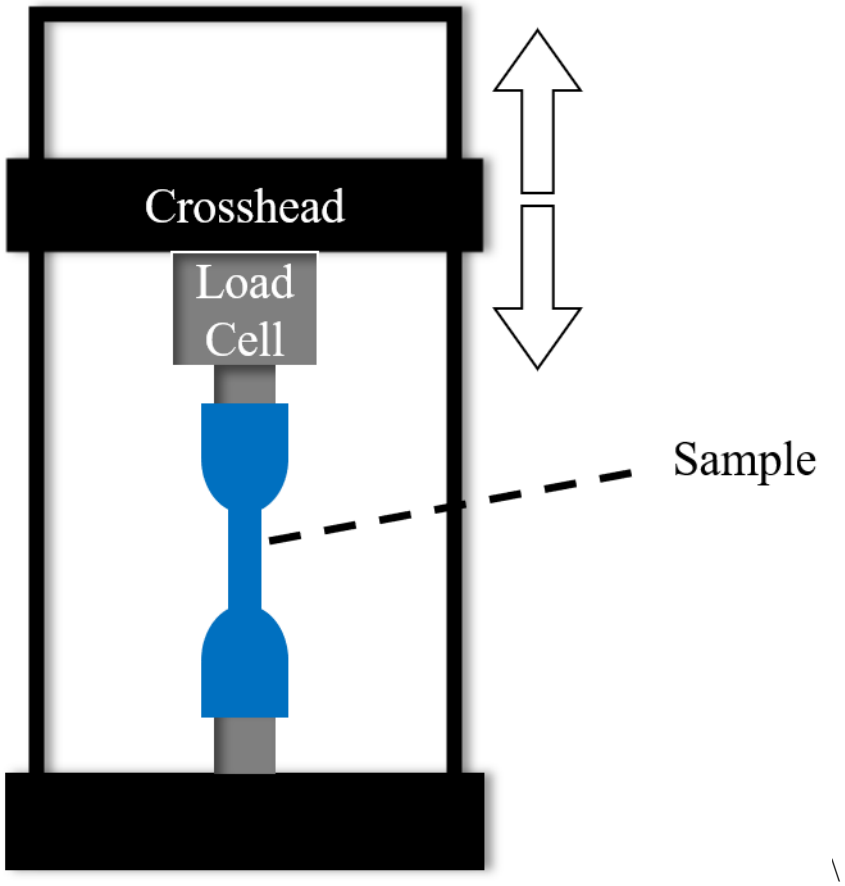

Figure 3.2 Testing apparatus of the uniaxial tensile test. The sample (shown in blue) was clamped in the fixture, while the cross head moved vertically.

3.2.2 Flexural Testing

Like the methodology of the uniaxial tensile test, the 3D printed shape memory polymers' flexural properties were examined under a 3-point bend configuration (see Figure 3.3). This test was based on ASTM D790, and utilized a universal testing device (Instron 5967), and a load cell (10 kN). Flat, rectangular specimens were placed between two supports and displaced at a rate of 1 mm/min until 5% strain, or fracture of the

sample occurred (whichever occurred first). Samples prepared with material extrusion technology measured 100 x 10 x 4 mm (l x w x h), while samples prepared via SLA measured 100 x 6 x 3 mm. A minimum of four samples were used to determine the average and standard deviation of the samples.

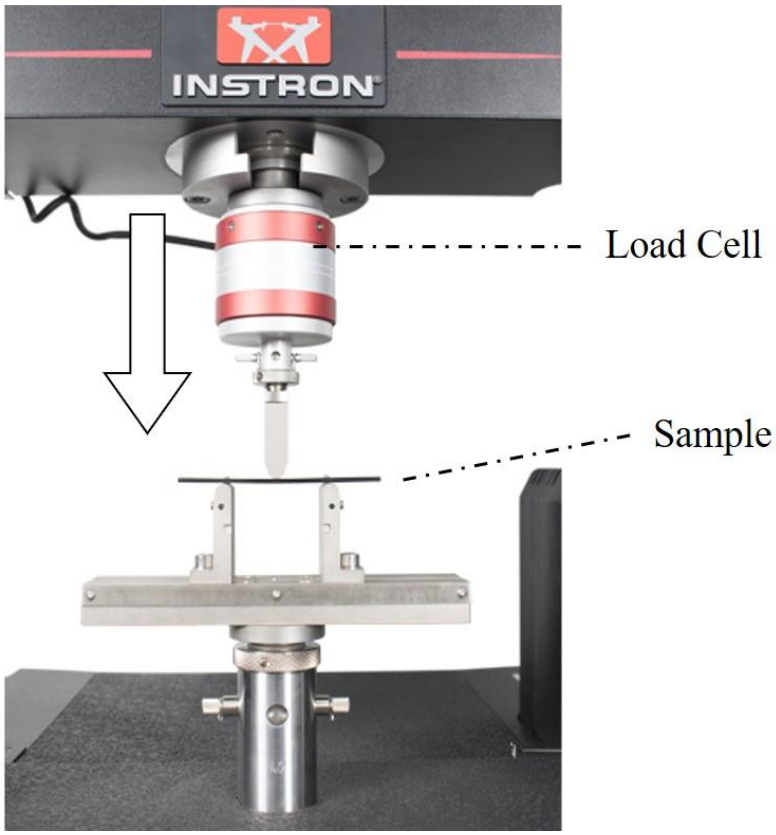

Figure 3.3 The testing apparatus for examination of flexural properties under 3 point bend [88]**.** The cross head compressed the sample between two equally spaced supports.

3.2.3 Dynamic Mechanical Analysis

Dynamic mechanical analysis (DMA) was used in characterizing the thermal and mechanical properties of the 3D printed shape memory polymers. Indeed, since shape memory polymers contain a distinct “glassy” and “rubbery” phase, DMA allowed for the

separation of these viscoelastic transitions in the material (see Figure 3.4). For this test, small rectangular coupons (30 x 5 x 0.5 mm) were clamped into a sample holder while an oscillating force was applied at different temperatures. This test was performed on the SMP blends manufactured via SLA, and all samples were tested twice, the second heating run was used to determine the tan delta peak, and the storage modulus of the material. Samples were tested using a Seiko Instruments (Chiba, Japan) DMS 200, dynamic mechanical analyzer. A frequency of 1Hz, with an amplitude of 10 μm was applied to the sample, as the sample was heated from ambient temperature to 200 °C at a rate of 2 °C/min, and then repeated after cooling to room temperature.

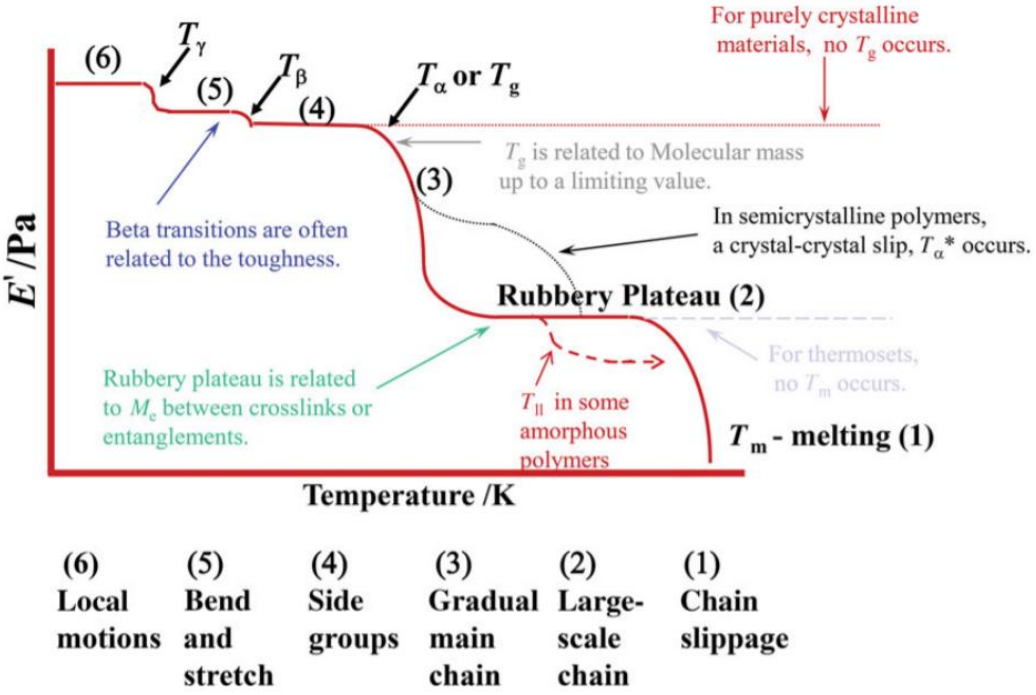

Figure 3.4 Typical Storage modulus curve collected via dynamic mechanical analysis [89]**.** Distinct step transitions in the storage modulus E' correspond to distinct thermal transitions. The glassy region (4) shows a large decrease in modulus to reach the rubbery plateau (2).

3.2.4 Prediction of The Mechanical Properties of Polymer Blends

Since the shape memory polymer blends used in SLA printing consist of a mixture of elastic and rigid material, it can be expected that the mechanical properties of these blends lie between that of the individual materials. To predict the properties of these polymer blends, two simple models (i) parallel and (ii) series were used to determine the interaction of the glassy and rubbery phase of the blended material (see Figure 3.5). If both Elastic 50A and Clear V4 polymers exist as distinct co-continuous phases, the tested properties should exhibit a proportional combination of the properties of each material. Here, the upper-bound parallel prediction of properties is given by the rule of mixtures (equation 3.1) and the series model (equation 3.2) predicts the lower bound [89].

$$M = M_1\phi_1 + M_2\phi_2 \qquad \textbf{3.1}$$

$$\frac{1}{M} = \frac{\phi_1}{M_1} + \frac{\phi_2}{M_2} \qquad \textbf{3.2}$$

Where M1, M2, are the mechanical properties of components 1 and 2, and ϕ1 and ϕ2 are the volume fractions of each component [90].

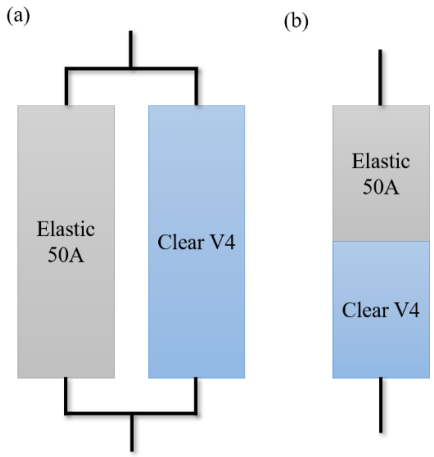

Figure 3.5 Mechanical modeling of polymer blends. (a) parallel model of each distinct polymer and (b) series model of the polymers acting in conjunction.

3.3 Thermal Characterization

After examining the mechanical properties of the material, additional thermal characterization techniques were employed to better examine and quantify the shape memory effect of the material. Differential scanning calorimetry, and thermomechanical analysis were both utilized in determining the phase transition, the shape recovery and shape fixity of the samples. Shape recovery quantifies the ability of shape memory materials to return to their original "permanent" shape from a temporary shape.

3.3.1 Differential scanning calorimetry

A common technique for examining thermal transformations is the use of differential scanning calorimetry (DSC). This technique was employed in determining the Tg, of the shape memory polymer materials, and was combined with DMA information

to investigate thermal events. For crystalline, or semi-crystalline materials (such as the SMP used for material extrusion), sharp peaks on the heating and cooling curves of DSC were used to determine the Tg of the shape memory polymer (see Figure 3.6). Here, small samples (5-10 mg) were prepared in aluminum pans with lids, and placed in a PerkinElmer Hyper DSC (Waltham, MA, USA). The samples were scanned from 25 °C to 230 °C at a rate of 10 °C/min, under multiple cycles. To determine the Tg, the second thermal cycle was utilized to mitigate the effects of the thermal history in the first heating cycle.

Differential scanning calorimetry was also employed on the thermoset SMP blends prepared via SLA. While the samples lacked a distinct crystalline phase, they exhibited the sign of a broad glass transition temperature. Once again, samples (5-10 mg) were prepared in aluminum pans with lids, and then tested under the heating-cooling scanning profile from 0 °C to 200 °C at a rate of 10 °C/min, under multiple cycles. The second thermal cycle was used for analysis, as the first thermal cycle for the thermoset materials can often show additional polymerization reactions from some small percentage of the material being unpolymerized (see Figure 3.6).

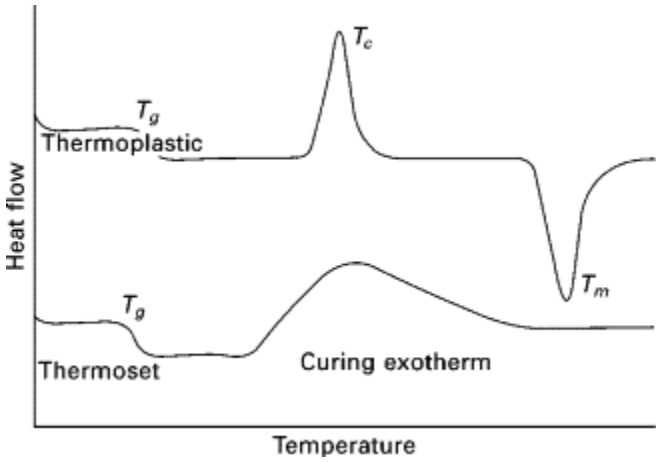

Figure 3.6 Typical DSC thermogram for polymers [91]**.** The thermoplastic sample (top) shows a distinct melting and crystallinity peak. The thermoset sample (bottom) shows a glass transition temperature, and the formation of crosslinks as seen by the curing exotherm.

3.3.2 Shape Recovery Cycles

Two main techniques of thermomechanical analysis were used to elucidate the shape recovery properties of the 3D printed shape memory polymers. As previously mentioned, the major characteristics of shape memory polymers are shape recovery, and shape fixity. In the case of the shape memory polymer manufactured by material extrusion, the so-called fold deploy test was used to quantify large deformations of a flat bar. Additionally, smaller specimens of both shape memory polymers (manufactured via material extrusion and SLA) were subjected to cyclical thermal and mechanical loadings to determine both the shape fixity and the shape recovery properties.

Shape fixity, or shape retention ratio, represents the ability of the studied material to hold its' "temporary" shape. Certainly, for a shape memory polymer to be functional, it must be stable under hysteresis to maintain a deformed shape. An example of the thermal mechanical loading known as a "shape recovery cycle" is outlined in Figure 3.7. Once a

load is applied to deform the sample (step 1 and 2), the shape memory polymer must then be cooled (T < Tg), and the load removed (step 3). Additional heating, free from an external load allows the part to return to its permanent shape (step 4).

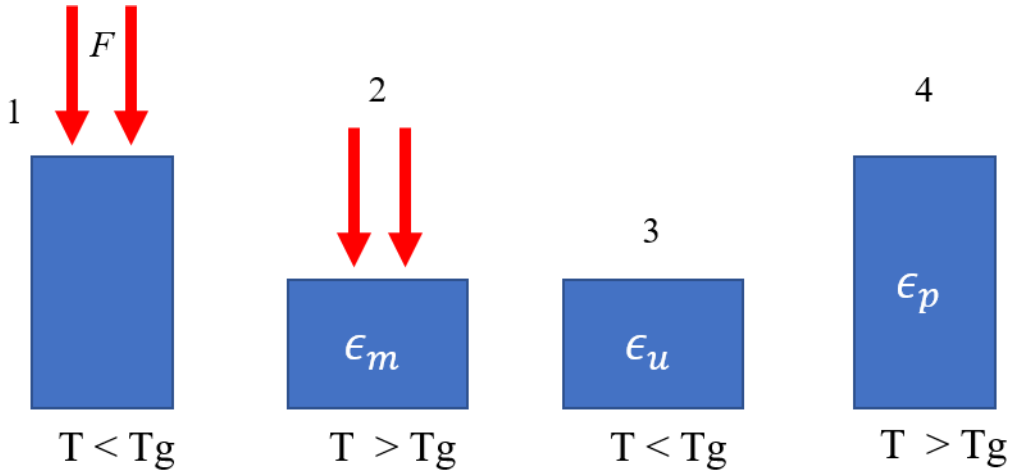

Figure 3.7 An illustrated shape recovery cycle. An external load (red arrow) is applied to a sample while it is heated above its glass transition temperature (steps 1 and 2). Once the sample is cooled, the load is removed, and the sample is in its temporary shape (state 3). Heating the sample free of external loads allows for the permanent shape to be recovered (state 4).

Small relaxations in the applied strain may occur, and lower the shape fixity, S_f, of the sample. This property is summarized simply in equation 3.3 developed by Tobushi et al (1998) [91]:

$$S_f = \frac{\epsilon_u(N) - \epsilon_p(N-1)}{\epsilon_m - \epsilon_p(N-1)} \qquad \textbf{3.3}$$

Where ε_m is the maximum applied strain, ε_u is the strain after the applied load is removed, ε_p is the strain value after unconstrained recovery of the sample (T > Tg), and *N* corresponds to the *N* th shape recovery cycle.

Once a deformation is applied to the shape memory polymer, the recovery can be quantified by measuring the strain upon additional heating. Utilizing the shape recovery cycle depicted in Figure 3.7, the shape recovery occurs between steps 3 and 4. Similar to the shape fixity, the shape recovery ratio, S_R, has been described by equation 3.4 [92]:

$$S_R(N) = \frac{\epsilon_u(N) - \epsilon_p(N)}{\epsilon_u(N) - \epsilon_p(N-1)} \qquad \textbf{3.4}$$

Where, ε_u, ε_p, are the same as equation 3.3 and represent the strain in the deformed shape and the strain in the recovered shape, respectively. In combination, the shape fixity and shape recovery ratio create a suitable definition for the performance and functionality for the shape memory properties of the investigated materials.

3.3.3 Fold-Deploy Test

The fold deploy test has been widely used [63,92–94] in categorizing macromolecular motion of the shape memory polymers on a benchtop, and can be used to quickly validate the shape recovery of a sample. This test was conducted on the material extrusion 3D printed shape memory polymer. In this case, rectangular bars (80 x 11 x 4 mm) were printed and then placed in boiling water to heat the material above its glass transition temperature. After 5 minutes, samples were removed and bent into a "U" shape around a 12mm diameter metal rod (see Figure 3.8) [83]. After cooling, the temporary "U" shape was retained, and the sample was placed back into hot water to recover for 5 minutes. The shape recovery could then be calculated using a modified version of equation 3.4, where the strain is measured as the angle, Θ. The shape recovery by the fold-deploy test is given by:

$$R_{FD} = \frac{\theta_p(N)}{\theta_p(N-1)} \quad \textbf{3.5}$$

Where Θ_p is the angle remaining in the recovered flat bar (see Figure 3.8) and N corresponds to the N th fold-deploy cycle.

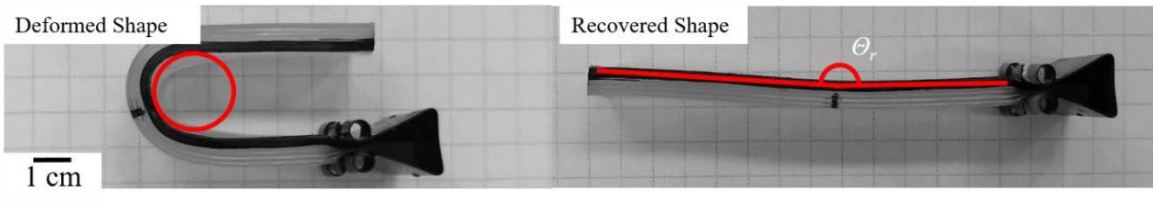

Figure 3.8 3D Printed SMP used in the fold-deploy test [83]**.** The recovered shape displays the angle of recovery, shown here as Θr.

3.3.4 Thermomechanical Analysis

To better quantify the stress, strain, and recovery of the shape recovery cycles, the use of a thermomechanical analyzer was employed. A TMA (Q800) thermomechanical analyzer (TA instruments, New Castle, DE, USA) was used to investigate these properties (see Figure 3.9). Here, shape memory polymer samples printed via SLA were analyzed in compression mode for a shape recovery cycle. Cubic samples (5 x 5 x 5 mm) were machined from SLA printed shape memory polymer blends. The samples were ramped to 100 °C and a force of (0.9 N) was applied until the sample cooled to 25 °C. Once cooled, the load was removed (to 0.001 N), and the sample was heated back to 100 °C while strain data was collected. This test allowed for the collection of temperature, strain, and load information over time.

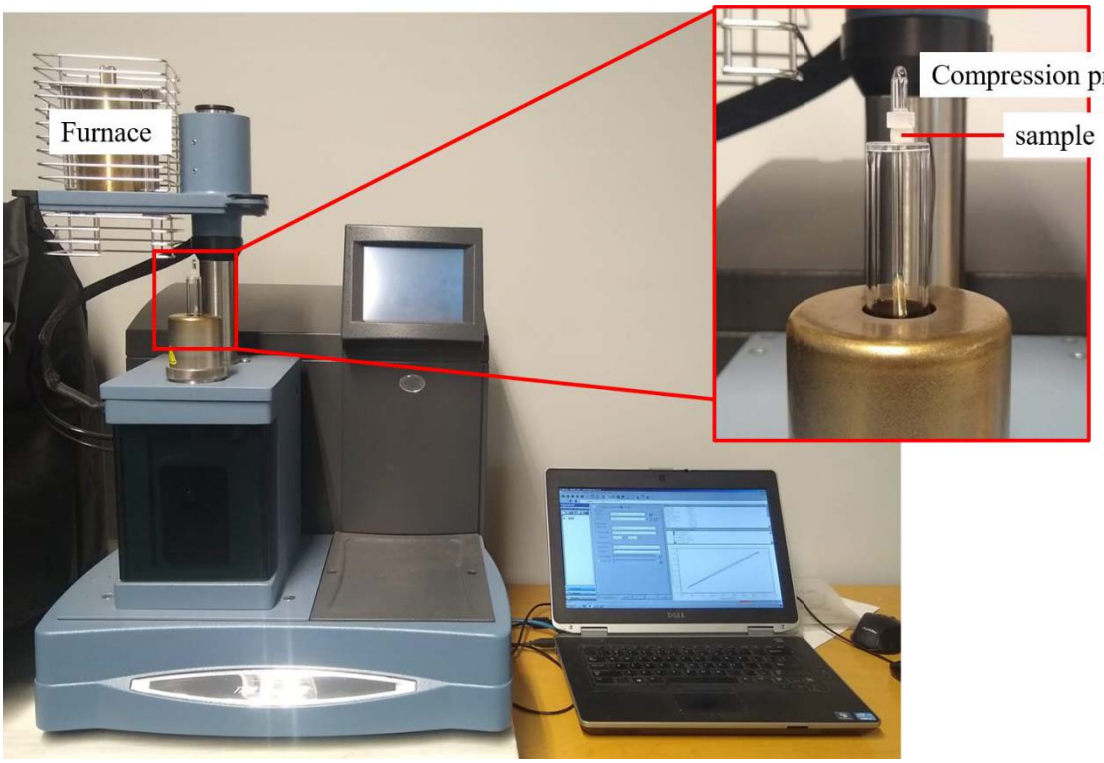

Figure 3.9 The TMA Q400, used for thermomechanical characterization of the shape memory polymers. The furnace rotates over the sample stage to heat samples above the glass transition temperature.

3.4 Smart Devices

As described previously, a focus of this work was to utilize additive manufacturing to produce shape memory polymers to be used as deployable structures and electronic actuators. While shape memory polymers can easily recover from a deformed shape, the polymers themselves still lack electronic functionality, acting as insulating materials. To overcome this hurdle, the manufactured shape memory polymers were incorporated into hybrid structures to act as electronic devices. Two main materials were utilized to achieve this: metal adhesive tape, and a liquid-metal material.

3.4.1 Fabrication of a 3D Printed SMP actuator

The shape memory polymers manufactured via material extrusion were utilized in fabricating a two-way thermal actuator. This thermal actuator utilized Nickel-Titanium shape memory alloy (SMA) wires (Dynalloy Inc, Irvine, CA USA) to provide two stable geometries that could be triggered without the use of an external load. Instead, the shape memory polymer's distinct rubbery phase allowed the shape memory alloy wires to return to the parent shape (straightened). Once the hybrid SMP switch was cooled, the shape memory alloy wires relaxed, and the entire switch went to a second distinct shape. This hybrid switch was assembled from a printed SMP sample (28 x 5 x 1 mm). After printing, shape memory alloy wires were glued to the sample, and copper tape was applied to the surface to provide conductivity (Figure 3.10 a) [83].

The application of the fabricated SMP / SMA hybrid thermal switch was tested as an actuator in a simple electronic circuit. Here, a microcontroller MSP430 (Texas Instruments, Dallas, TX, USA) was encoded with simple logic to collect temperature data based on the state of the hybrid switch. If the input pin voltage was high, data collection was started, and if the voltage was low, data collection stopped. The SMP/SMA hybrid switch was mounted to a breadboard and positioned such that at $T > 90$ °C, the switch straightened and contacted the signal pin. Once the system reached a lower temperature ($T < 90$ °C), the switch relaxed to the "*off*" position and data collection was stopped. The switch mounted on the MSP430 board is shown in Figure 3.10, along with an illustration depicting the *on* and *off* states [83].

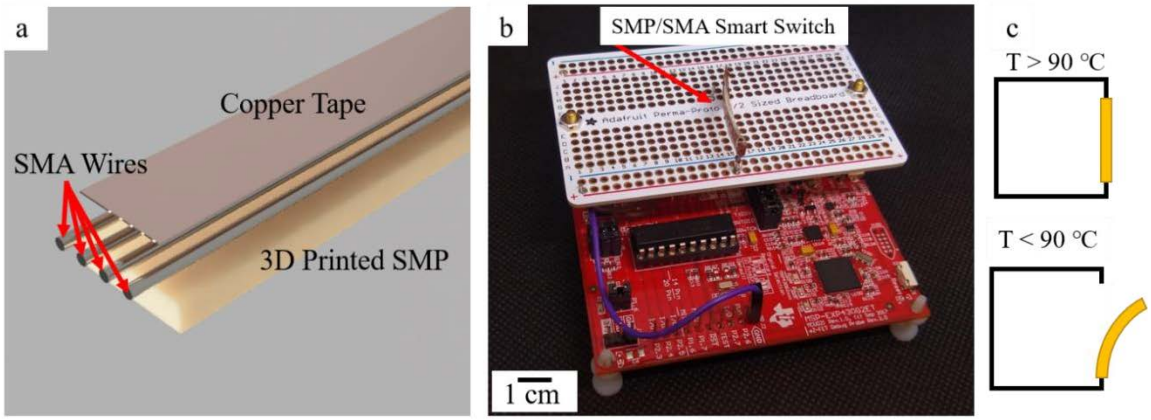

Figure 3.10 SMP / SMA thermal switch used as an actuator to control data collection [83]**.** (a) Digital render of the manufactured SMA/SMP hybrid switch. (b) the manufactured switch mounted to a breadboard on the MSP430 (c) illustration of the "on" state of the switch creating a closed circuit, and the "off" state of the switch creating an open circuit.

3.4.2 Development of a functional SMP antenna

To further explore the electronic capabilities of shape memory polymers printed via SLA, a functional antenna was designed and printed. By filling voids within the matrix with a liquid metal, conductive traces formed the functional components of the antenna, while the SMP matrix acted as scaffolding for the entire design. After printing, the microfluidic channels in the SMP part were cleaned with compressed air to eliminate excess resin from the voids. Galinstan liquid metal (Roto Metals, San Leandro, CA, USA) consisting of 65.8 % Ga, 21.5 % In, and 10% Sn metal was injected into the channels of the printed SMP, and a coaxial connector was glued into the part (see **Figure 3.11**).

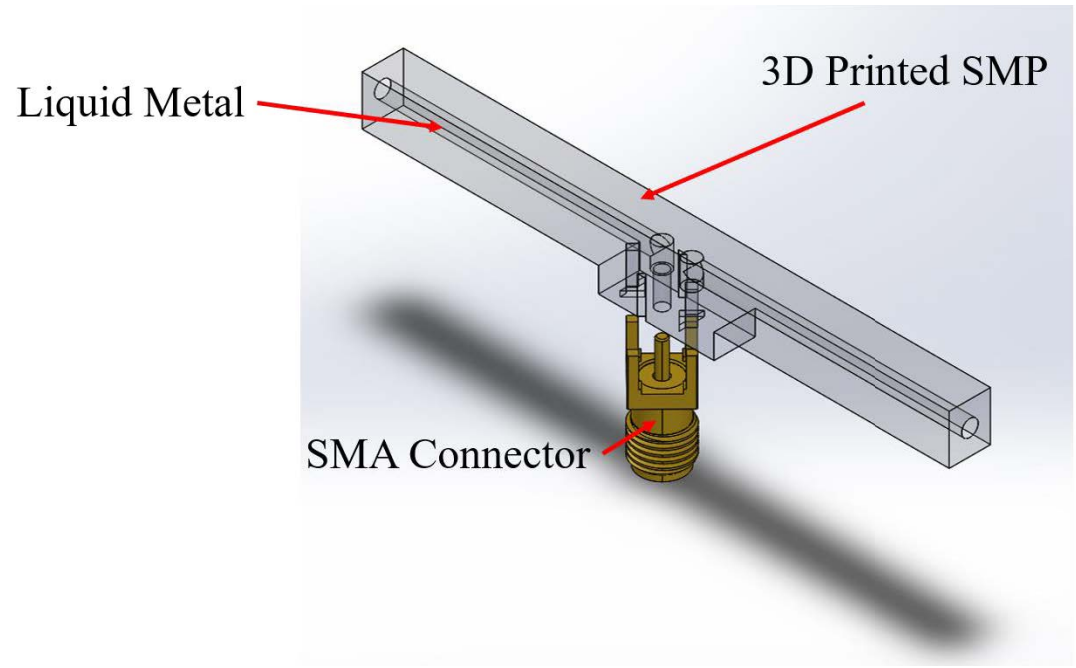

Figure 3.11 Digital rendering of the shape memory polymer dipole antenna. Empty channels in the SMP matrix were later filled with the liquid Galinstan metal.

The antenna performance was evaluated using a E5061B virtual network analyzer (VNA) (Agilent Technologies, Santa Clara, CA, USA) to examine the one port scattering parameter (S11) parameter performance (see Figure 3.12). In this case, the VNA frequency sweep was between 100 KHz to 3 GHz. The data collected for the S11 parameter plot could then be compared to a simulated antenna in the same frequency range, generated from ANSYS HFSS (Canonsburg, PA, USA). The performance of the manufactured antennas was primarily examined using the S-11 parameter plot to determine the resonant frequency of the antenna. To validate the shape memory properties, the liquid metal antenna was heated in an oven (100 °C), deformed into a curved shape, and retested with the VNA.

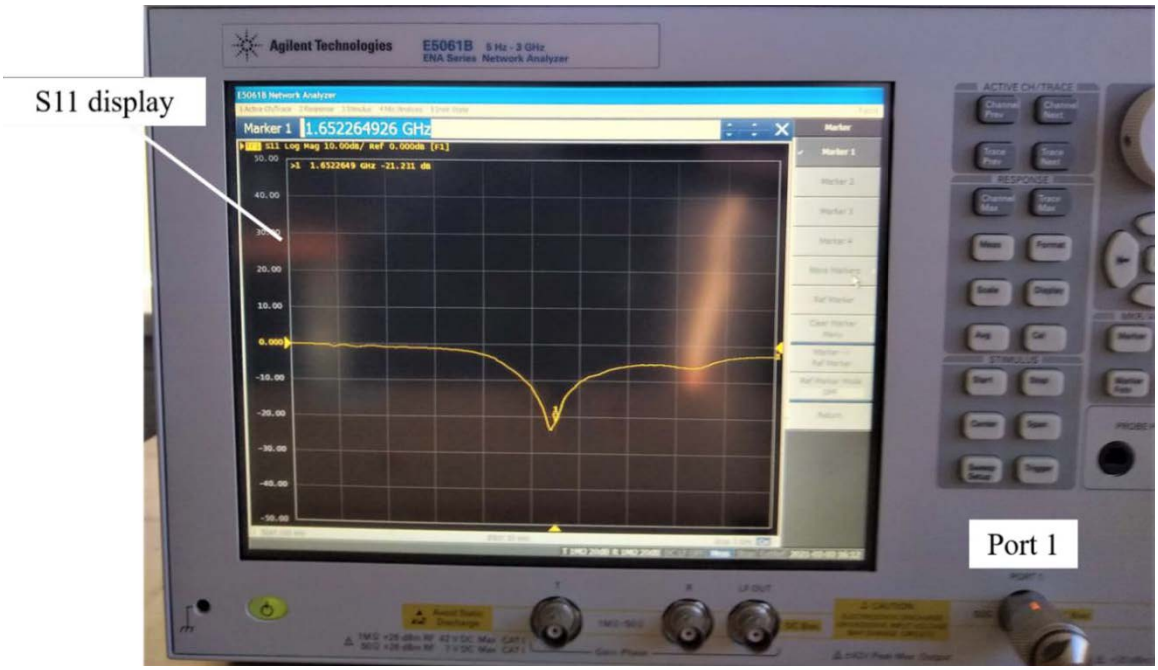

Figure 3.12 The Virtual Network Analyzer used to investigate the fabricated smart antennas. The fabricated antennas are connected to port 1 for analysis, and real time results are shown on the instruments display.

4 Results and Discussion

This chapter presents the results of experimentation on the additive manufacturing work performed on shape memory polymers. The chapter is separated by each technique of additive manufacturing used in this research program. First, the commercially available shape memory polymer that was printed via direct pellet extrusion was presented and characterized by mechanical testing and thermal testing. The results from the fabricated SMP hybrid switch are also presented. In the case of the shape memory polymer blends prepared via stereolithography, a further examination was conducted into the mechanical properties. A comparison of each shape memory polymer blend is presented, with the goal to suggest a single polymer blend for future work. The selected shape memory polymer blend is finally demonstrated as a functional smart antenna.

4.1 Shape Memory Polymers via Material Extrusion

4.1.1 Mechanical Properties

4.1.1.1 Tensile Testing

Uniaxial tensile testing elucidated the mechanical properties of the printed SMP pellets. During the tensile tests, the samples reached a yield point, with a visible necking zone (see Figure 4.1). This necking behavior was also observed in the stress-strain data from the tensile test. Here, an ultimate tensile strength of 55.58 MPa (± 2.29 MPa) was observed across the samples. The linear behavior of the stress-strain curve was also used to calculate the Young's Modulus of the printed samples, which was determined to be 1.01 GPa (± 0.063 GPa).

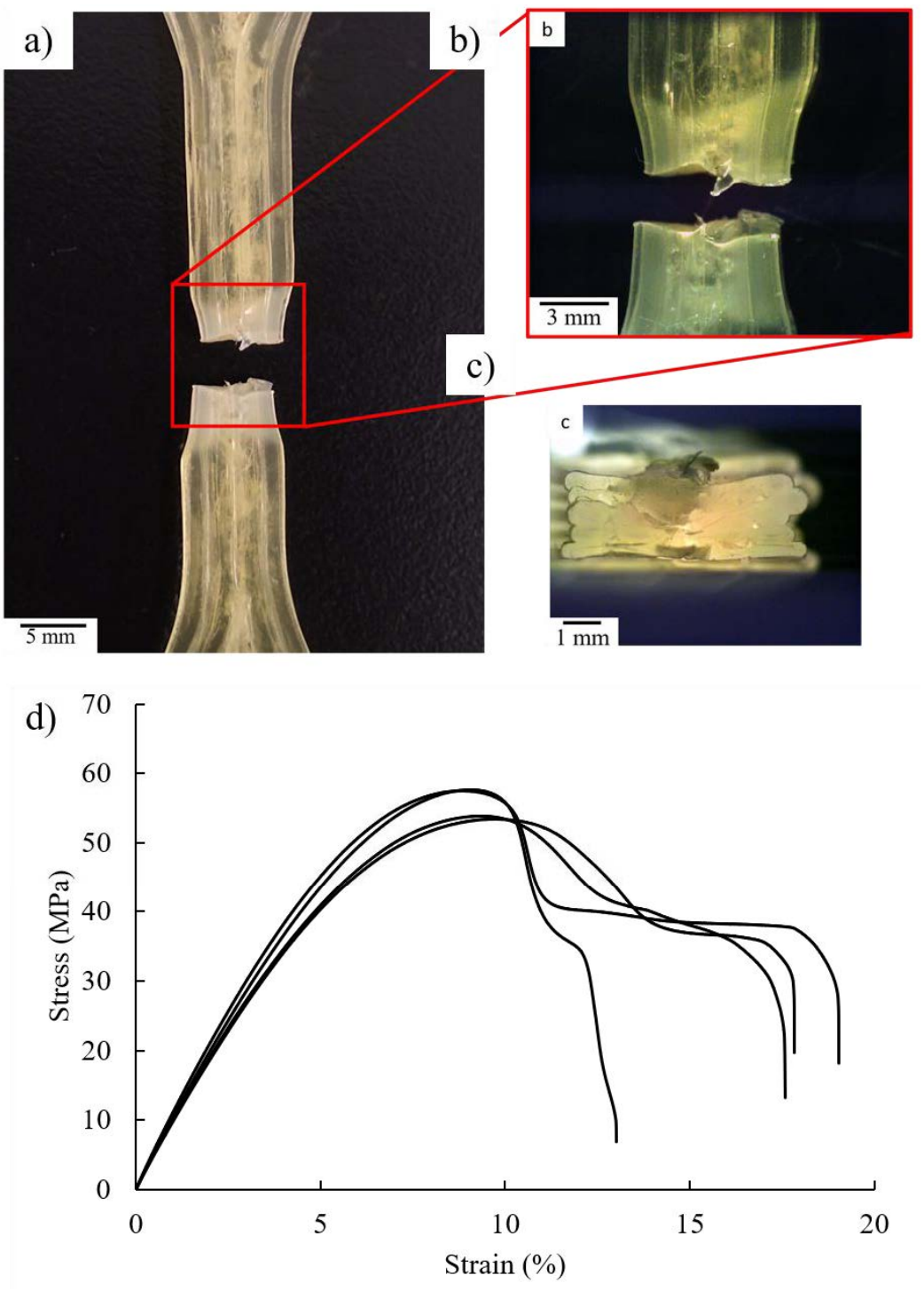

Figure 4.1 Tensile testing results of the SMP printed via material extrusion.(a, b) A fractured tensile specimen following the uniaxial tensile test. (c) A cross-sectional view of the fracture area). (d) Stress- strain data from the uniaxial tensile test, that exhibits the yield point and necking of the tensile samples.

The examined ultimate tensile strength of 55.58 MPa was indeed higher than that reported by the manufacturer (48 MPa) [100]. However, the manufacturer reported mechanical properties of the injection molded parts, but the measured tensile strength was calculated from the printed parts. As such, the observed difference of 7.5 MPa in the ultimate tensile strength is attributed here to the difference in the sample preparation. It should be noted, that in the printed samples, the filament bead was extruded longitudinally (in the same direction as the uniaxial loading for the tensile test). Thus, this increased strength could be associated with the alignment of the polymer chains. Anisotropy is common in fused filament fabrication parts, and changes in tensile strength are commonly factors of print orientation and processing parameters [26,96].

4.1.1.2 Flexural Testing

The Flexural testing of the 3D printed SMP Diaplex 9020 parts was based on the 3-point bend configuration. As illustrated by the stress – strain curves (see Figure 4.2), none of the examined samples fractured before the conclusion of the test (5 % strain). This resulted in an average flexural stress of 68.05 MPa (± 2.95 MPa) and a flexural modulus of 2.11 GPa (± 0.102 GPa). As it was seen seen in the tensile results, both the flexural strength and the flexural modulus were higher than those values reported by the manufacturer 55 MPa and 1.9 GPa, respectively [101]. Once again, the flexural specimens were printed in the longitudinal direction with a 100% infill. Here, the differences in flexural strength and modulus seem in agreement for the expected difference between injection molded counterparts and an optimized printing orientation [97,98].

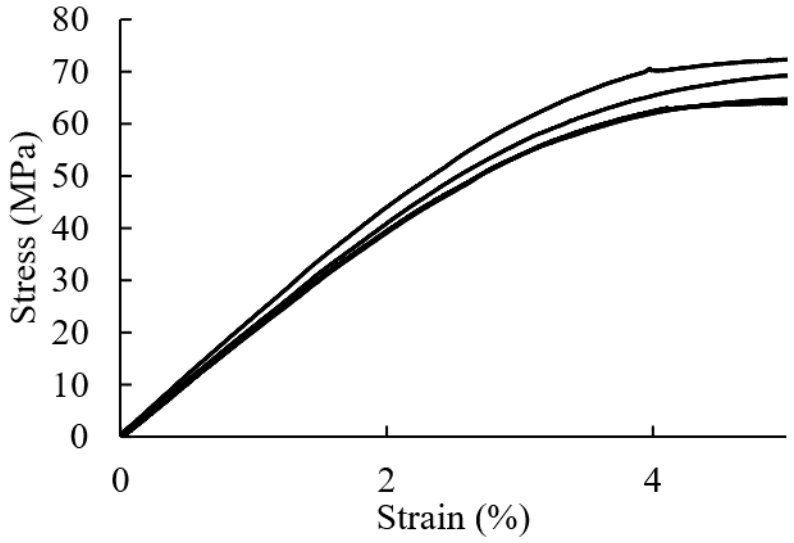

Figure 4.2 Flexural results of the shape memory polymer printed via material extrusion. The commercially available SMP printed samples resulted in a yielding profile without fracture.

4.1.2 Thermal Analysis

4.1.2.1 Differential Scanning Calorimetry (DSC)

The thermal events of the 3D printed and the as received SMP pellets were examined by differential scanning calorimetry. As seen from the resulting thermogram (see Figure 4.3), only one distinct thermal transition occurred between room temperature and 230°C. This event corresponds to the glass transition in the examined shape memory polymer. Here, the glass transition from the second heating cycle was determined to be 85.4 °C in the printed material, and 81.9°C from the cooling curve [83]. This temperature is slightly lower than the transition temperature reported by the manufacturer (90°C); however, the reported Tg was obtained by the manufacturer from a mechanical analysis [99,100]. This difference seems to be small (< 5 °C) and can be attributed to the difference in the measuring techniques.

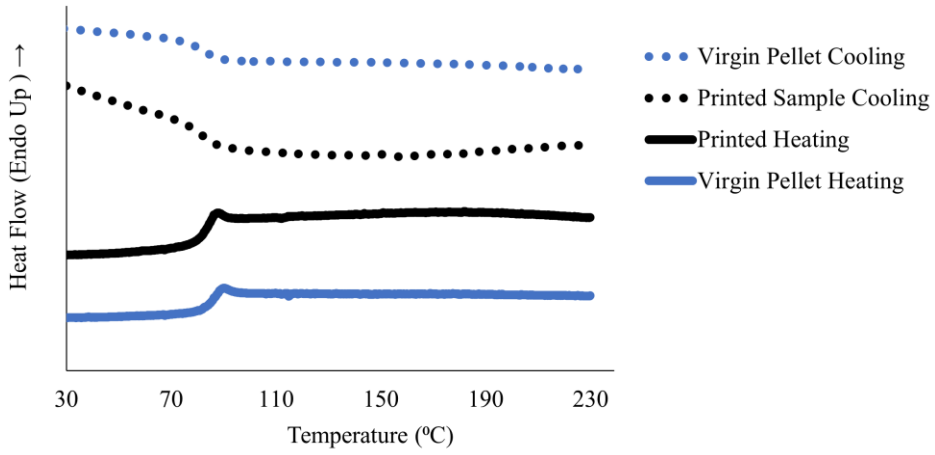

Figure 4.3 DSC results of the commercially available shape memory polymer [83]. Both the printed polymer (blue) and the as-received pellets (black) are shown for the second cooling and heating cycles.

4.1.3 Shape Recovery

4.1.3.1 Fold-Deploy Tests

Both the fold-deploy tests and the thermomechanical analysis showed that the 3D printed shape memory polymer pellets exhibited high levels of shape recovery and shape fixation. The "U" – shaped folded deploy testing of the shape memory polymer yielded an average shape recovery angle of 175.7 ° across five cycles, this resulted in an average shape recovery of 97.62 % [83]. From Figure 4.4, the first shape recovery cycle achieved a recovery ratio over 100%. This indicates that the angle of the "U" shaped bar returned to an angle higher than 180°, and it is likely attributed to the printing process. It is hypothesized that during the printing process, some degree of unintentional thermal programming may be applied on the printed specimens. However, after the first cycle, this internal strain is relaxed, and the shape recovers > 95% of the parent shape.

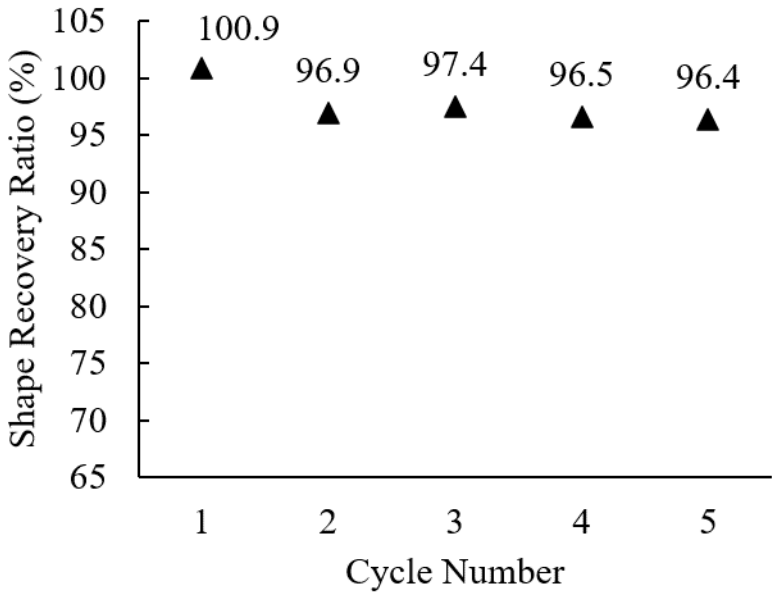

Figure 4.4 The shape recovery ratio of the 3D Printed SMP pellets. As the fold-deploy cycles increase, an average shape recovery ratio of about 97.6% is achieved.

4.1.3.2 Shape recovery cycle testing

The thermomechanical analysis of the 3D printed SMP pellet confirmed the high shape recovery properties of the printed material. This analysis allowed for determination of the shape fixity ratio, S_f, a ratio of the applied strain to the residual strain in the sample after the external load was removed (see equation 3.3). An examination of the strain vs time data from the cyclical test (see Figure 4.5 a), showed the location of the recovered strain (e_p), set strain (e_u), and maximum strain (e_m) used to calculate the shape fixity, and shape recovery seen in Figure 4.5 (b). The raw data for Figure 4.5 (a) have been zeroed from the initial strain point, the highest amount of applied strain was observed on the first cycle.

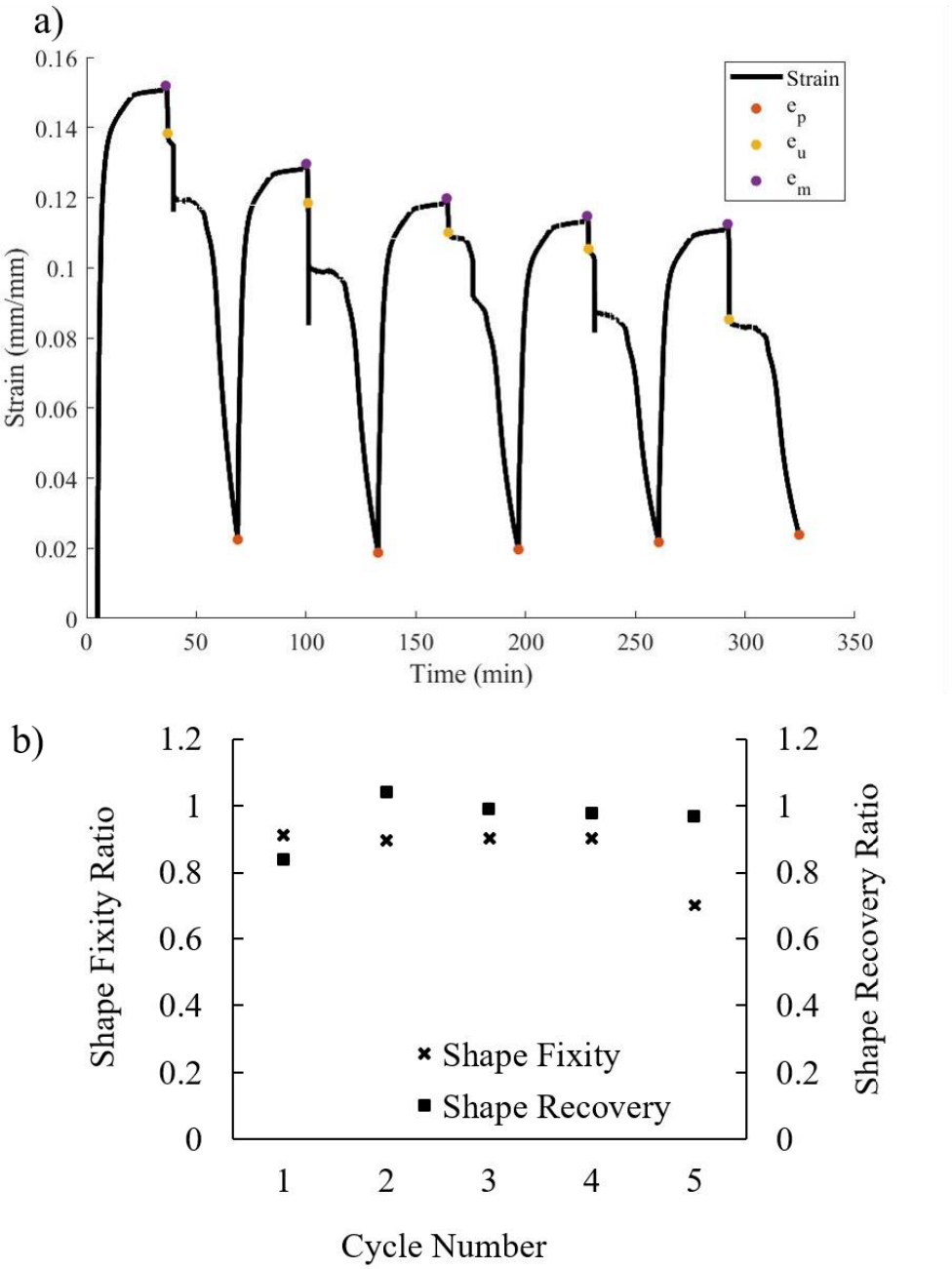

Figure 4.5 Results of the shape recovery cycle testing on the 3D printed SMP pellet. (a) Strain vs time plot of the shape recovery cycles by thermomechanical analysis. Here, the values for the maximum strain, em, and values of the fixed strain (after cooling), eu, were used to calculate the shape fixity for each cycle. The values of recovered strain, ep, are attributed to the strain recovered after heating, and as the initial strain for the next cycle. (b) Summarizes the values of shape fixity, Sf, and shape recovery, Sr, calculated from the strain values in (a).

However, as seen in Figure 4.5, the recovered and the starting strain values, e_r were near a nominal strain of 0.02, indicating an irrecoverable amount of strain was present in the sample from the first cycle, but also in the fifth cycle. This aligns well with the hypothesis from the fold-deploy test, claiming that some amount of strain has been induced on the shape memory polymer during the printing process. This test, which applied small deformations to the sample under compression, yielded an average shape fixity of 86.3%, as the fifth cycle resulted in the lowest shape fixity observed (70%) (see Figure 4.5b). Subsequent shape recovery cycles show consistent results, and the shape recovery approaches a value of 96.6% (see Figure 4.5), exhibiting similar results to the fold-deploy test (Figure 4.4).

4.1.4 Application of SMP as a Thermal Actuator

As previously mentioned, the 3D printed SMP was combined with shape memory alloy wires to create a counterbalanced hybrid thermal actuator switch. The entire hybrid actuator and MSP 430 were set in a laboratory oven to collect temperature data. The output from the MSP 430 (see Figure 4.6) clearly shows that above 90 °C, the thermal actuator initialized the data collection. All temperature data above 90 °C was collected until the oven door was open and the system rapidly dropped. The continuous collection of data is emphasized by the changes in temperature the oven underwent. Here, the continuous collection for data showcases how the hybrid smart switch has a distinct *on* and *off* state, possible only because of the actuation and relaxation of the hybrid switch. Once the switch returned to the *off* state, it was able to trigger data collection when it was heated once again.

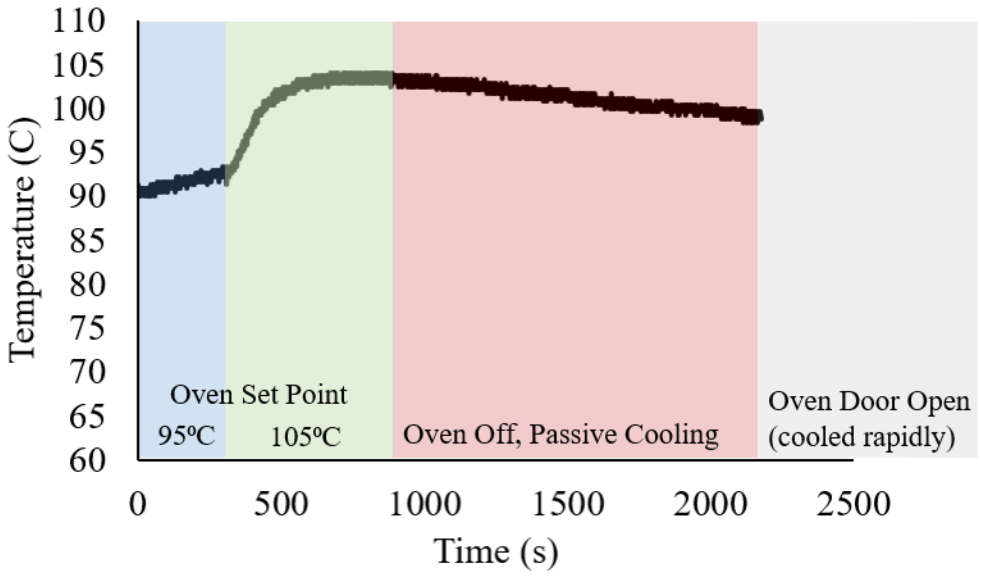

Figure 4.6 Collected data from the MSP430 actuated by the hybrid SMP / SMA switch[83]**.** Data collection started (t = 0) once the oven reached 90 °C. As the oven set point was increased to 105 °C, the entire system continuously collected the temperature data. Once the oven was switched off (red area), the passive cooling could be measured until the system rapidly cooled, and the actuator relaxed to the "off" position.

4.2 Shape Memory Polymers Printed via SLA

4.2.1 Printing of the Polymer Blends

The polymer blends used for 3D printing via SLA were all manufactured on the same 3D printer. Due to the closed-source nature of the Formlabs Form 2 printer, few processing parameters could be modified to affect the quality of the printed samples (see Figure 4.7). As a result, problems arose in the printing process for some polymer blends that could not be mitigated by modifying the printing parameters. The samples containing a mass fraction of 0, 0.1, and 0.2 of the Elastic resin printed without major problems. However, the samples containing a higher amount of Elastic resin (0.3, 0.4 mass fraction) showed higher degrees of part failure, which were observed as incomplete parts and delamination of the printed coupons (see Figure 4.7 c). Undeniably, the reaction kinetics for the clear and Elastic material are not identical, and the printing parameters used to cure these polymers differ from the processing used. Without a method to mitigate these parameters (laser exposure intensity, and scanning speed), it appeared beneficial to select one of the other two polymer blends for ease of printability. Nevertheless, enough testing coupons of all the polymer blends were successfully printed for analysis of the mechanical properties.

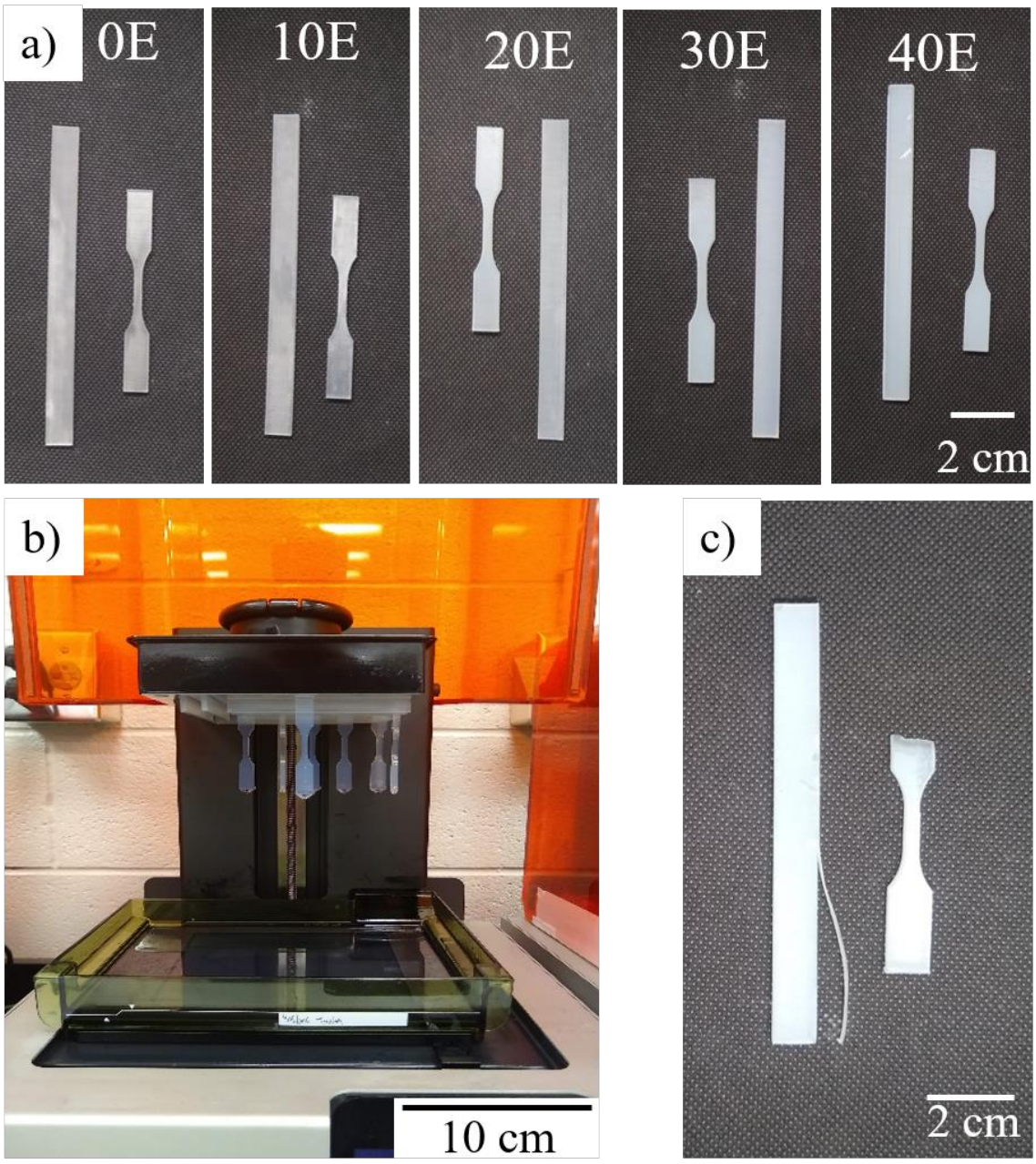

Figure 4.7 Polymer blends printed via SLA for the investigation of shape memory polymers. (a) Each polymer blend, for the samples containing a mass fraction of Elastic resin from 0 ("0E") to 0.4 ("40E"). (b) Samples after printing, suspended from the build plate of the inverted SLA 3D printer. (c) Examples of the failed/ incomplete prints seen in the 30E and 40E polymer blends.

4.2.2 Mechanical Properties

4.2.2.1 Tensile Testing

The uniaxial tensile testing was conducted for each blend of the examined materials (standard and elastic materials). From the stress- strain curves (see Figure 4.8) the brittle behavior of the neat Clear material was observed. In contrast, the plain Elastic material displayed a profile (see Figure 4.8 b) with a strain of about 0.56 mm/mm, which was 18 times higher than the Clear material. As the mass fraction of the Elastic material in the blends was increased, it was evident that the ductility of the material increased. Indeed, the polymer blends consisting of Elastic 50A resin all possessed a higher strain at failure than the neat Clear material, another indication that the brittleness of the samples was decreased. Additionally, the highest amount of elastic resin examined (40% by mass) showed the lowest tensile strength, but the highest elongation at break, indicating the incorporation of Elastic resin in the polymer blend had effectively created a "rubber-toughened" copolymer.

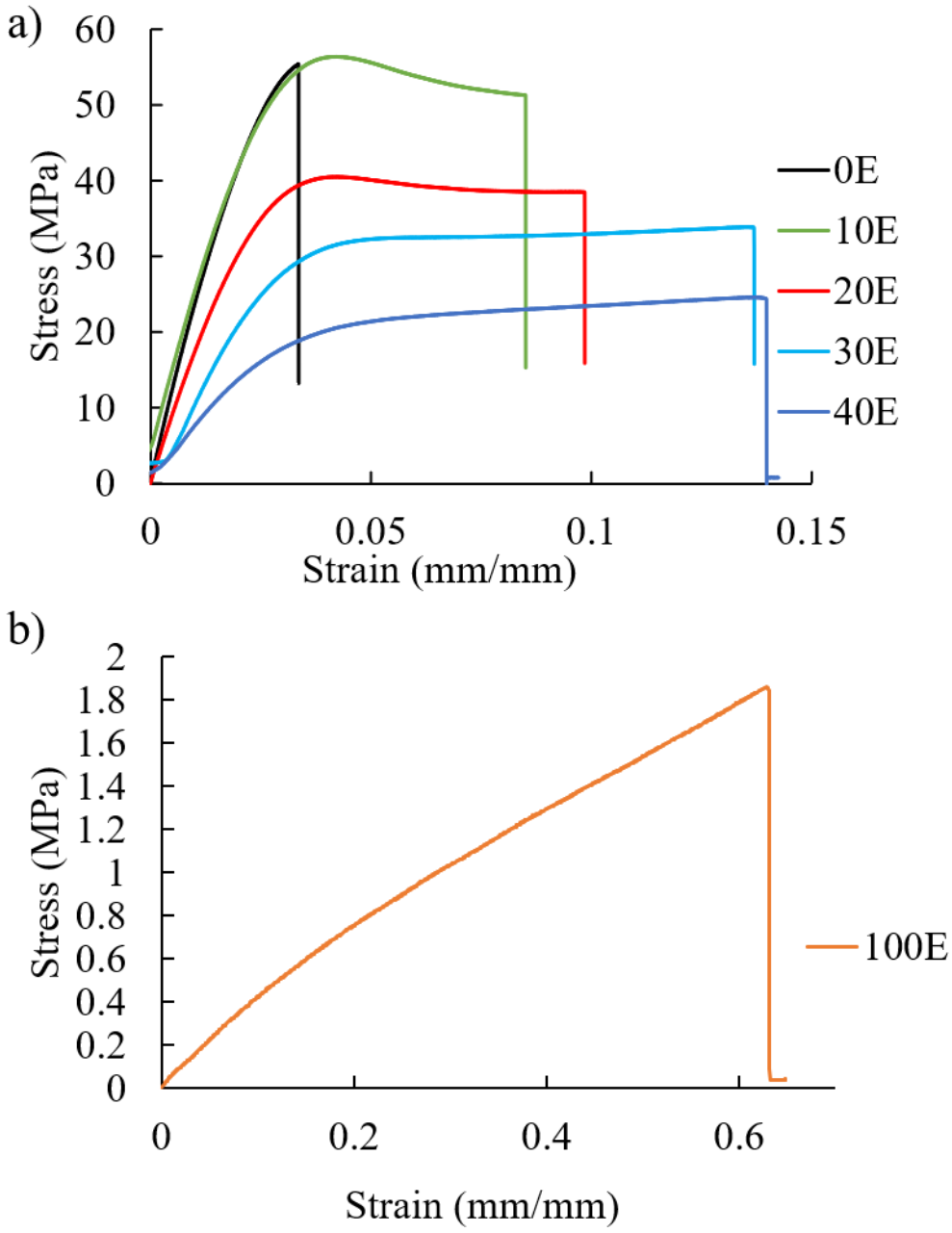

Figure 4.8 Stress-strain curves of the examined SLA polymer blends under tension.(a) A representative curve of each of the tested blends is being displayed. In the legend, the numbers indicate the mass fraction of Elastic Resin in the blend (i.e. 10E corresponds to 10% by mass of the Elastic material, 20E to 20%, and so on). (b) A representative curve of the pure Elastic material, exhibiting a much higher elongation at break than the Clear material.

The data collected from the uniaxial stress-strain tests was utilized in determining the values of tensile strength and Young's Modulus of the material. As seen from Figure 4.8, the ultimate tensile strength decreased with a higher content of Elastic 50A resin in the matrix. A similar trend was observed in the Young's Modulus of the material (see Figure 4.9). The neat Clear material exhibited an ultimate tensile strength of 53.1 MPa but had dropped to 25.1 MPa upon the addition of 40% Elastic resin by mass. Additionally, the Young's Modulus reached a minimum of 0.63 GPa for the polymer blend of 40% Elastic material, compared to 2.4 GPa for the unmodified Clear resin. Furthermore, the strain at break of each examined polymer blend increased with the addition of the Elastic resin (see Figure 4.9 b). Here, the strain at break increased five times, to a value of 0.15 mm/mm (± .04) for the polymer blend consisting of 40% Elastic resin. From these tests, it was clear that the addition of the Elastic resin to the polymer blends significantly increased the elongation, therefore mitigating the brittle nature observed in the unmodified material.

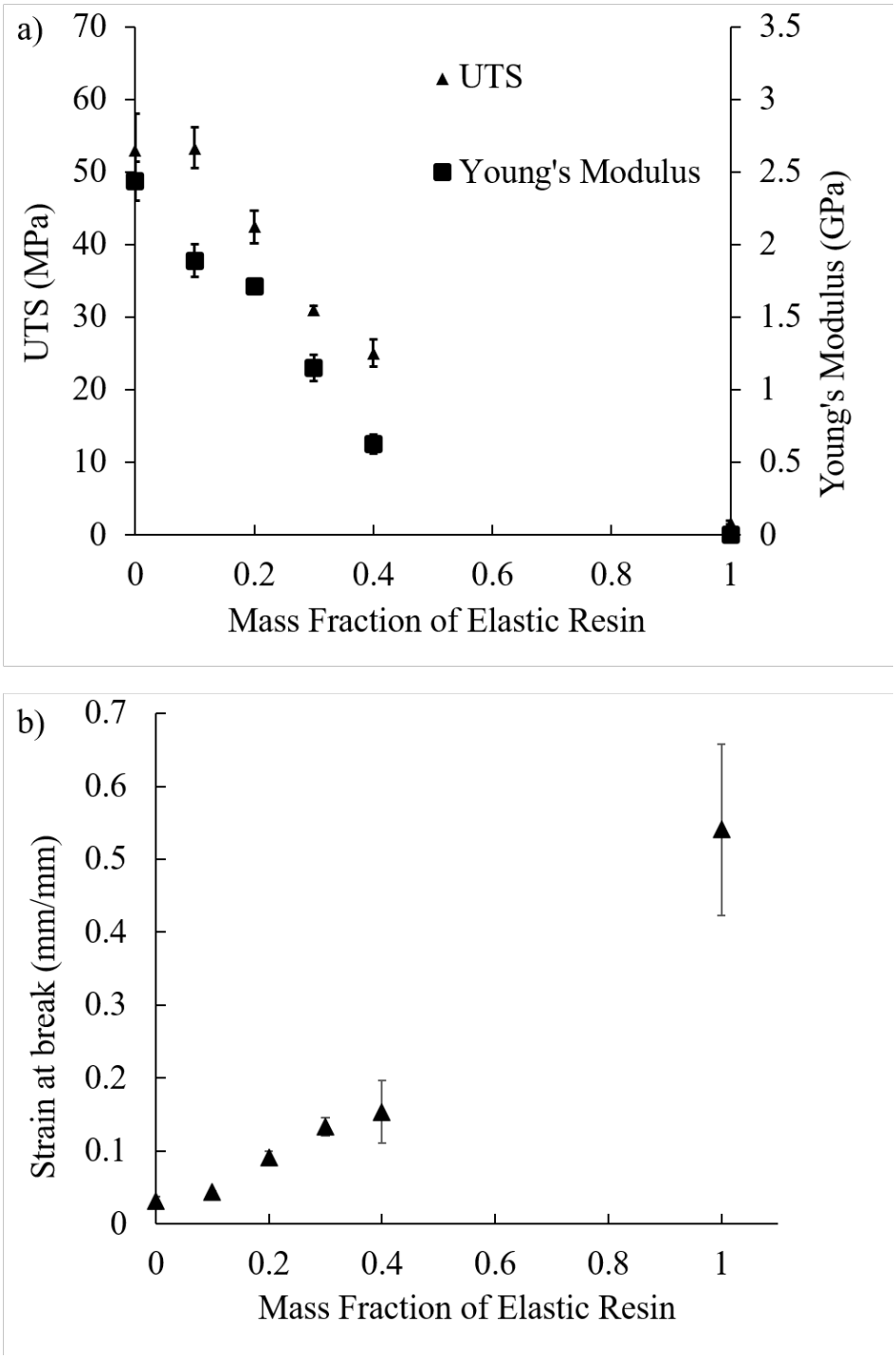

Figure 4.9 Mechanical properties of the polymeric blends for SLA under uniaxial tensile conditions. (a) As the mass fraction of Elastic resin increased (x-axis), the ultimate tensile strength (UTS) and Young's Modulus decreased. (b) The strain at break increased by increasing the mass fraction of the Elastic resin in the polymer blends.

The results of the tensile test showed a distinct correlation between mass fraction of Elastic resin and the ultimate tensile strength. The values of the ultimate tensile strength were plotted against the values for UTS via the series and parallel models (see Figure 4.10). It was observed that for the samples containing a fraction of 0.2 or more of Elastic resin, the parallel model closely predicted the value of the tensile strength. For the blend containing only 10% Elastic resin, it was observed that this value was greater than the maximum predicted value of the parallel model. In fact, the ultimate tensile strength of this polymer blend (53.3 ± .001 MPa) was very close to the value of the unmodified polymer (53.0 ± .006 MPa). Indicating, the polymer blend consisting of a mass fraction of 0.1 Elastic resin, was governed solely by the properties of the Clear resin in the matrix. This hypothesis was reinforced by inspection of the stress-strain curves (see Figure 4.8), and the measured strain at failure (see Figure 4.9 b). Overall, it was observed that the series model (or lower bound) was not an accurate predictor of mechanical properties, while the parallel model (upper bound) was more closely related to the examined properties. As might be expected, more complex and higher order models for continuous co-polymers are needed to accurately predict the mechanical response of this system [99,100].

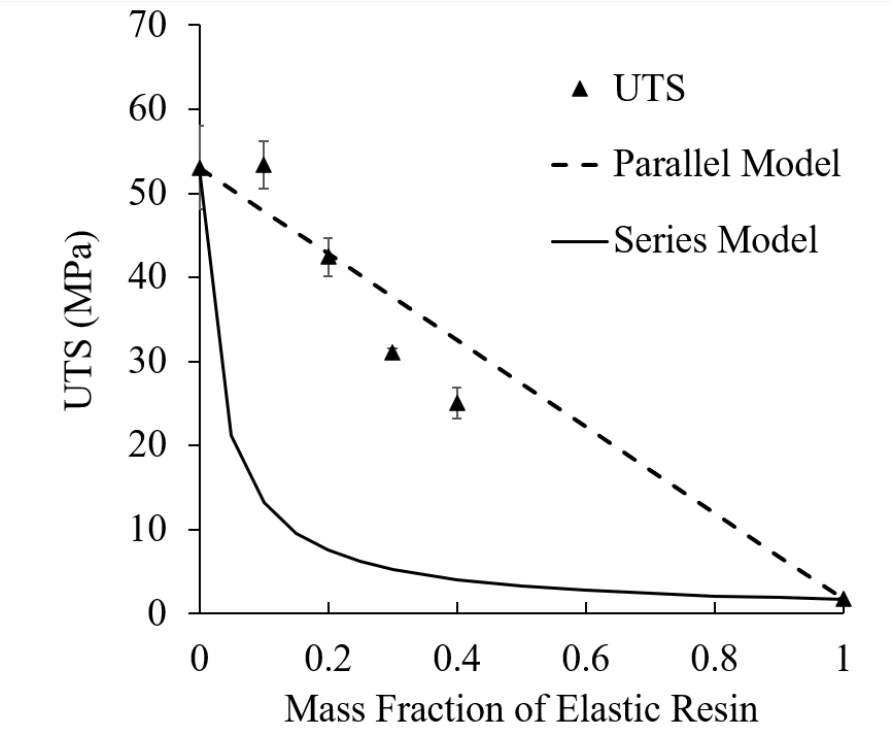

Figure 4.10 Ultimate tensile strength and the series and parallel model of copolymers. It was clear, the blend of 0.1 Elastic resin by mass was governed solely by the Clear Resin matrix. The measured ultimate tensile strength for the blends containing 0.2 to 0.4 Elastic resin clearly fall within the lower and upper bounds determined by the parallel and series model.

4.2.2.2 Flexural Testing

Three-point bend flexural testing confirmed similar trends as those seen in the uniaxial tensile testing. Here, once the mass fraction of the elastic resin in the polymer blend reached 0.2, the flexural stress decreased to a value 20% lower than the plain Clear material (see Figure 4.11). Ultimately, the lowest flexural stress recorded here was 23.2 (± 0.68) MPa, for the blend consisting of a mass fraction of 0.4 Elastic resin. As in the case of the commercially available SMP, the flexural specimens did not fracture during the 3-point bend test (< 5% strain).

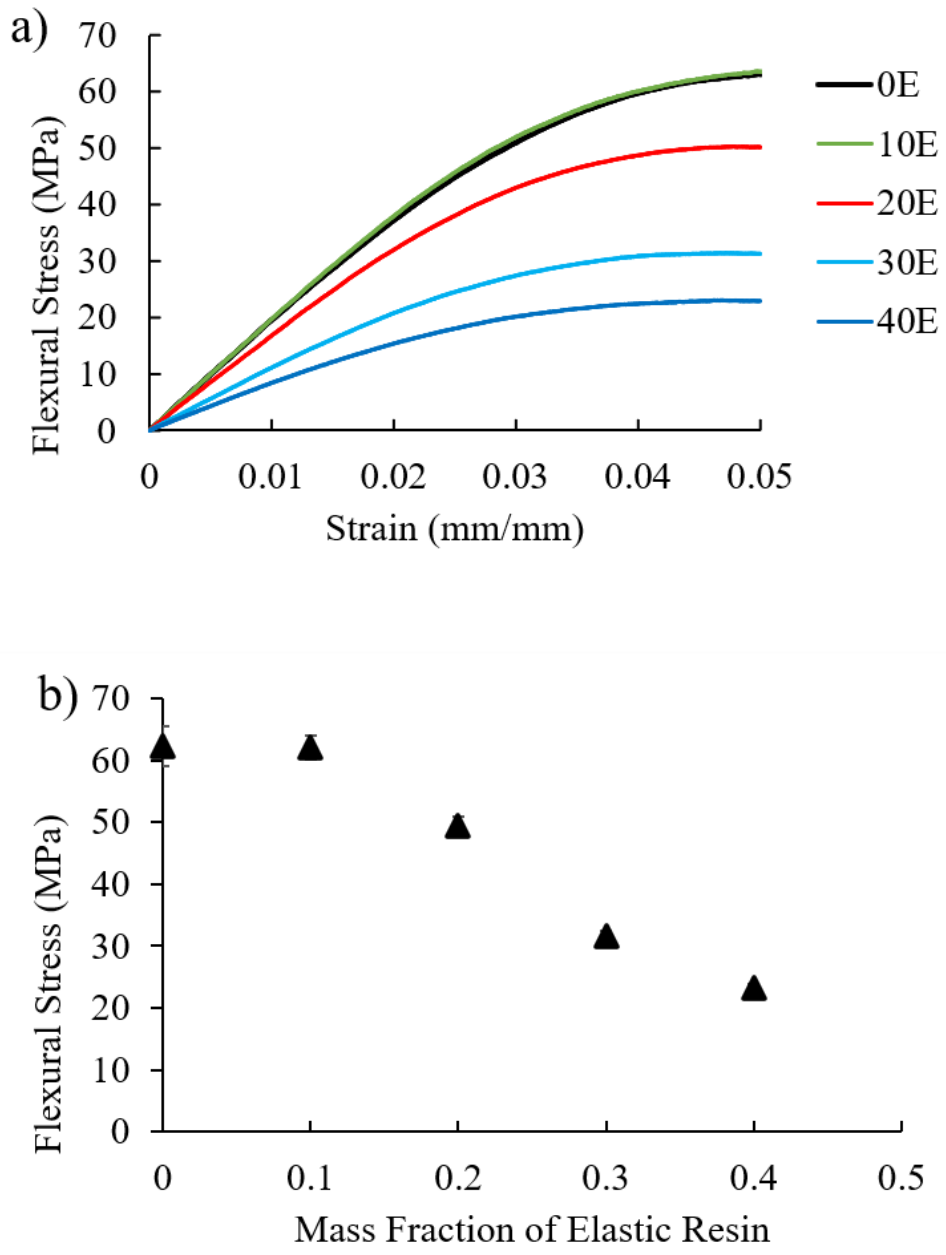

Figure 4.11 Flexural Properties of the SLA polymer blends. (a) Representative stress-strain curves of each polymer blend studied. (b) Flexural stress (MPa) vs mass fraction of Elastic resin in the polymer blend.

Overall, the bending modulus and flexural stress clearly decrease with the addition of Elastic resin to the polymer blend for all blends containing 20% or higher amounts of the Elastic 50A resin.

4.2.3 Thermal and Thermomechanical Analysis

4.2.3.1 DSC

The first tool used to investigate the thermal transitions of the SMP polymer blends prepared via SLA was differential scanning calorimetry. The results of the first and second thermal cycle are shown below (see Figure 4.12). Comparing the first heating run (a) to the second heating (b), the presence of a gradual exothermic event was observed in the first heating cycle that occurred above 160 °C, which was not observed in the second heating cycle. This was indicative of residual polymerization reactions in the printed samples. Additionally, the lack of distinct crystallization peaks observed in the second heating cycle confirmed the amorphous nature of this photopolymer material. However, this material has still been characterized by its "broad glass transition" as seen from the gradual slope of the second heating ramp (see Figure 4.12 b) [67].

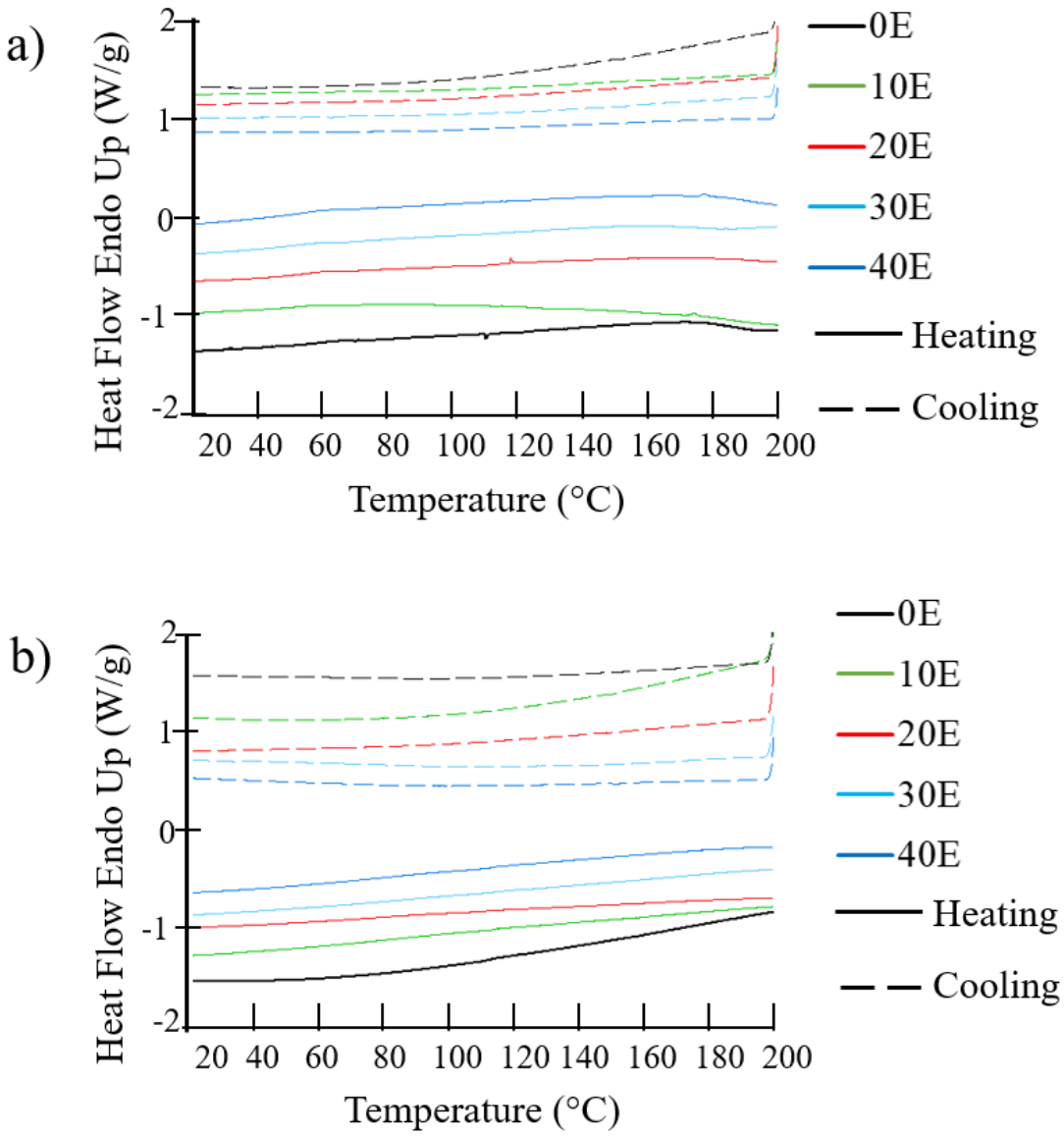

Figure 4.12 Differential scanning calorimetry thermograms of the SLA polymer blends. (a) The first heating run displayed exothermic events above 180 °C, attributed to additional polymerization in the sample. (b) The second heating and cooling cycle of the same samples shown in (a).

The broad glass transition events were utilized to calculate the onset of the glass transition temperature. Here, the measured values of the glass transition temperatures (see Table 4-1), ranged from 44 to 54 °C for the first cycle, and from 60 to 85 °C for the

second cycle. All samples showed an increase in the Tg from the first cycle to the second cycle. This observation, in addition to the exothermic event presented on the end of the first heating cycle is consistent with results of similar photopolymers [101]. Other researchers have studied the same neat Clear resin by DSC, and have found a transition temperature of 53 °C [67], and 107.2 °C [101]. As it can be seen from the DSC thermograms, the lack of distinct crystalline thermal events, presence of broad glass transitions, and range of literature reported values indicate that this measurement technique is less-than ideal for the characterization of the transition temperature of these SMP blends. While it was clear that the properties of the SLA printed SMP blends change with temperature, other techniques were employed to interpret these events.

Table 4-1. Glass transition temperatures for SLA SMP blends by DSC.

	Tg (°C)	
Sample	***1st Cycle***	***2nd Cycle***
0E	44.12	60.34
10E	47.69	84.97
20E	44.79	67.35
30E	49.36	76.33
40E	54.47	80.03

4.2.3.2 Dynamic Mechanical Analysis

To further examine the transitions that occurred in the SLA polymer blends, the mechanical properties were studied as the temperature of the sample was increased. The storage modulus of the material, E', and loss modulus of the material, E'', was gathered by dynamic mechanical analysis (DMA). As it can be seen in Figure 4.13, the initial

storage modulus exhibited similar trends to the Young's modulus evaluated at room temperature (see Figure 4.9). Here, as the mass fraction of Elastic 50A resin increased, the initial modulus of the material decreased. The storage modulus curve for all samples displayed a distinct rubbery plateau, in the order of 10^8, when compared to the initial modulus (in the order of 10^9), highlighting the distinct modulus drop of these shape memory polymers. From the loss modulus curves (displayed in Figure 4.13 b) a lack of distinct peaks in the for each polymer blend was observed, which provided little information of the thermal transitions in the polymer blends. The results shown in Figure 4.13 indicate that the blends displayed a large decrease in stiffness by increasing the temperature, a mechanism that is required to achieve the temporary shape stage.

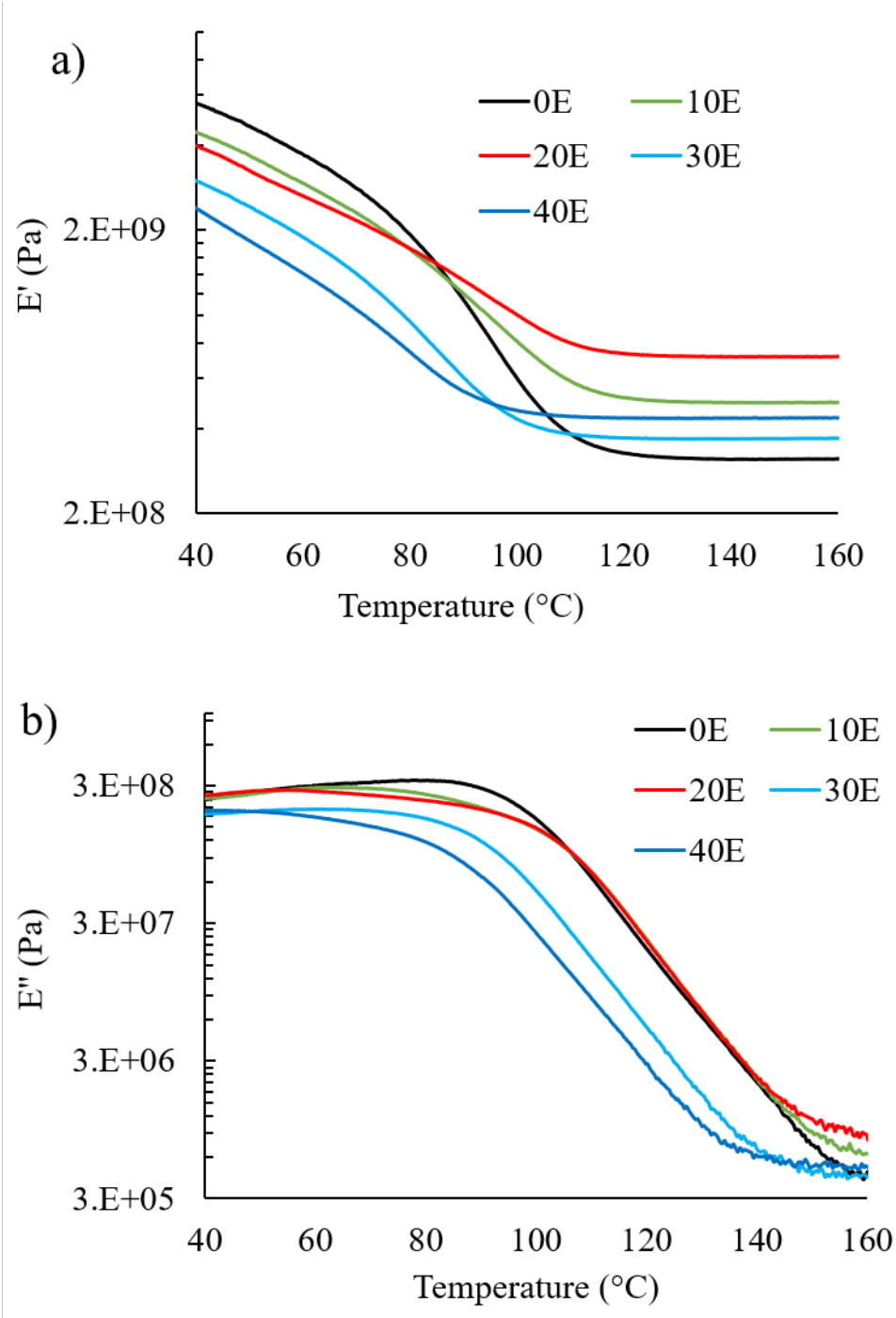

Figure 4.13 Storage modulus (a) and loss modulus (b) curves for the examined SLA polymer blends. The initial stiffness of the material steadily decreases as the amount of elastic resin in the blend increases (as seen from figure a). (b) the loss modulus vs temperature profiles for each tested shape memory polymer blend.

To quantify the transition temperature of each shape memory polymer blend, the ratio of elastic and viscous responses, known as tangent delta, was used (see Figure 4.14). The tan delta curves of each polymer blend vs temperature showed a clear maximum peak which was associated with the glass transition of the samples. This peak represented a physical response of the material transitioning into the rubbery phase [102]. Here, the peak of tan delta occurred between 80 to 97.5 °C (Table 4-2) for all the samples. Once again, this property mutually decreased as the amount of Elastic 50A resin increased in the samples. However, for the samples containing a mass fraction of 0 to 0.2 Elastic material, the values of the glass transition were within four degrees Celsius, whereas the samples containing 0.3 to 0.4 Elastic resin displayed a change in the glass transition temperature of more than 10 degrees Celsius. This observation indicated that higher concentrations of Elastic 50A resin in the polymer blend resulted in a significant decrease in the damping factor of the material.

Table 4-2. Tan delta peak temperature for each of the examined SLA SMP blends.

Sample	tan δ peak (°C)
0E	97.50
10E	96.92
20E	93.45
30E	87.62
40E	80.09

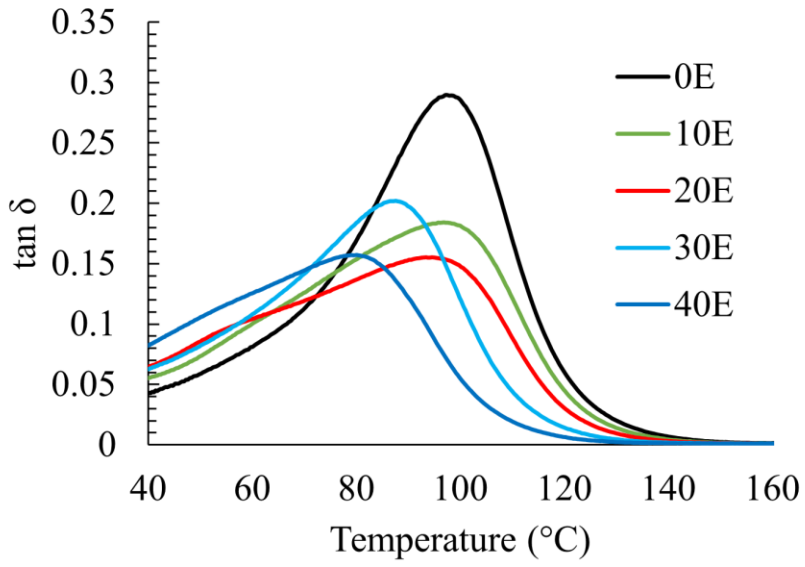

Figure 4.14 Tangent delta curve of the examined SLA polymer blends. The tan delta curve represents the "damping" ability of the material. As the amount of elastic resin increases, the peak of the tangent delta occurs at a lower temperature.

4.2.3.3 Shape Recovery Cycles

The SMP blends manufactured via SLA were examined in twenty compression cycles to characterize the shape recovery of the polymer blends. A plot of the strain vs force applied to the sample (as seen in Figure 4.15) was used to characterize the strain values achieved during this test. The results showed that across the polymer blends consisting of 0 to 0.4 fraction of the Elastic 50A resin, the samples approached a constant value of the recovered strain, e_p, and the fixed strain, e_u, as the number of thermal cycles increased. As it was observed in the shape memory polymer parts produced via material extrusion, the parts printed via SLA also exhibited a unique behavior on the first thermal cycle.

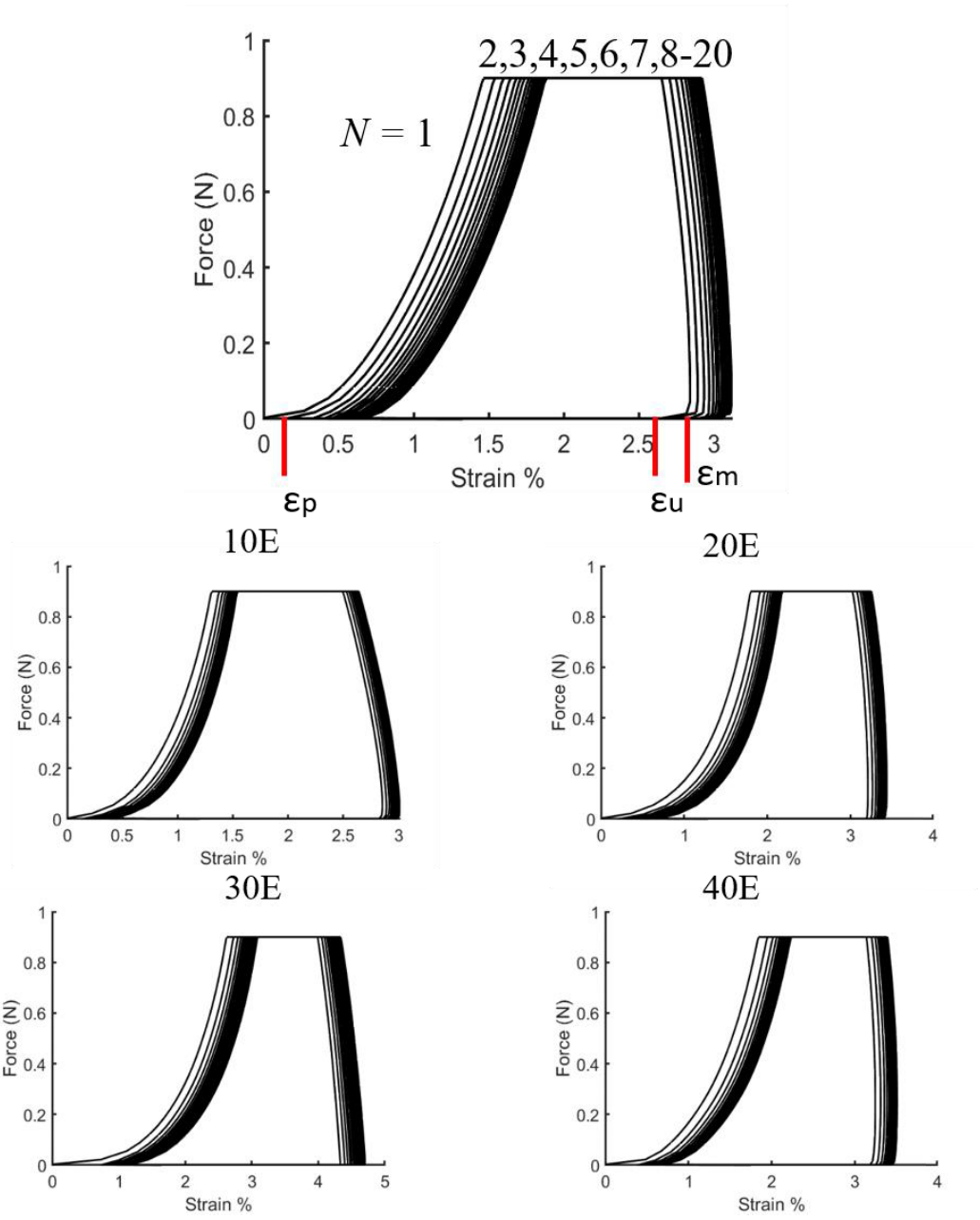

Figure 4.15 Force vs Strain curves from the shape recovery cycle testing. Here, each polymer blend underwent the same 20 cycles. 0E shows the value of the maximum applied strain, ε_m, the set strain, ε_u, and recovered strain, ε_p. Across each polymer blend, the cyclical strain approaches the same value.

This was attributed to an excess of reactive moieties being present in the samples (as it was recorded in both the differential scanning calorimetry results and the dynamic mechanical analysis). Nevertheless, as the prescribed shape recovery cycle number, *N*, increased, the applied strain approached a constant value for all samples.

The thermomechanical shape recovery tests on the polymer blends were also used to quantify the shape fixity and shape recovery ratio. As it was seen from the trends in the force vs strain data (see Figure 4.15), the first cycle resulted in the lowest values of the shape recovery for all the examined samples (Figure 4.16 a). However, following the first cycle, the samples have been completely polymerized, and the polymer networks have been fully developed. As such, the full ability of the polymer samples to store deformations in the temporary state was established. Samples containing some percentage of elastic material (0.1 to 0.4 mass fraction) approached a constant value of shape recovery (over 0.98) after twenty sequential cycles of shape recovery. Polymer blends consisting of 0.1 to 0.4 mass fraction Elastic resin also showed a high degree of shape fixity (Figure 4.16 b) and exhibited consistent values greater than 0.97 across twenty cycles. While the shape fixity and recovery appear excellent for polymer blends containing the Elastic 50A resin, inferior properties were observed for the unmodified Clear material.

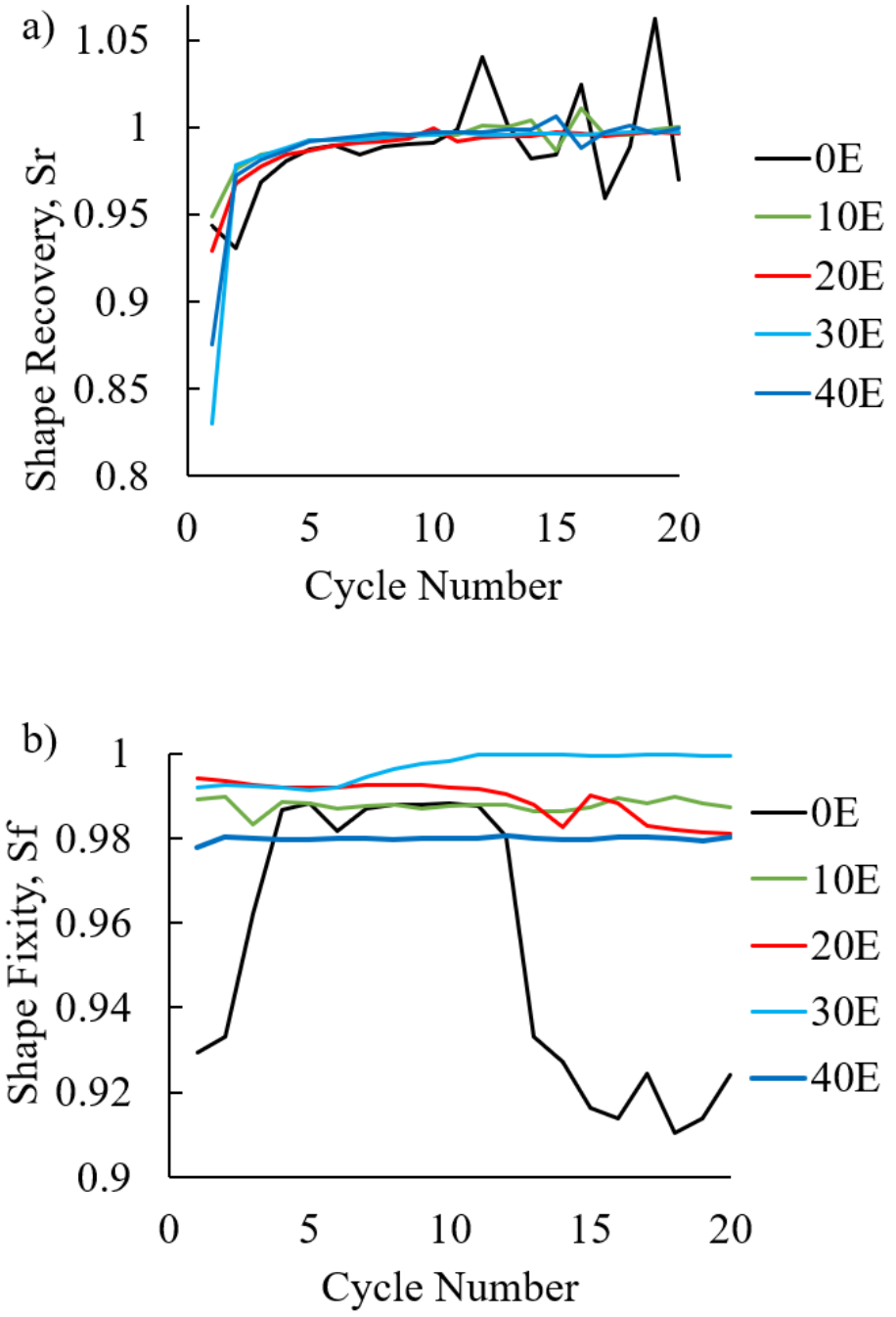

Figure 4.16 Shape recovery (a) and shape fixity (b) ratio of the SMP polymer blends during 20 shape recovery cycles. While the blends reinforced with Elastic resin (10-40E) approached a constant value of S_r (a), and S_f (b) after eleven thermal cycles, the properties of the neat Clear resin (0E) did not.

In the thermomechanical tests, the clear material (0 mass fraction of the Elastic resin), displayed values for shape recovery over 1.0, and a distinct drop in the shape fixity after eleven thermal cycles. Unlike the case for the previously examined material extrusion shape memory polymer, where a recovery over 1.0 was attributed to internal stresses created during the printing of the samples; here, the shape recovery over 1 corresponded to the twelfth shape recovery cycle. This shape recovery could not be attributed to internal stresses from the printing process, as these would be expected to occur on the first shape recovery cycle. Instead, these erroneous values of shape recovery were the result of unrecovered strain induced in the previous shape recovery cycle. As shown in equation 3.4, to determine the shape recovery of each cycle, the previous strain value is used as the initial strain of the sample. In this case, a lack of full recovery from the eleventh shape recovery cycle allowed for the recovered strain for the twelfth cycle, ε_p, to reach a value higher than the set strain, ε_u (as seen in Figure 4.17). These events corresponded to the erratic behavior observed in the shape fixity ratio of the sample as well. To eliminate the possibility of an anomaly, a new sample containing 0% Elastic was repeated in the 20 shape recovery cycles, and shape recovery over 1.0 was again observed in the new sample.

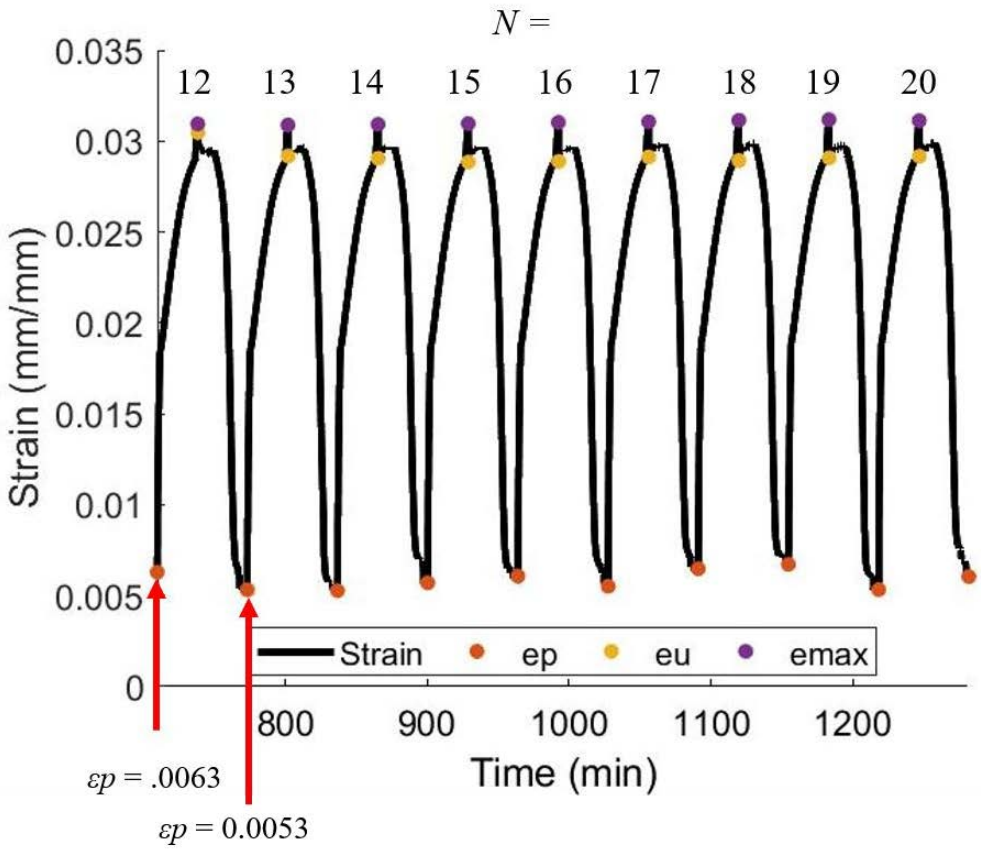

Figure 4.17 The 11th to 20th shape recovery cycle for the neat Clear resin. Here, the recovered strain of the eleventh cycle becomes the initial strain of the twelfth cycle, and the twelfth cycle reaches a recovered strain 0.001 higher than the initial strain for this cycle.

4.2.4 Shape Memory Polymer Functional Antenna

With the ability to successfully print and shape memory polymers via SLA, an antenna was fabricated as an exemplary application of this technology. From the work conducted in characterizing the polymer blends, the blend containing a mass fraction of 0.2 Elastic resin was selected as the best candidate from the observed mixtures. While each of the polymer blends displayed good shape recovery and shape fixity, this blend was selected for its high strain at break, while still exhibiting the ease of printing. While

the blends containing 0.3 and 0.4 mass fraction of the Elastic resin displayed higher strains at failure, the errors and defects that occurred while printing resulted in unreliable and sub-prime quality parts to be manufactured. For those reasons, the blend of 0.2 Elastic resin is used in the next section for the fabrication of a functional antenna.

4.2.4.1 The Liquid Metal Dipole Antenna

A 3D printed shape memory polymer antenna was printed with the blend of 0.2 mass fraction of the Elastic 50A resin. Empty channels in the SMP part were filled with liquid Galinstan metal and examined as a functional antenna. The final antenna included a coaxial connector that made electrical contact with the internal channels of Galinstan (see Figure 4.18). The SMP scaffolding allowed for typical shape recovery behavior (temporary deformation, and shape recovery to permanent shape). This was validated by placing the entire antenna in an oven (T = 100 °C), and then the antenna was deformed to a curved dipole shape (radius of curvature = 44 mm). Upon additional heating, the SMP-Galinstan antenna recovered back to its permanent shape of a straight dipole. Both configurations of the antenna (straight, and curved) were tested using a network analyzer to evaluate its performance.

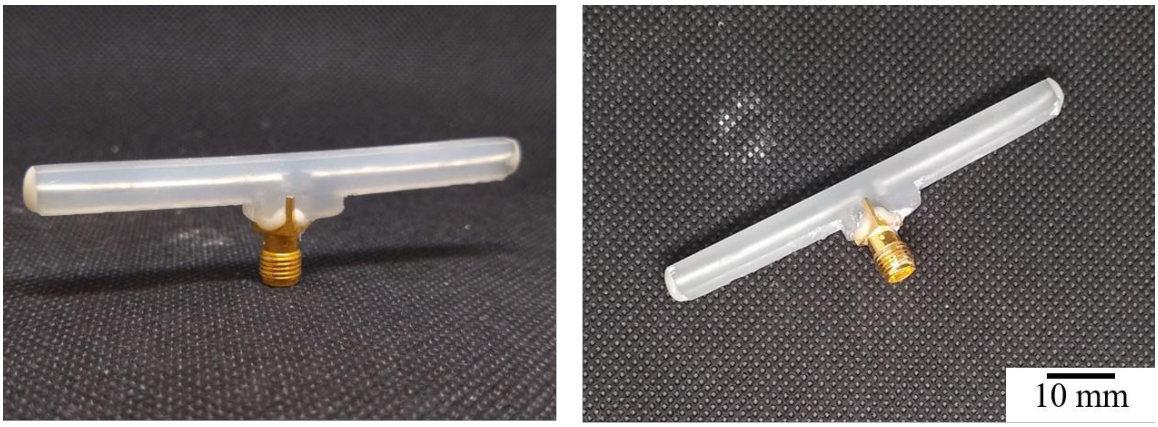

Figure 4.18 The 3D printed SMP antenna. The liquid Galinstan metal is visible within the shape memory polymer matrix.

4.2.4.2 Antenna Performance

A virtual network analyzer (VNA) was used to determine the S11-parameter plots for both the temporarily curved, and straightened dipole antennas (see Figure 4.19). This information was then compared to simulated results obtained from ANSYSS, considering the same geometry as the microfluidic channels. The straight dipole antenna exhibited a peak return loss at 1.68 GHz, compared to the simulated results of 1.89 GHz. A similar decrease in the resonant frequency was observed in the curved dipole which occurred at 1.70 GHz for the tested antenna, and 1.88 GHz in the simulated results. It should be noted, the simulation for the antennas utilized the conductivity of the Galinstan, but the dielectric properties of the SMP material were unavailable and not included in the simulation. As such, this observed frequency shift present in both antennas was attributed to the presence of the SMP matrix surrounding the conductive material of the antenna. This shift in the peak frequency is consistent with results of similar liquid metal filled 3D printed antennas [78].

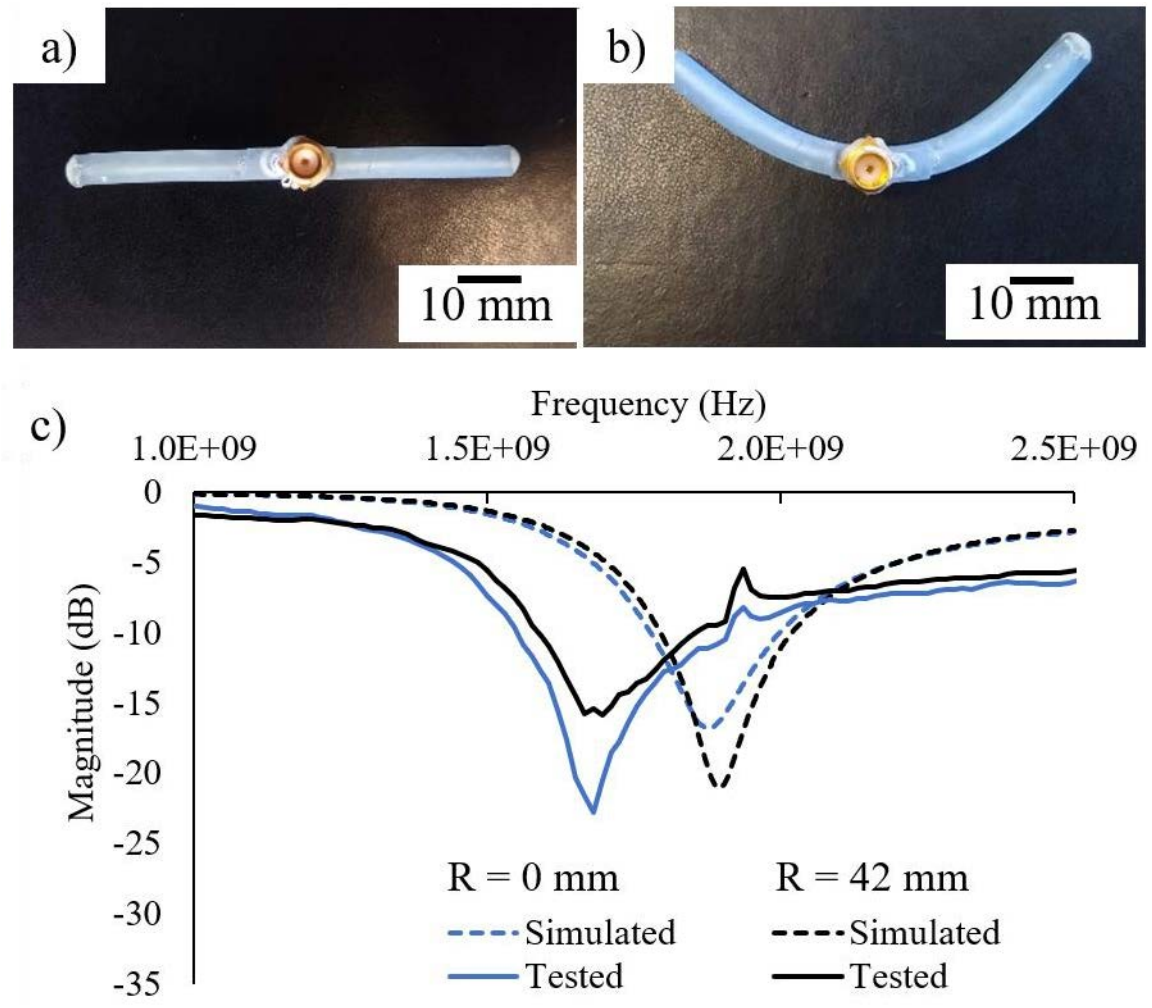

Figure 4.19 S11- Parameter plots for the simulated and tested SMP antennas. (a) The tested shape memory polymer antenna with a radius of curvature of 0 mm. (b) The antenna from (a) after heating and deformation to a radius of curvature of 42 mm. (c) Measured S-11 parameters for both antennas shown, compared to the simulated results

From the S11 parameter plot, the bandwidth and fractional bandwidth were calculated (see Table 4-3). In this case, the bandwidth was measured as the frequency for a return loss of -10 db. It was observed that the curved dipole antenna exhibited a narrower bandwidth of 0.25 GHz, compared to the straight dipole antenna bandwidth of 0.34 GHz. This of course, resulted in a lower fraction bandwidth of 0.15 for the curved

dipole. However, the fractional bandwidth of both the straightened dipole (0.21) and curved dipole (0.15), were higher than the simulated bandwidth of 0.12 (for both the curved and straightened). Overall, the curved dipole antenna exhibited a narrower frequency band, while the straightened antenna offered a lower peak loss at the resonant frequency.**Table 4-3 The tested and simulated performance of the liquid-metal 3D printed SMP antenna.**

	Radius of Curvature	***Peak Frequency (GHz)***	***Maximum Return Loss (dB)***	***Bandwidth (GHz)***	***Fractional Bandwidth***
Tested	0 mm	1.68	-22.81	0.34	0.21
Simulated		1.88	-16.78	0.22	0.12
Tested	42 mm	1.70	-15.90	0.25	0.15
Simulated		1.89	-21.07	0.22	0.12

5 Conclusions and Future Work

Shape memory polymers have successfully been processed via both additive manufacturing techniques investigated: material extrusion and vat polymerization. This work demonstrated that commercially available SMP pellets intended for injection molding applications can be printed on a modified, open-source FFF 3D printer. Additionally, this work has expanded the use of commercially available photopolymers resins to develop adaptive co-polymers with mitigated brittleness and tuned thermo-mechanical performance.

5.1 Material Extrusion of Shape Memory Polymers

The commercially available shape memory polymer pellets printed via material extrusion resulted in the following conclusions:

- A slightly higher mechanical properties than their injection molded counterparts.
- A high shape recovery (over 96%) after five thermal cycles in fold deploy tests. Similarly, after 5 thermomechanical tests the printed parts exhibited a shape recovery approaching 96.6%.
- The shape fixity of the printed SMP had an average of 86.3%. although it decreased to 76% on the fifth thermal cycle.
- By combining the 3D printed SMP matrix with shape memory alloy wires and copper tape, a functional bi-directional hybrid switch was manufactured and tested. This hybrid switch was successfully used on the actuation data collection of a microcontroller based on a thermal stimulus.

5.2 Vat Polymerization of Shape Memory Polymers

The initial efforts concentrated on formulating a shape memory polymer, validating and investigating its thermo-mechanical properties, and demonstrating the fabrication of functional deployable structures. The formulation of a shape memory polymer for SLA used the backbone of the shape memory effect of an available photopolymer resin. It was here found:

- The addition of a Elastic 50A resin allowed for polymer blends of varying mass ratios to be printed on a Formlabs unit.
- As the mass fraction of a Elastic 50A resin increased, the mechanical properties of the blend polymer (tensile strength, modulus, flexural strength) decreased. Furthermore, the strain at break of the polymer blends increased with the addition of Elastic 50A resin indicating the brittleness of the Clear resin was successfully mitigated.
- While the initial storage modulus of the polymer blends decreased with the addition of Elastic 50A, the change in modulus from the glassy region to the rubbery region was still large enough to preserve the shape memory effect.
- The polymer blend that exhibited the high degree of shape recovery, and mechanical properties, without sacrificing quality or printability of samples, was the blend based on 20% Elastic 50A and 80% Clear resin. This polymer blend exhibited a Tg of 93.45 °C, and a shape recovery over 97% after twenty thermomechanical cycles.

- The selected polymer blend was utilized to manufacture functional dipole antennas based on microfluidic channels printed in the SMP matrix, which were filled with a Gallium-Indium liquid metal. These antennas exhibited a shape memory effect allowing the production of a deployable smart antenna.
- The SMP-liquid metal Antennas were tested using a virtual network analyzer and exhibited a peak resonant frequency between 0.18 and 0.21 GHz lower than simulated values.

5.3 Future Work

It is known that vat polymerization additive manufacturing has several benefits over material extrusion, and further investigation into the newly produced shape memory polymer blend would benefit from further characterization. Primarily, this work established the presence of the shape memory effect in each polymer blend and investigated the primary mechanical properties at room temperature. However, further mechanical characterization at elevated temperatures ($T > Tg$) is still required to fully characterize and understand these systems in the rubbery region. Additionally, while the thermomechanical cycle tests used in this work to characterize the printed SMP provided useful information, the applied strain (due to the equipment available for these tests) were rather small (< 5%). It would be highly beneficial to examine these materials at higher applied and recovered strain values.

Furthermore, the additive manufacturing of functional electronics and antennas is of high interest. This work produced a functional SMP-liquid metal antenna, but characterization of the dielectric properties is needed to generate better simulations of the

manufactured antennas. Additionally, a simple dipole antenna was used as a proof of concept, but a major achievement by using additive manufacturing is the fabrication of geometrically complex and functional antennas. Lastly, the liquid metal used in this work acted as a functional conductor for the tested antennas, however, its incorporation on the SMP was rather difficult, and the parts had to be manufactured with larger dimensions. As a result, when deforming the sample, only small deformations could be applied without cracking the sample and allowing the liquid metal to seep out. Thus, alternative approaches to create the functional conductor of these antennas may be more practical in the future.

REFERENCES

1. Ntouanoglou K, Stavropoulos P, Mourtzis D. 4D Printing Prospects for the Aerospace Industry: a critical review. Procedia Manufacturing. 2018;18: 120–129. doi:10.1016/j.promfg.2018.11.016

2. Liu Y, Du H, Liu L, Leng J. Shape memory polymers and their composites in aerospace applications: a review. Smart Mater Struct. 2014;23: 023001. doi:10.1088/0964-1726/23/2/023001

3. Jamie D. Adidas Release their 3D Printed Shoes: The Futurecraft 4D. In: 3D Natives [Internet]. 23 Jan 2018 [cited 15 Nov 2020]. Available: https://www.3dnatives.com/en/adidas-futurecraft-4d-220120184/

4. The First Truly Accessible 3D Printed Denture Solution. [cited 14 Dec 2020]. Available: https://dental.formlabs.com/blog/now-shipping-3d-printed-digital-dentures/

5. Holmes M. Additive manufacturing continues composites market growth. Reinf Plast. 2019;63: 296–301. doi:10.1016/j.repl.2018.12.070

6. González RG. Brief History of Additive Manufacture and the Effect of Patents. American Scientific Research Journal for Engineering, Technology, and Sciences (ASRJETS). 2019;54: 56–67. Available: http://asrjetsjournal.org/index.php/American_Scientific_Journal/article/view/4758

7. Langnau L. 2019 Additive Manufacturing market growth surpassed $10B worldwide. [cited 7 Dec 2020]. Available: https://www.makepartsfast.com/2019-additive-manufacturing-market-growth-surpassed-10b-worldwide/

8. Schmidt DF. Perspectives on the future of additive manufacturing. 2020 [cited 7 Dec 2020]. Available: https://dc.engconfintl.org/imam/6/

9. Dao TD, Ha NS, Goo NS, Yu W-R. Design, fabrication, and bending test of shape memory polymer composite hinges for space deployable structures. J Intell Mater Syst Struct. 2018;29: 1560–1574. doi:10.1177/1045389X17742728

10. Baer GM, Small W 4th, Wilson TS, Benett WJ, Matthews DL, Hartman J, et al. Fabrication and in vitro deployment of a laser-activated shape memory polymer vascular stent. Biomed Eng Online. 2007;6: 43. doi:10.1186/1475-925X-6-43

11. Sokolowski W, Metcalfe A, Hayashi S, Yahia L, Raymond J. Medical applications of shape memory polymers. Biomed Mater. 2007;2: S23-7. doi:10.1088/1748-6041/2/1/S04

12. Pretsch T, Ecker M, Schildhauer M, Maskos M. Switchable information carriers based on shape memory polymer. J Mater Chem. 2012;22: 7757–7766. doi:10.1039/C2JM16204K

13. Li F, Liu Y, Leng J. Progress of shape memory polymers and their composites in aerospace applications. Smart Mater Struct. 2019;28: 103003. doi:10.1088/1361-665X/ab3d5f

14. Zhang R, Guo X, Liu Y, Leng J. Theoretical analysis and experiments of a space deployable truss structure. Compos Struct. 2014;112: 226–230. doi:10.1016/j.compstruct.2014.02.018

15. Raos P, Klapan I, Galeta T. Additive Manufacturing of Medical Models--Applications in Rhinology. Coll Antropol. 2015;39: 667–673. Available: https://www.ncbi.nlm.nih.gov/pubmed/26898064

16. Tanikella NG, Wittbrodt B, Pearce JM. Tensile strength of commercial polymer materials for fused filament fabrication 3D printing. Additive Manufacturing. 2017;15: 40–47. doi:10.1016/j.addma.2017.03.005

17. Honigmann P, Sharma N, Okolo B, Popp U, Msallem B, Thieringer FM. Patient-Specific Surgical Implants Made of 3D Printed PEEK: Material, Technology, and Scope of Surgical Application. Biomed Res Int. 2018;2018: 4520636. doi:10.1155/2018/4520636

18. Osswald TA, Puentes J, Kattinger J. Fused filament fabrication melting model. Additive Manufacturing. 2018;22: 51–59. doi:10.1016/j.addma.2018.04.030

19. Moreno Nieto D, Casal López V, Molina SI. Large-format polymeric pellet-based additive manufacturing for the naval industry. Additive Manufacturing. 2018;23: 79–85. doi:10.1016/j.addma.2018.07.012

20. Woern AL, Byard DJ, Oakley RB, Fiedler MJ, Snabes SL, Pearce JM. Fused Particle Fabrication 3-D Printing: Recycled Materials' Optimization and Mechanical Properties. Materials . 2018;11. doi:10.3390/ma11081413

21. Meraz Trejo E, Jimenez X, Billah KMM, Seppala J, Wicker R, Espalin D. Compressive deformation analysis of large area pellet-fed material extrusion 3D printed parts in relation to in situ thermal imaging. Additive Manufacturing. 2020;33: 101099. doi:10.1016/j.addma.2020.101099

22. Volpato N, Kretschek D, Foggiatto JA, Gomez da Silva Cruz CM. Experimental analysis of an extrusion system for additive manufacturing based on polymer pellets. Int J Adv Manuf Technol. 2015;81: 1519–1531. doi:10.1007/s00170-015-7300-2

23. Shah J, Snider B, Clarke T, Kozutsky S, Lacki M, Hosseini A. Large-scale 3D printers for additive manufacturing: Design considerations and challenges. Int J Adv

Manuf Technol. 2019;104: 3679–3693. Available: https://idp.springer.com/authorize/casa?redirect_uri=https://link.springer.com/article/10.1007/s00170-019-04074-6&casa_token=TgtrCrtTRIQAAAAA:ZW8BHeBEsKyZlVAtEINJvsc3oV1GOFn89elSQRGNNSrThlkgCNdB_phvpP2scgBScKkXiApu0OQ_B6My

24. Love LJ, Duty C. Cincinnati big area additive manufacturing (BAAM). Oak Ridge, TN. 2015. Available: https://info.ornl.gov/sites/publications/files/Pub54708.pdf

25. Sanchez FAC, Lanza S, Boudaoud H, Hoppe S, Camargo M. Polymer Recycling and Additive Manufacturing in an Open Source context: Optimization of processes and methods. Annual international solid freeform fabrication symposium, ISSF 2015. hal.univ-lorraine.fr; 2015. pp. 1591–1600. Available: https://hal.univ-lorraine.fr/hal-01523136

26. Laureto JJ, Pearce JM. Anisotropic mechanical property variance between ASTM D638-14 type i and type iv fused filament fabricated specimens. Polym Test. 2018;68: 294–301. doi:10.1016/j.polymertesting.2018.04.029

27. Ahn S, Montero M, Odell D, Roundy S, Wright PK. Anisotropic material properties of fused deposition modeling ABS. Rapid Prototyping Journal. 2002;8: 248–257. doi:10.1108/13552540210441166

28. McCausland T. 3D Printing's Time to Shine. Research-Technology Management. 2020;63: 62–65. doi:10.1080/08956308.2020.1790290

29. 3D Printing Trends Report 2020. Makerbot, L L C; 2020. Available: https://pages.makerbot.com/pro3DPrintingTrendReport.html

30. 3D Systems Reduces Price on ProX SLS 500 to Expand 3D Printing Market and Gain Market Share. 12 Apr 2017 [cited 18 Nov 2020]. Available: https://www.3dsystems.com/press-releases/3d-systems-reduces-price-prox-sls-500-expand-3d-printing-market-and-gain-market

31. Form 3. [cited 18 Nov 2020]. Available: https://formlabs.com/3d-printers/form-3/

32. Melchels FPW, Feijen J, Grijpma DW. A review on stereolithography and its applications in biomedical engineering. Biomaterials. 2010;31: 6121–6130. doi:10.1016/j.biomaterials.2010.04.050

33. What Does Resolution Mean in 3D Printing? [cited 12 Dec 2020]. Available: https://formlabs.com/blog/3d-printer-resolution-meaning/

34. Quan H, Zhang T, Xu H, Luo S, Nie J, Zhu X. Photo-curing 3D printing technique and its challenges. Bioact Mater. 2020;5: 110–115. doi:10.1016/j.bioactmat.2019.12.003

35. Photon Series. [cited 13 Dec 2020]. Available: https://www.anycubic.com/collections/anycubic-photon-3d-printers

36. Voet VSD, Strating T, Schnelting GHM, Dijkstra P, Tietema M, Xu J, et al. Biobased Acrylate Photocurable Resin Formulation for Stereolithography 3D Printing. ACS Omega. 2018;3: 1403–1408. doi:10.1021/acsomega.7b01648

37. Borrello J, Nasser P, Iatridis J, Costa KD. 3D Printing a Mechanically-Tunable Acrylate Resin on a Commercial DLP-SLA Printer. Addit Manuf. 2018;23: 374–380. doi:10.1016/j.addma.2018.08.019

38. Bird D, Caravaca E, Laquidara J, Luhmann K, Ravindra NM. Formulation of Curable Resins Utilized in Stereolithography. TMS 2019 148th Annual Meeting & Exhibition Supplemental Proceedings. Springer International Publishing; 2019. pp. 1575–1587. doi:10.1007/978-3-030-05861-6_148

39. Products. [cited 14 Dec 2020]. Available: https://www.liqcreate.com/products/

40. Gong H, Beauchamp M, Perry S, Woolley AT, Nordin GP. Optical Approach to Resin Formulation for 3D Printed Microfluidics. RSC Adv. 2015;5: 106621–106632. doi:10.1039/C5RA23855B

41. Marlon WMC, Jonas de C. Development of acrylate-based material using a multivariable approach: additive manufacturing applications. Rapid Prototyping Journal. 2014;20: 121–132. doi:10.1108/RPJ-11-2012-0098

42. Layani M, Wang X, Magdassi S. Novel Materials for 3D Printing by Photopolymerization. Adv Mater. 2018;30: e1706344. doi:10.1002/adma.201706344

43. Mendes-Felipe C, Oliveira J, Etxebarria I, Vilas-Vilela JL, Lanceros-Mendez S. State-of-the-art and future challenges of UV curable polymer-based smart materials for printing technologies. Advanced Materials Technologies. 2019;4: 1800618. Available: https://onlinelibrary.wiley.com/doi/abs/10.1002/admt.201800618

44. Garcia EA, Ayranci C, Qureshi AJ. Material Property-Manufacturing Process Optimization for Form 2 Vat-Photo Polymerization 3D Printers. J Mater Process Manuf Sci. 2020;4: 12. doi:10.3390/jmmp4010012

45. Cosmi F, Dal Maso A. A mechanical characterization of SLA 3D-printed specimens for low-budget applications. Materials Today: Proceedings. 2020;32: 194–201. doi:10.1016/j.matpr.2020.04.602

46. Wang S, Ma Y, Deng Z, Zhang K, Dai S. Implementation of an elastoplastic constitutive model for 3D-printed materials fabricated by stereolithography. Additive Manufacturing. 2020;33: 101104. doi:10.1016/j.addma.2020.101104

47. Lendlein A, Jiang H, Jünger O, Langer R. Light-induced shape-memory polymers. Nature. 2005;434: 879–882. doi:10.1038/nature03496

48. Zhao Q, Qi HJ, Xie T. Recent progress in shape memory polymer: New behavior, enabling materials, and mechanistic understanding. Prog Polym Sci. 2015;49–50: 79–120. doi:10.1016/j.progpolymsci.2015.04.001

49. Diani J, Gilormini P, Frédy C, Rousseau I. Predicting thermal shape memory of crosslinked polymer networks from linear viscoelasticity. Int J Solids Struct. 2012;49: 793–799. doi:10.1016/j.ijsolstr.2011.11.019

50. Hu J, Chen W, Fan P, Gao J, Fang G, Cao Z, et al. Epoxy shape memory polymer (SMP): Material preparation, uniaxial tensile tests and dynamic mechanical analysis. Polym Test. 2017;62: 335–341. doi:10.1016/j.polymertesting.2017.07.001

51. Tobushi H, Hayashi S, Kojima S. Mechanical Properties of Shape Memory Polymer of Polyurethane Series : Basic Characteristics of Stress-Strain-Temperature Relationship. JSME international journal Ser 1, Solid mechanics, strength of materials. 1992;35: 296–302. doi:10.1299/jsmea1988.35.3_296

52. Wagermaier W, Kratz K, Heuchel M, Lendlein A. Characterization Methods for Shape-Memory Polymers. In: Lendlein A, editor. Shape-Memory Polymers. Berlin, Heidelberg: Springer Berlin Heidelberg; 2010. pp. 97–145. doi:10.1007/12_2009_25

53. Behl M, Lendlein A. Shape-memory polymers. Kirk-Othmer Encycl Chem Technol. 2000; 1–16. Available: https://onlinelibrary.wiley.com/doi/abs/10.1002/0471238961.1908011612051404.a01.pub2

54. Behl M, Razzaq MY, Lendlein A. Multifunctional shape-memory polymers. Adv Mater. 2010;22: 3388–3410. Available: https://onlinelibrary.wiley.com/doi/abs/10.1002/adma.200904447?casa_token=KAW7qJ6XiPEAAAAA:zWgU3SCokjTSWPmxxf8Ql12SgcVA7OLh-7CRCl9DTJuP29HHBAmQI2sWI3tl7QDyVMSHwQ2c7BETuPY

55. Petisco-Ferrero S, Fernández J, Fernández San Martín MM, Santamaría Ibarburu PA, Sarasua Oiz JR. The relevance of molecular weight in the design of amorphous biodegradable polymers with optimized shape memory effect. J Mech Behav Biomed Mater. 2016;61: 541–553. doi:10.1016/j.jmbbm.2016.04.027

56. Sun Y-C, Wan Y, Nam R, Chu M, Naguib HE. 4D-printed hybrids with localized shape memory behaviour: Implementation in a functionally graded structure. Sci Rep. 2019;9: 18754. doi:10.1038/s41598-019-55298-1

57. Pandey A, Singh G, Singh S, Jha K, Prakash C. 3D printed biodegradable functional temperature-stimuli shape memory polymer for customized scaffoldings. J Mech Behav Biomed Mater. 2020;108: 103781. doi:10.1016/j.jmbbm.2020.103781

58. Koualiarella A, Arvanitidis A, Argyros A, Kousiatza C, Karakalas A, Lagoudas D, et al. Tuning of shape memory polymer properties by controlling 3D printing strategy. CIRP Ann. 2020;69: 213–216. doi:10.1016/j.cirp.2020.04.070

59. Khoo ZX, Teoh JEM, Liu Y, Chua CK, Yang S, An J, et al. 3D printing of smart materials: A review on recent progresses in 4D printing. Virtual Phys Prototyp. 2015;10: 103–122. doi:10.1080/17452759.2015.1097054

60. Kashyap D, Kishore Kumar P, Kanagaraj S. 4D printed porous radiopaque shape memory polyurethane for endovascular embolization. Additive Manufacturing. 2018;24: 687–695. doi:10.1016/j.addma.2018.04.009

61. Yang Y, Chen Y, Wei Y, Li Y. 3D printing of shape memory polymer for functional part fabrication. Int J Adv Manuf Technol. 2016;84: 2079–2095. doi:10.1007/s00170-015-7843-2

62. Zhang B, Zhang W, Zhang Z, Zhang Y-F, Hingorani H, Liu Z, et al. Self-Healing Four-Dimensional Printing with an Ultraviolet Curable Double-Network Shape Memory Polymer System. ACS Appl Mater Interfaces. 2019;11: 10328–10336. doi:10.1021/acsami.9b00359

63. Yu R, Yang X, Zhang Y, Zhao X, Wu X, Zhao T, et al. Three-Dimensional Printing of Shape Memory Composites with Epoxy-Acrylate Hybrid Photopolymer. ACS Appl Mater Interfaces. 2017;9: 1820–1829. doi:10.1021/acsami.6b13531

64. Miao S, Zhu W, Castro NJ, Nowicki M, Zhou X, Cui H, et al. 4D printing smart biomedical scaffolds with novel soybean oil epoxidized acrylate. Sci Rep. 2016;6: 27226. doi:10.1038/srep27226

65. Yu K, Ritchie A, Mao Y, Dunn ML, Qi HJ. Controlled sequential shape changing components by 3D printing of shape memory polymer multimaterials. Procedia IUTAM. 2015;12: 193–203. Available: https://core.ac.uk/download/pdf/82582195.pdf

66. Choong YYC, Maleksaeedi S, Eng H, Wei J, Su P-C. 4D printing of high performance shape memory polymer using stereolithography. Mater Des. 2017;126: 219–225. doi:10.1016/j.matdes.2017.04.049

67. Inverardi N, Pandini S, Bignotti F, Scalet G, Marconi S, Auricchio F. Sequential Motion of 4D Printed Photopolymers with Broad Glass Transition. Macromol Mater Eng. 2020;305: 1900370. doi:10.1002/mame.201900370

68. Villacres J, Nobes D, Ayranci C. Additive manufacturing of shape memory polymers: effects of print orientation and infill percentage on mechanical properties. Rapid Prototyping Journal. 2018;24: 744–751. doi:10.1108/RPJ-03-2017-0043

69. Ge Q, Qi HJ, Dunn ML. Active materials by four-dimension printing. Appl Phys Lett. 2013;103: 131901. doi:10.1063/1.4819837

70. Zarek M, Layani M, Cooperstein I, Sachyani E, Cohn D, Magdassi S. 3D Printing of Shape Memory Polymers for Flexible Electronic Devices. Adv Mater. 2016;28: 4449–4454. doi:10.1002/adma.201503132

71. Shan W, Chen Y, Hu M, Qin S, Liu P. 4D printing of shape memory polymer via liquid crystal display (LCD) stereolithographic 3D printing. Mater Res Express. 2020;7: 105305. doi:10.1088/2053-1591/abbd05

72. An Y, Kim J, Goo NS, Kim Y, Park JK, Yu W-R. Quantitative evaluation of the three-dimensional deployment behavior of a shape memory polymer antenna. Smart Mater Struct. 2018;27: 105007. doi:10.1088/1361-665X/aad936

73. Jape S, Garza M, Ruff J, Espinal F, Sessions D, Huff G, et al. Self-foldable origami reflector antenna enabled by shape memory polymer actuation. Smart Mater Struct. 2020;29: 115011. doi:10.1088/1361-665X/abaac2

74. Shemelya C, Zemba M, Liang M, Yu X, Espalin D, Wicker R, et al. Multi-layer archimedean spiral antenna fabricated using polymer extrusion 3D printing. Microw Opt Technol Lett. 2016;58: 1662–1666. Available: https://onlinelibrary.wiley.com/doi/abs/10.1002/mop.29881?casa_token=lWdxHm6CIF8AAAAA:fwcDd9bM2wWi1E5hh9bMZkU9f-5c0cNpSYXYeLsMEE1YLbCPyYusutPGaNuuLCol7blxHkOe9kFWRmo

75. Yu Y-Z, Lu J-R, Liu J. 3D printing for functional electronics by injection and package of liquid metals into channels of mechanical structures. Mater Des. 2017;122: 80–89. doi:10.1016/j.matdes.2017.03.005

76. Ladd C, So J-H, Muth J, Dickey MD. 3D printing of free standing liquid metal microstructures. Adv Mater. 2013;25: 5081–5085. doi:10.1002/adma.201301400

77. Ota H, Emaminejad S, Gao Y, Zhao A, Wu E, Challa S, et al. Application of 3D printing for smart objects with embedded electronic sensors and systems. Adv Mater Technol. 2016;1: 1600013. doi:10.1002/admt.201600013

78. Bharambe VT, Ma J, Dickey MD, Adams JJ. Planar, Multifunctional 3D Printed Antennas Using Liquid Metal Parasitics. IEEE Access. 2019;7: 134245–134255. doi:10.1109/ACCESS.2019.2942058

79. Zhou Y, Fang S, Liu H, Wang Z, Shao T. A Function Reconfigurable Antenna Based on Liquid Metal. Electronics. 2020;9: 873. doi:10.3390/electronics9050873

80. Bharambe V, Parekh DP, Ladd C, Moussa K, Dickey MD, Adams JJ. Liquid-Metal-Filled 3-D Antenna Array Structure With an Integrated Feeding Network. IEEE Antennas Wirel Propag Lett. 2018;17: 739–742. doi:10.1109/LAWP.2018.2813309

81. mahor·xyz. [cited 31 Jan 2021]. Available: https://mahor.xyz/

82. Shape Memory Polymer (SMP) Guide for Injection/Extrusion molding. SMP Technologies; Available: http://www2.smptechno.com/tech/

83. Cersoli T, Cresanto A, Herberger C, MacDonald E, Cortes P. 3D Printed Shape Memory Polymers Produced via Direct Pellet Extrusion. Micromachines (Basel). 2021;12. doi:10.3390/mi12010087

84. Formlabs. Clear Resin. Safety Data Sheet; 2020 Feb. Available: https://formlabs-media.formlabs.com/datasheets/1801037-SDS-ENEU-0.pdf

85. Formlabs. Elastic 50A Resin. Safety Data Sheet; 2020 Jun. Available: https://formlabs-media.formlabs.com/datasheets/2001417-SDS-ENEU-0.pdf

86. Tech specs for the Form 2. [cited 25 Mar 2021]. Available: https://formlabs.com/3d-printers/form-2/tech-specs/

87. The definitive guide to ASTM D790 flexure testing of plastics. [cited 26 Mar 2021]. Available: https://www.instron.us/en-us/testing-solutions/by-test-type/flexure/the-definitive-guide-to-astm-d790

88. Menard KP, Menard NR. Dynamic mechanical analysis in the analysis of polymers and rubbers. Encyclopedia of polymer science and technology. 2002; 1–33. Available: https://onlinelibrary.wiley.com/doi/abs/10.1002/0471440264.pst102.pub2

89. Asaletha R, Kumaran MG, Thomas S. Thermoplastic elastomers from blends of polystyrene and natural rubber: morphology and mechanical properties. Eur Polym J. 1999;35: 253–271. doi:10.1016/S0014-3057(98)00115-3

90. Ratna D. 3 - Thermal properties of thermosets. In: Guo Q, editor. Thermosets. Woodhead Publishing; 2012. pp. 62–91. doi:10.1533/9780857097637.1.62

91. Tobushi H, Hashimoto T, Ito N, Hayashi S, Yamada E. Shape Fixity and Shape Recovery in a Film of Shape Memory Polymer of Polyurethane Series. J Intell Mater Syst Struct. 1998;9: 127–136. doi:10.1177/1045389X9800900206

92. Liu Y, Han C, Tan H, Du X. Thermal, mechanical and shape memory properties of shape memory epoxy resin. Materials Science and Engineering: A. 2010;527: 2510–2514. doi:10.1016/j.msea.2009.12.014

93. Fan M, Yu H, Li X, Cheng J, Zhang J. Thermomechanical and shape-memory properties of epoxy-based shape-memory polymer using diglycidyl ether of

ethoxylated bisphenol-A. Smart Mater Struct. 2013;22: 055034. doi:10.1088/0964-1726/22/5/055034

94. Wu X, Yang X, Zhang Y, Huang W. A new shape memory epoxy resin with excellent comprehensive properties. J Mater Sci. 2016;51: 3231–3240. doi:10.1007/s10853-015-9634-4

95. SMPtechno. Shape Memory Polymer "SMP" Material Properties. In: SMP Technologies [Internet]. 2019 [cited 5 Aug 2020]. Available: http://www2.smptechno.com/en/smp/

96. Schirmeister CG, Hees T, Licht EH, Mülhaupt R. 3D printing of high density polyethylene by fused filament fabrication. Additive Manufacturing. 2019;28: 152–159. doi:10.1016/j.addma.2019.05.003

97. Kaynak C, Varsavas SD. Performance comparison of the 3D-printed and injection-molded PLA and its elastomer blend and fiber composites. J Thermoplast Compos Mater. 2019;32: 501–520. doi:10.1177/0892705718772867

98. Akhoundi B, Behravesh AH. Effect of filling pattern on the tensile and flexural mechanical properties of FDM 3D printed products. Exp Mech. 2019;59: 883–897. doi:10.1007/s11340-018-00467-y

99. Jose S, Thomas S, Biju PK, Karger-Kocsis J. Mechanical and dynamic mechanical properties of polyolefin blends: effect of blend ratio and copolymer monomer fraction on the compatibilisation efficiency of random copolymers. J Polym Res. 2013;20: 1–13. Available: https://idp.springer.com/authorize/casa?redirect_uri=https://link.springer.com/article/10.1007/s10965-013-0303-5&casa_token=zVCze7Sp01wAAAAA:vKgtohDdrYgWw90DKjAd2a21TL4ET32iNuqbVKhpyCU_LGUBSlcQwlbxK3EenJgRaduiLuaTbUzX3s-t

100. Veenstra H, Verkooijen PCJ, van Lent BJJ, van Dam J, de Boer AP, Nijhof APHJ. On the mechanical properties of co-continuous polymer blends: experimental and modelling. Polymer . 2000;41: 1817–1826. doi:10.1016/S0032-3861(99)00337-7

101. Mendes-Felipe C, Patrocinio D, Laza JM, Ruiz-Rubio L, Vilas-Vilela JL. Evaluation of postcuring process on the thermal and mechanical properties of the Clear02^{TM} resin used in stereolithography. Polym Test. 2018;72: 115–121. doi:10.1016/j.polymertesting.2018.10.018

102. Menard KP, Menard N. Dynamic mechanical analysis. Encyclopedia of Analytical Chemistry: Applications, Theory and Instrumentation. 2006; 1–25. Available: https://onlinelibrary.wiley.com/doi/abs/10.1002/9780470027318.a2007.pub3